Discover Chemical Engineering

Discover

Review

Chemical looping reforming: process fundamentals and oxygen carriers

Hao Zheng[1] · Xiaofeng Jiang[1] · Yanxiu Gao[1] · Andrew Tong[2] · Liang Zeng[1]

Received: 29 April 2022 / Accepted: 13 June 2022
Published online: 25 July 2022

Abstract
Chemical looping reforming (CLR) provides a viable process intensification approach for clean and efficient syngas production from carbonaceous fuel with inherent gas–gas separation. The rational design of metal oxide-based oxygen carriers and the scale-up of associated CLR reactor systems play important roles in CLR process development. This review first introduces the concept and advantages of CLR as well as its historical development. The process fundamentals, including basic schemes, reaction stoichiometry, thermodynamics, kinetics and reactor system design, are reviewed. The integral approach for CLR process development is illustrated, showing that the design and compatibility of oxygen carriers and reactor systems are critical for CLR performance. The reaction principle during the reduction of oxygen carriers is discussed, followed by strategies for improving the redox reactivity and stability. We further review and discuss the latest exciting advances on this subject with the purpose of illustrating factors that govern fundamental mechanisms in the redox reaction chemistry of oxygen carriers and their design principles for sustained chemical looping reactor applications. It is expected that these new advances will inspire more effective oxygen carriers and efficient reactor systems for the development and deployment of various CLR processes.

1 Introduction

1.1 Chemical looping concept

Carbonaceous fuels (natural gas, oil, coal, biomass and their derivatives) are currently the dominant energy source and are projected to supply > 70% of the global energy through 2050 [1]. They can be fully oxidized with oxygen from air to CO_2 and H_2O through combustion process for heat and electricity generation [2, 3]. They can also be partially oxidized through either gasification or reforming process to produce synthesis gas (or syngas, a mixture of primarily CO and H_2), which is an important intermediate for H_2, liquid fuel and chemical synthesis [4, 5]. Existing processes for carbonaceous fuel conversion, however, consist of multiple costly unit operations for upstream raw material reaction and clean-up as well as downstream product synthesis and separation/purification. These multiple processing steps results in significant process inefficiencies and pollutant release. In addition, the utilization of carbonaceous fuels emits a tremendous amount of CO_2, which is the main cause of the alarming global warming problem. In 2021, energy-related CO_2 emissions

Hao Zheng and Xiaofeng Jiang are co-first authors.

✉ Andrew Tong, tong.48@osu.edu; ✉ Liang Zeng, zengl@tju.edu.cn | [1]Key Laboratory for Green Chemical Technology of Ministry of Education, School of Chemical Engineering and Technology, Tianjin University, Tianjin 300072, China. [2]William G. Lowrie Department of Chemical and Biomolecular Engineering, 151 W. Woodruff Avenue, Columbus, OH 43210, USA.

grew by 4.8% as demand for coal, oil and gas rebounded with the economy, reaching 31.5 billion metric tons [1]. Cutting greenhouse gas emissions to limit the increase in average global temperatures to 1.5 ℃ by 2050 is key to averting the worst effects of climate change [6]. A growing number of countries have committed to carbon neutrality strategies to meet the 2050 target. To realize the goal, International Renewable Energy Agency (IRENA) predicted that the annual energy intensity improvement rate needs to rise to 2.9%, nearly 2.5 times the historical trend, and the global energy intensity must reduce by 60% before 2050 [7]. To achieve clean, efficient and cost-effective utilization of carbonaceous fuels, transformative conversion technologies with intensified process schemes, low environmental impacts and high energetic efficiencies are necessary. As shown in Fig. 1, the concept of chemical looping promises to solve these problems in conventional carbonaceous fuel conversion, representing an energy conversion technology that is potentially an affordable, clean and efficient alternative for power generation and syngas [8–11].

In a broad sense, chemical looping is an approach for process intensification in which a given reaction and/or separation can be decomposed into multiple subreactions via reacting and regenerating chemical intermediates in isolated steps or spaces [12]. The typical design of chemical looping schemes is to integrate reaction and separation with circulating metal oxide-based oxygen carriers in one unit operation and thus intensify the overall process with increased efficiency, lowered emission and reduced cost. In the 1.5 °C Scenario, some emissions persist in 2050 from residual uses of fossil fuels and some industrial processes [7]. Therefore, the remaining CO_2 will have to be captured and sequestered. The concept of chemical looping can be applied for the conversion of carbonaceous fuels to produce electricity, syngas and H_2 with inherent CO_2 control. This concept has been quickly adopted as high-temperature solids looping cycles in the past couple of decades for the in situ removal of CO_2 during the carbonaceous fuel combustion process [3, 10, 13, 14].

In conventional pulverized coal-fired power plants, coal and air are mixed together in the boiler and combusted to release heat while producing a flue gas containing ~ 15% CO_2 in volume. For CO_2 capture from flue gas, a well-established monoethanolamine scrubbing technology could be used, however, it will increase the cost of electricity (COE) by more than 50% [15]. Chemical looping combustion (CLC) is a promising second-generation oxy-fuel combustion technique and has been highlighted as the R&D focus in the European Strategic Energy Plan (SET-Plan) [14, 16–18]. The CLC system mainly consists of a reducer/fuel reactor and a combustor/air reactor, between which oxygen carriers are circulated to convey both heat and oxygen. In the reducer, oxygen carriers provide lattice oxygen to fully oxidize their fuel to CO_2 and H_2O. A high purity CO_2 stream can be obtained by condensing the water with minimal energy penalty. The reduced oxygen carriers are regenerated with air in the combustor, where sensible heat is released for electricity generation. The CLC approach achieves in situ CO_2 capture during the combustion process, circumventing energy- and cost-intensive air separation and CO_2 separation units. In addition, thermal NO_x formation is significantly reduced during its flameless combustion process [19, 20]. Techno-economic analysis shows that the CLC process can capture > 90% CO_2 with < 30% increase in the COE while reducing environmentally hazardous pollutants such as NO_x [21].

In addition to the CLC application for full oxidation of carbonaceous fuel with in situ CO_2 capture, the CLR process can also be used for partial oxidation to improve the production of CO and/or H_2. The CLR process has more potential for the chemical and fuel industries due to the wide utilization of CO and H_2. This review focuses on the research and development of CLR processes and associated oxygen carriers for CO and/or H_2 production from non-solid carbonaceous fuels such as natural gas and alcohol. Chemical looping gasification of solid fuels and thermochemical splitting of CO_2 and/or H_2O without involving carbonaceous fuels are not discussed in this review [22–27]. The concept and advantages of CLR are first introduced and followed by the historical development of related technologies. The various aspects of the CLR

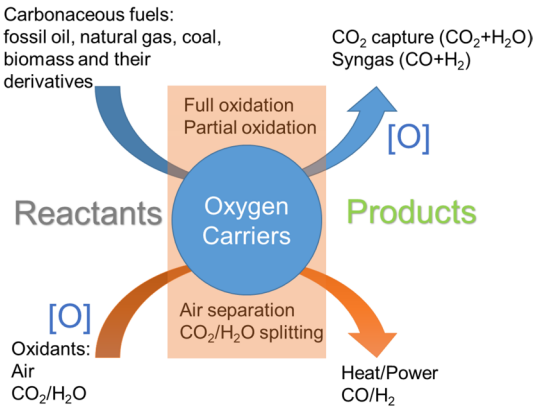

Fig. 1 Chemical looping concept for carbonaceous fuel conversion

process, including basic schemes, reaction stoichiometry, thermodynamics, kinetics, and reactor design, are reviewed. The design strategy and recent development on oxygen carrier materials are discussed. It is expected that these process fundamentals and recent advances will inspire more effective oxygen carrier particles and reaction systems to be developed and deployable in CLR processes.

1.2 Chemical looping reforming

Conventional reforming process usually consists of a high-temperature catalytic reformer for syngas production, intermediate-temperature water gas shift (WGS) unit for H_2 enrichment, and low-temperature chemical/physical separation for CO_2 removal [5, 28]. Taking methane reforming as an example, steam reforming of methane (Eq. 1) is the most common approach, which requires an excess amount of steam to enhance carbonaceous fuel conversion and suppress coke deposition. Consequently, the resulted syngas is rich in H_2 (H_2:CO molar ratio > 3), which is suitable for H_2 production but not good for fuel and chemical synthesis. Dry reforming with CO_2 (Eq. 2) has been proposed to adjust the H_2:CO ratio for various downstream applications, but requires excess CO_2 injection to avoid carbon deposition, resulting lower syngas purity. Nevertheless, both reforming reactions are strongly endothermic and carried out in catalytic tubular reactors with external heating (Eq. 3). Such design requires high costs for reactor material of construction and fabrication as well as external fuel combustion to provide the heat necessary to drive the endothermic reactions. Carbon dioxide exists in both syngas from the tube side and flue gas from the furnace side, which complicates carbon capture scheme for natural gas reforming applications. Partial oxidation (POX, Eq. 4) and autothermal reforming (ATR, combination of Eqs. 1, 3, 4) have also been commercialized for syngas production, which is usually followed by WGS reaction for H_2 enrichment and CO_2 separation for H_2 purification. However, the associated air separation unit (ASU) and acid gas removal unit increase both the energy penalty and capital cost compared to SMR processes.

$$CH_4 + H_2O = CO + 3H_2 \ \Delta H^{o}_{1073K} = 225 \text{ KJ mol}^{-1} \tag{1}$$

$$CH_4 + CO_2 = 2CO + 2H_2 \ \Delta H^{o}_{1073K} = 259 \text{ KJ mol}^{-1} \tag{2}$$

$$CH_4 + 2O_2 = CO_2 + 2H_2O \ \Delta H^{o}_{1073K} = -802 \text{ KJ mol}^{-1} \tag{3}$$

$$CH_4 + 0.5O_2 = CO + 2H_2 \ \Delta H^{o}_{1073K} = -23 \text{ KJ mol}^{-1} \tag{4}$$

CLR offers a viable process intensification approach for effective syngas production integrated with in situ gas–gas separation. Figure 1 shows the concept of CLC/CLR for carbonaceous fuel conversion [29–33]. The overall reactions of the CLC and CLR systems are full oxidation (e.g., Eq. 3) and partial oxidation (e.g., Eqs. 1, 2, and 4), respectively. Rational design of CLR reactor system to decouple these reactions and oxygen carriers with high fuel conversion and product selectivity could directly produce high-quality syngas (high CO/H_2 concentrations and desirable ratios) without the need for gas–gas separation units such as air separation and acid gas removal units. For example, Fan et al. [34–37] developed a three-reactor CLR process, and the overall reaction is the same as the conventional ATR process. Iron-based oxygen carriers are used to convert carbonaceous fuel to CO_2/H_2O in a moving bed reducer, and the reduced oxygen carrier then reacts with the steam to directly generate H_2 in a moving bed oxidizer, both of which adopt a gas–solid counter-current flow pattern in the reactor design. The iron-based oxygen carrier is fully regenerated in a bubbling fluidized bed combustor by reacting with air and then recycled back to the reducer to provide both lattice oxygen and sensible heat. Both CO_2 and H_2 are separated in situ with near zero energy penalty in this three-reactor CLR system, which significantly reduces the separation costs and intensifies the H_2 production processes.

The concept of chemical looping is also advantageous from an exergy point of view [38–41]. The exergy loss in the carbonaceous fuel conversion process could be reduced by either recuperating the low-grade heat while producing more high-grade heat or designing suitable oxygen carriers in chemical looping processes. As shown in Fig. 2, in the conventional steam methane reforming process, the exergy losses are approximately 12.0% and 8.8% from steam reforming and WGS reactions, respectively. An iron-based CLR scheme is designed and analysed based on the same assumptions [40]. Approximately 5.7% exergy loss occurs in the reducer due to the generation of medium exergy rate iron from low exergy rate iron oxides, and near zero exergy loss is achievable in the oxidizer, as it only requires a small amount of low-grade heat. As a result, the exergy loss for H_2 production using the CLR scheme is significantly reduced compared

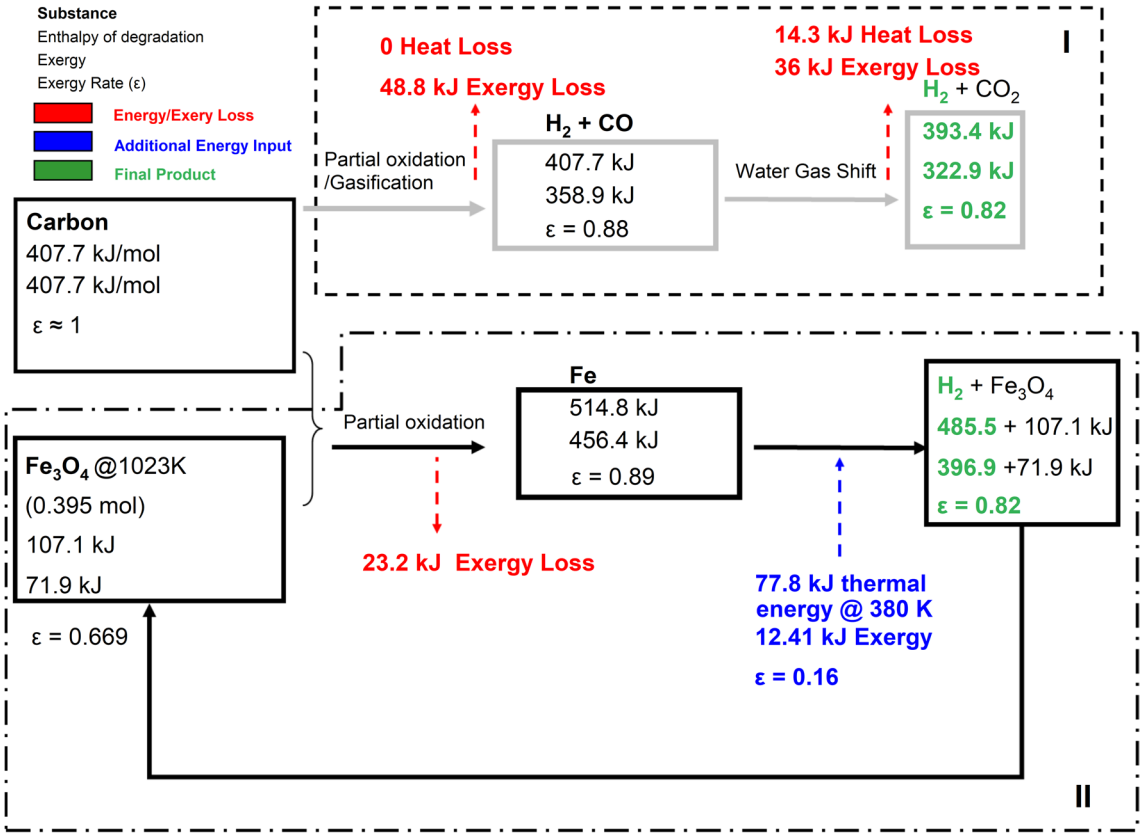

Fig. 2 Exergy recovering scheme for the carbon gasification–WGS process (reaction temperature is assumed to be 1123 K for scheme II). Reproduced from ref. [40] with permission from the American Chemical Society, copyright 2010

to the conventional process. In summary, through careful design of CLR schemes, significant improvements could be achieved in syngas production and separation with high exergy efficiency and low production cost. These advantages have attracted and inspired tremendous efforts for understanding reaction mechanisms and process fundamentals as well as developing oxygen carriers and reactor systems for various CLR processes.

1.3 Historical development of chemical looping reforming

Some representative historical and recent developments of CLR technologies are listed in Table 1. The Howard Lane process was the first industrial application of CLR for H_2 production, which can be traced back to the 1910s [42]. A fixed bed reactor was filled with iron ore and externally heated to reaction temperatures. A mechanical valve system was used for periodic switching between reducing gas (producer gas) and oxidizing gas for conducting redox cycles, a similar pattern used in most current laboratory research. In the Lane process, iron oxide was first reduced with coal-derived producer gas and then regenerated with steam while producing H_2 through the steam-iron reaction. The Lane process achieved an annual H_2 production capacity of 24 million m^3 by 1913 but shortly could not compete with the fast development of natural gas and oil reforming technologies. The low recyclability of iron ores and the poor fuel conversion in the fixed bed reactor system were two critical factors affecting the economics of the Lane process, which reflects that the oxygen carrier and reactor system are the two key components in the development of the CLR process.

The steam-iron process was further developed with the use of fluidized bed reactors design to enhance the mass and heat transfer between carbonaceous fuel and oxygen carriers [43]. In the early 1950s, Lewis and Gilliland studied the feasibility of copper or iron oxides as oxygen carriers in a circulating fluidized bed (CFB) system for converting solid fuels to high purity CO_2 [44–48]. Steam and/or CO_2 were used to fluidize the bed materials and promote the reaction between metal oxides and solid fuels in one reactor. The reduced metal oxide was then regenerated by air in a separate reactor. Various reactor designs have been proposed, including multistage fluidized bed, stoker-type or moving bed with gas–solid countercurrent flow pattern, to improve fuel conversion. However, the redox pairs were set to be Fe_2O_3/Fe_3O_4

Table 1 Representative chemical looping reforming process development

Developer	Year	Fuel	Product	Overall reaction	Oxygen carriers	Reactor design and gas–solid flow pattern
Lane	1910s	Syngas	H_2	$CO+H_2O=CO_2+H_2$	Fe_3O_4–Fe	Fixed bed, gas switching, solid fixed
Lewis and Gilliland	1950s	Solid fuel	CO_2	$C+O_2=CO_2$	CuO–Cu_2O or Fe_2O_3–Fe_3O_4	Circulating fluidized bed, moving bed, mixed flow
IGT	1970s	Syngas	H_2	$CO+H_2O=CO_2+H_2$	Fe_3O_4–Fe	Two-stage fluidized bed, countercurrent flow
Otsuka	1990s	CH_4	Syngas	$2CH_4+O_2=2CO+4H_2$	Supported cerium oxide	Fixed bed, gas switching, solid fixed
Fan	2000s	Syngas	H_2	$CO+H_2O=CO_2+H_2$	Fe_2O_3–Fe/FeO	Moving bed, countercurrent flow
Fan	2010s	CH_4	Syngas	$2CH_4+O_2=2CO+4H_2$	Fe_2TiO_5–$FeTiO_3$	Moving bed, co-current flow

and CuO/Cu_2O in their proposed designs, which is thermodynamically not suitable for syngas production in the CLR process. In the 1960s, the Institute of Gas Technology (IGT) developed the HYGAS process for gasifying coal under a H_2 atmosphere to enhance natural gas synthesis [49]. A high-pressure steam-iron process was proposed for H_2 production using synthesized iron-based oxygen carriers and a two-stage fluidized bed reactor design. The countercurrent gas–solid contacting pattern in a such design could improve the fuel gas and iron oxide conversions and thus the H_2 production efficiency. The HYGAS process was demonstrated at the pilot scale. However, it was not commercialized due to the wide discovery of natural gas resources and the poor reactivity and recyclability of the oxygen carriers.

In 1987, Ishida introduced the term chemical looping in order to reduce the irreversibility and exergy loss in the combustion process [38]. Later, in the 1990s, Otsuka studied syngas generation from the partial oxidation of methane using cerium oxides in a CLR scheme [50]. Cerium oxides have been widely used in the three-way catalysts of commercial automotive converters in light of their excellent oxygen storage/release capacity [51]. From the standpoint view of thermodynamics, CeO_2 has a moderate oxidizing capability that could potentially provide complete CH_4 conversion and a high syngas selectivity. However, the redox kinetics of cerium oxide are relatively slow and need to be promoted with various dopants [25, 52]. It is noted in Table 1 that all the net reactions in the listed processes are exothermic, which indicates that the corresponding CLR processes could be autothermally operated. CLR processes with net reactions being endothermic (e.g., steam/dry reforming reactions, Eqs. 1 and 2) have also been developed at lab scales. These endothermic CLR processes can still effectively integrate reaction and separation to generate the desired syngas product but usually require external heating for the activation of fuel and metal oxides, which can be provided from nuclear or solar energy [25, 32, 53–55]. Nevertheless, the high cost in the scaling-up and engineering of high-temperature reactors and the incomprehension in the design and development of oxygen carriers are the main causes for the slow development of these early CLR processes.

Since the early 2000s, due to the advantage of in situ CO_2 capture during carbonaceous fuel conversion, various chemical looping processes have been proposed and developed. Chalmers University has demonstrated the CLC process for both gas and solid fuel conversion at 10 and 100 kW_{th}, and recently tested steel converter slag as oxygen carriers in a 12 MW_{th} CFB boiler [13, 19, 56–64]. A 1 MW_{th} CLC pilot plant has been demonstrated for the conversion of both solid and gaseous fuels at Technical University of Darmstadt with naturally occurring materials such as iron ore and ilmenite as oxygen carriers [65–67]. In addition, two MW_{th}-level CLC pilot units are being designed or constructed supported by the National Key R&D Program of China [16, 68, 69]. All these large-scale CLC pilot units have adopted CFB reactor design. For CLR applications, Ohio State University (OSU) has developed an iron oxide-based syngas chemical looping (SCL) process to produce H_2 from coal-derived syngas since the 2000s [12, 35, 70–77]. The reducer and the oxidizer adopt a moving bed reactor design with gas–solid countercurrent flow pattern, which is helpful for simultaneously and separately obtaining high purity CO_2 and H_2. A 250 kW_{th} high-pressure SCL pilot unit has been demonstrated at the National Carbon Capture Center of the United States [34]. In the past decade, a shale gas to syngas (STS) process has also been developed at bench and sub-pilot scales [5, 33, 37, 78]. A moving bed reducer design with a gas–solid cocurrent flow pattern is adopted for controlling the conversions of iron titanium composite metal oxides (ITCMO) for high CH_4 conversion and high syngas selectivity. These recent works are driven by the need for clean and efficient schemes for carbonaceous fuel conversion. A few studies have reviewed the recent development of CLR processes [79, 80], solely emphasizing either oxygen carriers or process design. Nevertheless, oxygen carriers, reactor design and feedstocks all play an essential role in understanding and prompting the application of CLR. This review intends to provide an overview of the research and development of the CLR process. Specifically, the process fundamentals are reviewed, and the integral approach for the iron oxide based CLR process development is illustrated, showing that the design and compatibility of oxygen carriers and reactor systems are critical for CLR performance. We also update the state of the art and new areas of CLR, with a comprehensive review on the problems and guidelines for the design and development of both oxygen carriers and CLR reactor systems.

2 Process fundamentals

2.1 Basic schemes of chemical looping reforming

To date, various CLR processes have been developed with different feedstocks (e.g., natural gas, oil and ethanol) and oxygen carriers (e.g., Ni, Cu, Mn, and Fe oxides) [81–83]. Figure 3 illustrates the basic schemes applied for these CLR processes. The corresponding overall reaction is also shown under each scheme, with red and blue colors representing exothermic and endothermic reactions, respectively. Figure 3a shows the most commonly applied autothermal CLR

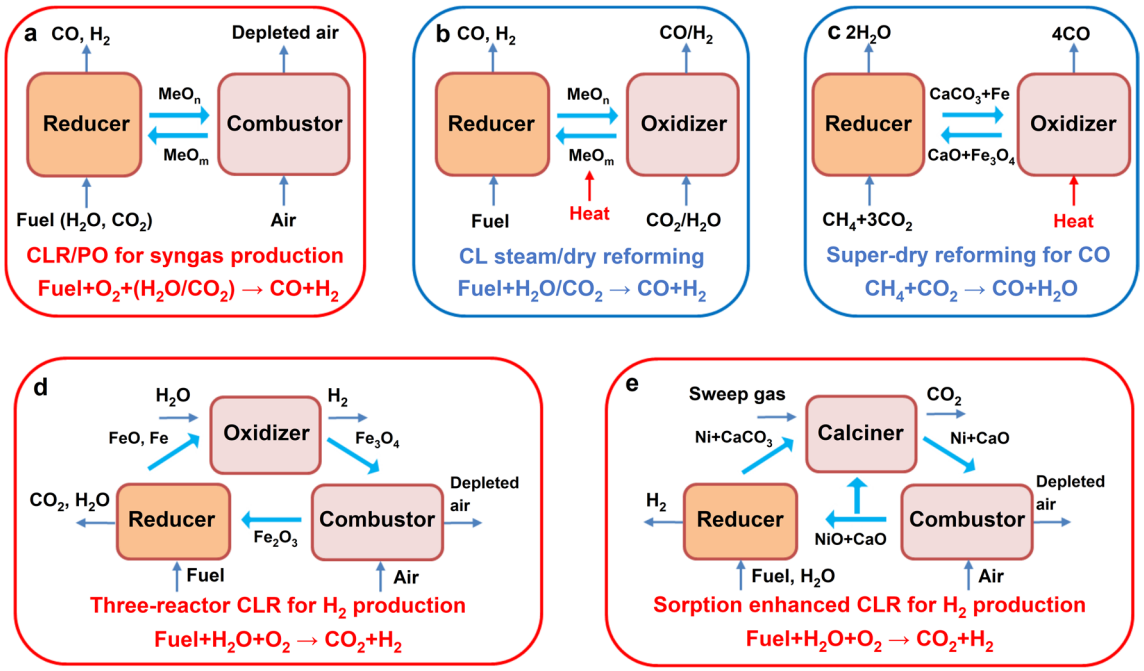

Fig. 3 Basic schemes of chemical looping reforming

scheme in previous studies. Such a scheme decouples the overall reaction of POX or ATR in two reactors. In the reducer, carbonaceous fuel reacts with oxygen carriers forming syngas, and H_2O and/or CO_2 can be introduced to assist the fluidization and reaction as well as adjust the H_2:CO ratio. The reduced oxygen carriers are then regenerated in the combustor with air while releasing heat for autothermal operation.

Different types of metal oxides have been investigated under this scheme for CH_4 conversion. Zafar et al. [83] studied the use of SiO_2-supported Ni, Cu, Mn, and Fe oxides as both reforming catalysts and oxidizing agents. They found that NiO/SiO_2 was the best candidate with high reduction reactivity and high H_2 selectivity. However, the reaction rate decreased as a function of cycle due to the formation of irreversible metal silicates, which do not react at a sufficient rate. Different supports and additive materials have been explored to increase the performance of Ni-based oxygen carriers [84]. Ryden et al. [85] synthesized NiO with $MgAl_2O_4$ support and conducted tests in a laboratory reactor consisting of two interconnected fluidized beds. The results showed that $NiO/MgAl_2O_4$ had good stability and high reactivity for complete CH_4 conversion and high syngas selectivity, and coke deposition could be reduced or eliminated by 25 vol% steam to methane. He et al. [86] added Fe, Cu and Mn oxides to CeO_2-based oxygen carriers and showed that the CLR reactivity could be improved with these transition-metal oxides (especially iron oxides) at >800 °C. However, the fundamental causes of these promotion effects are still unclear.

In addition to CH_4, the autothermal CLR scheme has been applied for the conversion of other gas or liquid fuels, such as bio oil [87] and ethanol [82]. Dupont et al. [82] studied the CLR of waste cooking oil for H_2 production in a fixed bed reactor with NiO/Al_2O_3 oxygen carriers. With a high steam-to-carbon molar ratio (S:C) of 4 and a WHSV of 2.64 h^{-1}, both high fuel and steam conversions could be achieved under a few redox cycles between 600 and 700 °C. Wang et al. [81] investigated the thermodynamic and experimental aspects on CLR of ethanol using a Cu-based oxygen carrier and showed that a H_2 yield of 2.25 mol per mole of ethanol was achieved at 700 °C and a CuO to ethanol molar ratio of 1. Dou et al. [88–92] conducted a series of studies on the CLR of ethanol and glycerol in fixed-bed and moving bed reactors using various Ni-based oxygen carriers between 500 and 650 °C. The results show that the confinement effect by nanostructures could maintain the particle size of Ni-based oxygen carriers and promote their reducibility and reactivity in the CLR process. Recently, Sun et al. [93] prepared Cu_2O–$Ca_2Fe_2O_5$ oxygen carriers for chemical looping oxidative steam reforming of methanol and realized a high methanol conversion with 40% Cu_2O sample at 240 °C, due to the suitable catalytic activity and lattice oxygen migration performance. Compared with CH_4 conversion, the autothermal CLR conversion of these biomass-derived liquid fuels can be conducted at lower

temperatures, which reduces the difficulties in maintaining the physical and chemical properties of oxygen carriers and engineering the associated reactor system.

Figure 3b and c show the endothermic CLR schemes without oxygen/air feeding. Both schemes require specific considerations of reactor design with external heating. Flue gas containing CO_2 could be generated during the external heating provided with carbonaceous fuel combustion, which defeats the purpose of using the chemical looping concept. Such a dilemma could be avoided by using renewable sources such as biomass and solar energy instead. Furthermore, oxygen carriers that cannot be regenerated by H_2O and CO_2 are excluded from the endothermic schemes. Specifically, Ni- and Cu-based oxygen carriers that have been widely applied in the first autothermal CLR scheme cannot be used, however, metallic Ni and Cu can still be incorporated, serving as reforming catalysts in endothermic CLR schemes.

The CLR scheme shown in Fig. 3b can be considered as a spinoff of the thermochemical splitting of water and/or carbon dioxide processes, which started around the 1980s [25, 26, 94]. The original thermochemical redox process consists of high-temperature (> 1300 °C) decomposition of metal oxides releasing O_2 and low-temperature (< 700 °C) reoxidation with CO_2/H_2O forming CO/H_2. The temperature difference between the two steps is too high to carry out the redox cycles in a practical reactor system with sustained oxygen carriers. With the introduction of carbonaceous fuel in the reducer, as shown in Fig. 3b, the reduction temperature could be lowered below 900 °C, and useful syngas could be obtained at the same time. Li et al. [32, 95, 96] developed a series of perovskite structured oxygen carriers for hybrid water splitting and syngas generation. They rationally optimized the thermodynamic properties of perovskite oxides, including oxygen partial pressure and oxygen vacancy formation energy (E_{vac}), with the assistance of Ellingham diagrams and density functional theory (DFT) calculations. Experimental studies validated that these perovskite-based oxygen carriers could reach up to 90% selectivity for syngas and H_2 in the reducer and oxidizer, respectively. Li and Zhu found that Fe–Ce mixed oxides had excellent redox performance in methane reforming and water splitting and provided fundamental insights into the redox reaction mechanism and morphology migration of oxygen carriers [97–99]. They recently proposed a chemical looping scheme for co-splitting of H_2O and CO_2 with CeO_2–$LaFeO_3$ oxygen carriers, which is efficient and flexible in syngas composition adjustment for various chemical and fuel synthesis [100].

Figure 3c reproduces Galvita and Marin's super-dry reforming process for producing high purity CO from greenhouse gases CH_4 and CO_2 [101]. In addition to using iron oxide as an oxygen carrier, this scheme also adopted nickel as a reforming catalyst and calcium oxide as a CO_2 sorbent. In the reducer, methane dry reforming is carried out over the Ni catalyst, while the resulting syngas is oxidized by Fe_3O_4 to CO_2 and H_2O. Under the reducer temperature, CO_2 is in situ captured by CaO, further enhancing the previous two reactions and finally leaving H_2O as the only effluent gas from the reducer. At the same time, the looping particles change from a mixture of Ni, CaO and Fe_3O_4 to that of Ni, $CaCO_3$ and Fe in the reducer. In the oxidizer, external heating is provided to decompose $CaCO_3$ into CaO and CO_2, and the latter subsequently reoxidizes Fe back to Fe_3O_4. The super-dry reforming scheme can achieve a CO yield of 45% higher than that of the traditional approach, which offers an alternative pathway for efficient CO_2 and CH_4 utilization.

Figure 3d and e show three-reactor CLR schemes for H_2 production, where the overall reactions are the same as the autothermal reforming process. Both schemes share similar reactor configurations and produce three hot gas streams containing concentrated CO_2, high purity H_2 and high-temperature flue gas separately. Such scheme integrates CLC to provide heat for CLR or sorption-enhanced reforming (SER), thus avoiding the external heating needed in the endothermic reforming schemes in Fig. 3b and c. The redox pairs of Fe_2O_3–Fe_3O_4 and NiO–Ni are used for CLC to generate heat, while the pairs of Fe_3O_4–FeO/Fe and CaO–$CaCO_3$ are adopted for CLR and SER, respectively, for H_2 production. More steam usage could cause the overall reaction endothermic compromising the autothermal operation, while more oxygen usage could generate excess heat, sacrificing the H_2 yield. Based on the heat of combustions and reforming reactions and thermodynamic equilibrium, the minimal oxygen and steam usage could be estimated for the design and optimization of three-reactor CLR reactor systems.

The iron-based three-reactor CLR scheme shown in Fig. 3d specifically represents the SCL process developed by Fan, which can coproduce H_2 and electricity with high efficiency. In the reducer, iron-based oxygen carriers are used to fully convert syngas or natural gas into H_2O and CO_2, and Fe_2O_3 is reduced to a mixture of Fe and FeO at approximately 900 °C. The oxidizer operates below 800 °C to conduct steam-iron reaction to produce high purity H_2 and reoxidize the reduced iron to Fe_3O_4. The combustor then completely regenerates Fe_2O_3 oxygen carriers and provides heat for autothermal operation. From the iron-based three-reactor CLR scheme, three hot gas streams are produced: a concentrated H_2O/CO_2 stream from the reducer, a H_2O/H_2 stream from the oxidizer and the flue gas stream from the combustor. The flue gas could be sent to an expander to recover the high-grade heat, and the exhausted gas, together with the other two streams, is routed to the heat recovery and steam generation section. After condensing out the steam, high purity CO_2

and H_2 streams can be obtained separately. The SCL process is more efficient than the conventional process due to its efficient energy management and integrated CO_2 separation scheme.

Figure 3e shows the scheme of sorption-enhanced chemical looping reforming (SECLR), which is the combination of SER and CLC. SER for H_2 production can be accomplished by the addition of CO_2 sorbent (e.g., CaO) for in situ CO_2 removal and thus driving the steam reforming and WGS reaction equilibrium towards H_2-rich products, while CLC can be achieved by the addition of oxygen carriers (e.g., NiO) to provide lattice oxygen and catalytic sites (reduced Ni) for fuel reforming. Calcium carbonate can be separately calcined to yield a pure CO_2 stream for its subsequent sequestration, and the calcium-based sorbent can be regenerated and recycled back. The nickel-based oxygen carrier can be regenerated with air to provide heat for the reforming reaction as well as the calcination reaction. By applying this scheme, higher H_2 yield and purity can be directly obtained with in situ CO_2 capture using reusable sorbents and metal oxides without additional gas–gas separation units.

Dupont et al. [102] The results showed that > 95% purity of H_2 was produced at 600 °C and 1 atm. Zeng et al. [103] conducted SE-CLR of ethanol with Ni-based catalyst and CaO sorbent and studied the NiO loading as well as reaction conditions of the reforming reactor. Increasing NiO loadings could lead to higher catalytic activity as it provided more active surface sites to accelerate intermediates to H_2 and CO. The highest ethanol conversion and H_2 selectivity were obtained at 650 ℃ with 20% loading of NiO, achieving a conversion of 98% and H_2 selectivity of 93%. Dou et al. [92] revealed that high purity H_2 production from glycerol could be achieved via SECLR using a continuous dual moving-bed reactor over NiO/$NiAl_2O_4$ oxygen carriers and lime-based sorbent. Hafizi et al. [104] investigated the performance of Fe-Ce-based oxygen carriers and CaO-based sorbents on the SECLR of CH_4 using a fixed-bed reactor. The results showed that H_2 purity of 89% could be obtained at 600 °C, S:C ratio of 1.5 and sorbent to oxygen carrier mass ratio of 3. Recently, they applied Co_3O_4/SiO_2 oxygen carrier and a cerium-promoted calcium-based sorbent in the SECLR process, and showed that up to 95% H_2 purity could be achieved at 550 °C, which is comparable to 84% in the CLR process [105]. Also, formic acid was realized as a prospective hydrogen carrier, and a sodium looping-based formic acid reforming was proposed and simulated for high-purity H_2 production. Conditions, i.e., temperature, pressure, and ratio of H_2O/HCOOH as well as Na_2CO_3/HCOOH, for three reactors were optimized to promote H_2 production and CO_2 absorption. Results showed a high H_2 production rate with a high purity of 97.9% and an ultra-low CO concentration of 11.97 ppm [106]. The continuous operation of all three reactors, however, has not yet been demonstrated in the SECLR process. With three interconnected fluidized bed reactors simultaneously exchanging a mixture of two looping particles, i.e., the CO_2 sorbent and the oxygen carrier, the operation and control requires a systematic approach. Issues that need to be further addressed include the simultaneous handling of mixed sorbent and oxygen carrier, sorbent and oxygen carrier reactivity and recyclability, heat transfer and solid/gas leakage among the reactors.

2.2 Product selectivity: stoichiometry, thermodynamics and kinetics

The product selectivity, i.e., the concentration and ratio of H_2 and CO in the syngas, in a CLR process could be affected by many factors, including reaction stoichiometry, thermodynamic equilibrium, surface reaction path and reactor system configuration. The reactor system configuration has been briefly discussed in the previous section. For example, the three-reactor CLR system could be designed to directly produce both H_2 and CO_2 in high purity from separate reactors, as shown in Fig. 3d and e. Amini et al. [80] have recently reviewed the effect of pressure in chemical looping system, concluding that high pressure is beneficial for the reaction kinetics and hydrogen production process. More review and discussion on the effect of reactor system configuration are addressed in Sect. 2.3.

The overall reaction stoichiometry determines the syngas selectivity and H_2:CO ratio based on the fuel and oxidant input. Based on Eqs. 1, 2 and 4, the theoretical H_2:CO ratios in the syngas from steam reforming, dry reforming and partial oxidation of methane are 3:1, 1:1 and 2:1, respectively. The contents of C, H, and O elements in other carbonaceous fuels, such as biomass-derived oil and alcohols, could vary to certain extents. Accordingly, the syngas composition could be adjusted for different downstream applications by varying the stoichiometric ratios of different feedstocks introduced to the CLR system. As discussed in the previous section, the stoichiometric ratio also determines the heat of the overall reaction based on the first law of thermodynamics.

As a chemical looping process consists of cyclic gas–solid reactions, successful operation relies on the performance of the oxygen carriers. In a typical chemical looping scheme, the overall reaction can be regarded as combustion and partial oxidation/reforming of the fuels, which requires distinct oxygen carrier properties so that the product selectivity can be properly controlled. For example, with a substoichiometric ratio of available lattice oxygen to fuel, partial oxidation of hydrocarbons for syngas production could be performed by metal oxides such as NiO and CuO. However, the resulting

syngas concentration is highly dependent on the oxygen-to-fuel ratio in this case. The second law of thermodynamics suggests that the reaction equilibrium could vary significantly with different oxygen carriers and operation conditions. The performance of oxygen carriers, typically metal oxides, can be estimated based on their equilibrium oxygen potential at high temperatures. The oxygen potential of various metal oxides could be studied and categorized with ease via the Ellingham diagram or the oxygen partial pressure diagram, as shown in Fig. 4 [107]. The corresponding oxygen partial pressure for combustion and reforming/gasification of representative fuels such as CH_4, C, CO and H_2 are also included. The active metal oxides could be sorted into the following groups.

The combustion or CLC group, including the oxides of manganese, iron, copper, etc., is located at the top pink zone of Fig. 4, where metal oxides have strong oxidizing capability. These metal oxides could be used as active components in oxygen carriers for complete fuel oxidation to CO_2 and/or H_2O in CLC processes, as their oxygen partial pressures are above the lines of CO and H_2 combustion. Molecular oxygen could be directly generated by exposing metal oxides such as Mn_2O_3, Co_3O_4 and CuO at high temperatures where their decomposition oxygen partial pressure could exceed 0.01 bar, which could facilitate the conversion of solid fuels in the so-called chemical looping with oxygen uncoupling (CLOU) process [108]. In contrast, the lines of $CaSO_4$, NiO and CoO are near the bottom of this zone, indicating that there is a small portion of uncovered fuel present in the reduction step. In general, the oxygen carriers in this group are mostly studied for CO_2 capture-oriented CLC processes.

The CLR group is in the blue zone located below the CLC group and above the line of CO formation. Thus, metal oxides in this region are able to gasify carbon to CO but cannot further oxidize CO and H_2 due to their moderate oxidizing capability. As a result, metal oxides in this group can be used for syngas production from various carbonaceous fuels. The advantage of using metal oxides in the CLR group is that they can thermodynamically ensure the stable production of high purity syngas while minimizing carbon deposition [33]. The inset of Fig. 4 also lists a subgroup of metal oxides suitable for CO and H_2 production when their reduced form interacts with steam, including FeO, Fe_3O_4, WO_2, WO_3 and MoO_2. These metal oxides are in the vicinity of the line of CO/H_2 combustion, which is thermodynamically feasible for both their reduction by CO/H_2-rich gas and reoxidation by CO_2/H_2O. It is noted that iron oxides have a series of oxidation states with both high and intermediate oxidizing capabilities, including Fe_2O_3, Fe_3O_4 and FeO, making them suitable for both CLC and CLR applications.

The third group is located at the bottom zone of Fig. 4, where the metal oxides have limited or no oxidation capability. This group is able to partially or selectively oxidize hydrocarbons. However, coke deposition or incomplete fuel conversion is inevitable. Metal oxides in this group can also be used as support materials such as TiO_2, SiO_2 and Al_2O_3. Under reaction conditions, the support could interact with the abovementioned active metal oxides in many ways. For example, iron oxides can also react with TiO_2, SiO_2 and Al_2O_3, forming $FeTiO_3$, $FeSiO_3$ and $FeAl_2O_4$, which could alter their thermodynamic and kinetic properties during chemical looping applications. Specifically, ITCMO oxygen carriers have been selected to improve the syngas selectivity and yield with minimal carbon deposition based on the following thermodynamic analysis [33].

The ratio of reducible oxygen provided by the metal oxides to CH_4 ([O]:CH_4) significantly affects the syngas composition and the possibility of carbon formation. As shown in Fig. 5, for both iron oxides and ITCMOs, when this ratio is lower than 1, a substoichiometric amount of oxygen is provided, which results in possible carbon deposition, carbide formation,

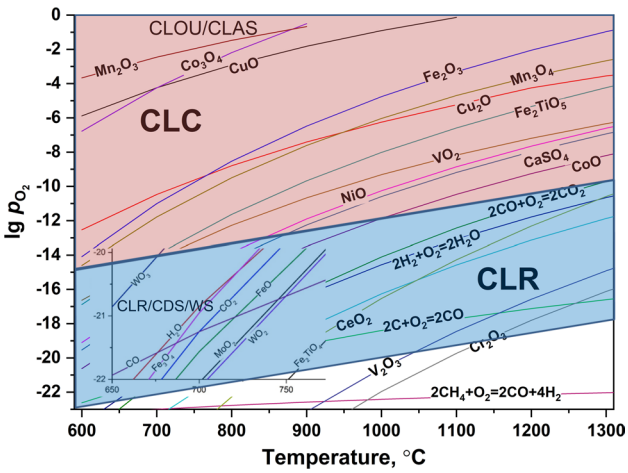

Fig. 4 Equilibrium oxygen partial pressure of metal oxides at various temperatures

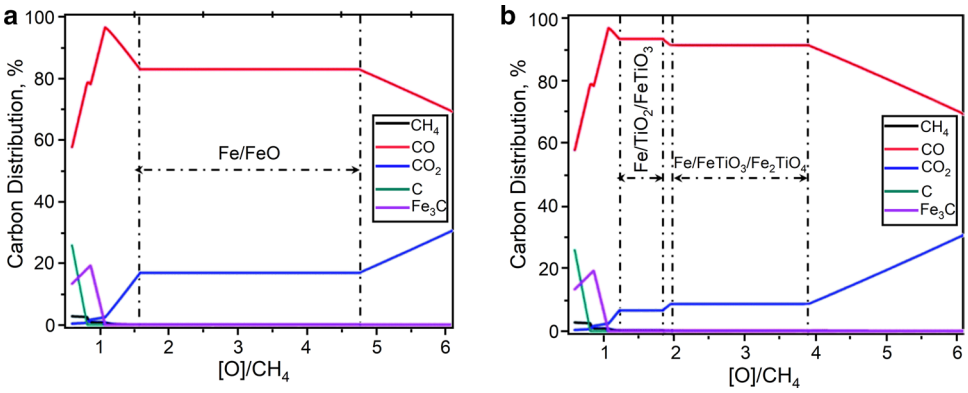

Fig. 5 Carbon distribution with various [O]:CH_4 ratio at 900 °C, 1 bar. **a** Fe_2O_3/Fe, **b** Fe_2TiO_5-Fe/Fe_2TiO_4/$FeTiO_3$. Reproduced from ref. [33] with permission from the Royal Society of Chemistry, copyright 2014

and/or unconverted CH_4 leakage. When the [O]:CH_4 ratio is higher than 1, most of the carbon is converted to either CO or CO_2. Figure 5a shows that iron oxide can achieve a low CO_2 selectivity (< 15%) when the [O]:CH_4 ratio is below 1.5. Under such conditions, however, metallic iron is the only reduced solid product and can catalytically decompose CH_4, causing carbon deposition. Carbon deposition/formation may be avoided by reducing the extent of metal oxide reduction by increasing the [O]:CH_4 ratio. Conversely, increasing this ratio results in an increase in CO_2 and H_2O levels to more than 30 mol%, lowering the syngas selectivity and yield. Thus, the use of single metal oxide material poses challenges in syngas quality control.

The ITCMO oxygen carriers possess a better equilibrium property toward syngas generation. With proper iron oxide and titanium oxide ratio, the effective reduced compounds can be $FeTiO_3$ and/or Fe_2TiO_4. As shown in Fig. 5b, ITCMO with a Fe to Ti ratio of 2 can partially oxidize CH_4 to syngas with minimal byproducts such as C, CH_4, CO_2 and H_2O. Unlike single metal oxide materials such as FeO, the syngas composition produced using ITCMO is very stable and of high concentration (> 90% CO selectivity) when the [O]:CH_4 ratio varies in a wide range between 1.5 and 4. Without any steam injection, the CH_4 reaction with ITCMO can produce syngas at a H_2:CO ratio slightly below 2. The H_2:CO ratio can be improved to 2 by introducing steam at 10% of the CH_4 molar flow. In the conventional autothermal reforming process, a steam-to-methane ratio of more than 20% is required to obtain a similar syngas composition. Thus, the ITCMO is promising for high-efficiency, high-quality syngas production.

In summary, the diagram of equilibrium oxygen partial pressure can guide the selection of active components and estimate the syngas selectivity preliminarily in CLR system. Nevertheless, the syngas selectivity could be also affected by the selection of supporter, ionic diffusion and catalytic kinetics, which will be further reviewed and discussed in Sect. 3.

2.3 Reactor system design

The reactor system design plays a critical role in determining the chemical looping process performance. It has been widely recognized that the combustor or air reactor should be operated in a fluidized bed mode for better heat and mass transfer, and the associated reactions are intrinsically fast and are thermodynamically favored. However, unlike the oxidation reaction in the combustor, the reactions with carbonaceous fuel in the reducer are complicated and could be limited by thermodynamic equilibrium and be relatively slow. It is therefore necessary to study the gas–solid contacting pattern and to optimize the reducer design, targeting high reliability and low capital-intensity while maximizing solid and gas conversions.

Based on the feeding mode, chemical looping reactor systems can be categorized into batch reactor system with gas-switching mechanical valves and circulating bed system with continuous gas and solid flow. A variety of reactor designs with different Geldart particle grouping and solid flow behaviors have been developed, including fixed bed, moving bed, and fluidized bed [12, 16, 109]. Among these reactors, the fixed bed reactor is simple in its design, and poses the least requirements on the mechanical strength of oxygen carrier particles. Thus, fixed bed has been widely used in lab-scale tests and was first commercialized in the Lane process for H_2 production [42]. However, fixed bed reactors can only handle gaseous fuel and require frequent gas switching at high temperatures, which is not suitable for large-scale operation. In addition, the poor heat transfer between gas and solids in the fixed bed reactor could cause hot spots that further lead to sintering and deactivation of oxygen carriers. To solve these problems, researchers have developed alternative reactor systems for continuous chemical looping operation. Figure 6 shows three major types of gas–solid contacting patterns for chemical looping reactors, which include mixed flow, countercurrent flow, and cocurrent flow. The mixed flow pattern mainly occurs

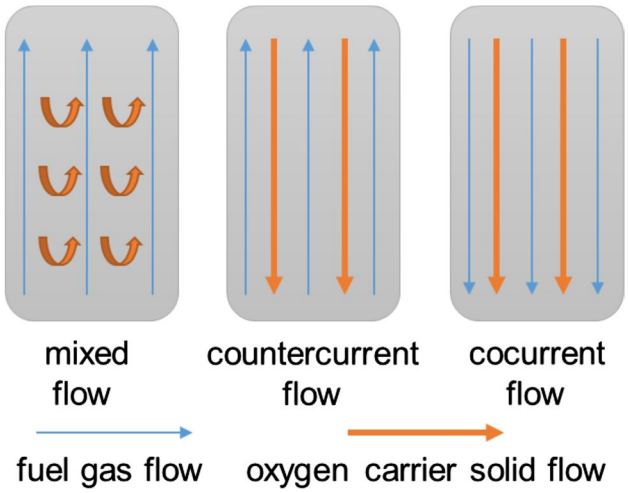

Fig. 6 Gas solid flow patterns in chemical looping reactor system

in the single-stage fluidized bed reactor, while the countercurrent and cocurrent flow patterns could be achieved in a moving bed or a series of interconnected fluidized bed system.

To date, various fluidized bed configurations, such as bubbling-, turbulent- and spout-fluidized bed operations, have been applied to provide good mixing characteristics and uniform heat transfer in CLC applications. However, back mixing and channelling in a fluidized bed usually results in poor fuel conversion and low product purity, and the separation among oxygen carriers, solid fuel and ash remain a major challenge. These aspects are closely related to the reaction kinetics between carbonaceous fuels and oxygen carriers as well as the design and operation of chemical looping reactors. Song and Shen reviewed the solid fueled CLC reactor system, and suggested proper design of the feeding position and bed internals to address operational problems [16]. Zhao et al. [109] recently updated their progress in chemical looping process development, and emphasized the importance of numerical simulation in the design, optimization, and scale-up of fluidized bed reactors. In the following, the fundamental and design of two iron-based CLR moving bed reactor system, i.e., the STS process and the SCL process, are discussed.

The STS process produces syngas from shale gas via the redox cycle of ITCMO oxygen carriers discussed in the previous section. To make full use of the thermodynamic properties of ITCMO oxygen carriers, a cocurrent moving bed reducer design is adopted [33]. The cocurrent gas–solid contact configuration controls the proper redox time and the extent of the oxygen carrier conversion while preventing carbon deposition. At the inlet of the reactor, the concentrated fuel source reacts with Fe_2TiO_5/Fe_3O_4, which is highly oxidative and unlikely to catalyze carbon deposition. At the outlet of the reactor, although reduced oxygen carriers contain metallic Fe, the atmosphere of diluted fuel and the lattice oxygen in $Fe_2TiO_4/FeTiO_3$ could help prevent carbon deposition. The reduced ITCMO consisting of Fe and $Fe_2TiO_4/FeTiO_3$ yields a corresponding thermodynamically high syngas purity with a H_2:CO ratio of ~2:1. The cocurrent moving bed reducer is advantageous over a fluidized bed reducer in that the moving bed reducer does not suffer a reduced shale gas conversion and/or undesirable syngas composition due to gas channelling and back mixing of particles with different oxidation states, which are unavoidable in a fluidized bed reactor. A set of experiments was conducted to characterize the ITCMO performance and validate the cocurrent moving bed concept [33].

The SCL scheme is shown in Fig. 3d, in which high syngas conversion and high steam-to-hydrogen conversion are two of the most important criteria for evaluation. In a fluidized-bed reactor such as a dense-phase fluidized bed, significant gas and solid mixing occurs. Thus, in a fluidized-bed reducer, the fresh syngas feedstock is diluted by the gaseous product, which is rich in H_2O and CO_2. Table 2 lists the equilibrium compositions between FeO_x and $CO/CO_2/H_2/H_2O$ at 850 °C, indicating that the dilution of the syngas by CO_2 and H_2O decreases the reducing capability of the syngas. For example, in order to achieve 100% conversion of syngas, iron oxides cannot be reduced to an oxidation state lower than Fe_3O_4. This indicates that the

Table 2 Equilibrium gas compositions with different oxidization states of iron at 850 °C

Redox pair	CO_2/H_2O	CO/H_2
Fe_2O_3/Fe_3O_4	99.9955%/99.995%	45 ppmv/50 ppmv
Fe_3O_4/FeO	80.3%/78.0%	19.7%/22.0%
FeO/Fe	38.0%/34.8%	62.0%/65.2%

Fe_2O_3 conversion cannot be higher than 11% with 100% syngas conversation in a fluidized bed reducer. Therefore, the gas and solid conversions in the fluidized-bed reducer are constrained.

Contrary to the fluidized bed reactor, a moving bed reactor has minimal axial mixing between the gas and solid phases. The SCL process uses a moving bed reactor with a countercurrent gas–solid contacting pattern for the reducer design. Based on the thermodynamic data shown in Table 2, at the bottom of the moving bed reducer, a fresh syngas feed with high H_2 and CO concentrations could react with iron at lower oxidation states. Meanwhile, the partially converted syngas with low H_2 and CO concentrations flows upward to meet iron at higher oxidation states. A multistage equilibrium model has been developed for the countercurrent moving bed reactor, which predicts that 100% syngas could be converted and Fe_2O_3 could be reduced by ~50% to a mixture of Fe and FeO [74]. Thermodynamic analysis has attempted to provide insight into the operational conditions of the SCL system using a moving bed reducer. The theoretical results confirm that the gas–solid countercurrent moving bed reducer with iron oxide oxygen carriers can achieve high fuel conversions to CO_2 and H_2O with a minimal solid circulation rate, is resistant to carbide and sulfide contamination, and has the capability of producing high purity H_2.

Furthermore, a one-dimensional dynamic model was developed to simulate the moving bed reducer in the SCL process [70, 110]. As shown in Fig. 7a, the bench-scale experimental data validated both the multistage equilibrium model and the 1-D dynamic model [70]. Both experimental and modeling results show that the gas and solid conversion profiles have opposite trends because of the countercurrent contact pattern. Under the current operating conditions and reducer design, an individual particle quickly completes the reduction from Fe_2O_3 to Fe_3O_4 and then to FeO at the top. The reduction from FeO to Fe is then limited by thermodynamic equilibrium before the gas profile is changed at the bottom, where fresh syngas is introduced. The steady-state simulation results with different reducer heights are shown in Fig. 7b. The results suggest that there is a minimal height to achieve the same reducer performance. In summary, the 1-D moving-bed reactor model provides insights into optimizing the countercurrent moving bed reducer design and operation.

The above examples illustrate the integral approach for the iron oxide based circulating moving bed CLR process development. Adanez et al. [2] have reviewed the progress in chemical looping combustion and reforming technologies, including various reactor and process development up to 2010. Most existing CLR processes proposed dual fluidized bed reactor design for high temperature natural gas reforming applications. In recent years, gas-switching concept was also studied to avoid solids attrition and circulation problems in the scale-up process [80]. Such system requires high temperature mechanical valves, which is practical for temperatures below 600 °C and could be applied for the CLR of oxygenated fuels including methanol [111, 112], ethanol [113, 114], etc. Various reactor configurations and associated experimental results are out of the scope of this review, and related discussion could be found from recent reviews [16, 80, 109].

In summary, the basic schemes and process fundamentals of the CLR system are discussed. The reaction stoichiometry, thermodynamic equilibrium, and reactor system configuration are all factors that could affect the gas product yield, and

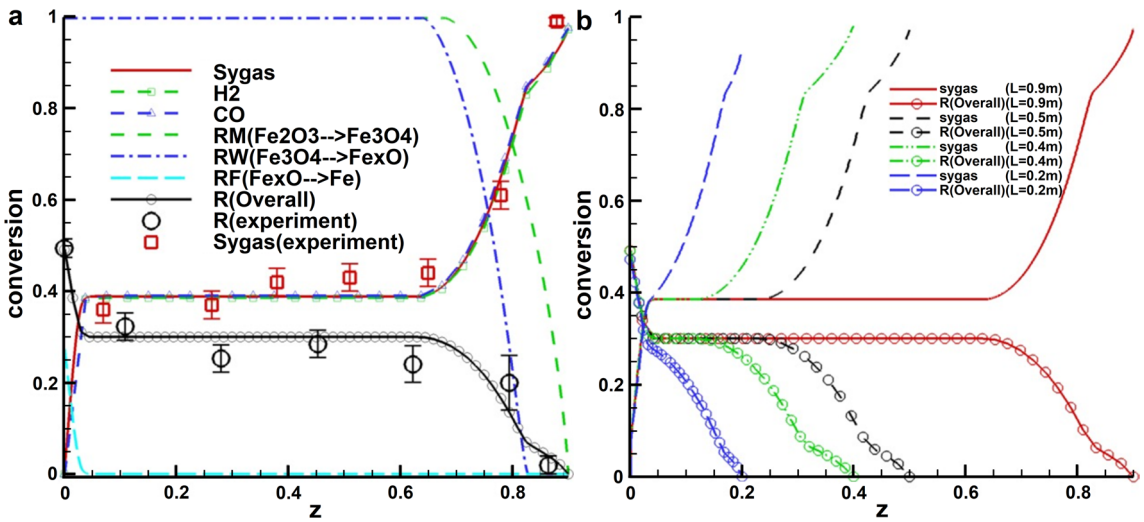

Fig. 7 1-D SCL reducer modelling **a** comparison of the gas and solid conversions between the numerical results and the experimental data in the moving bed reducer; **b** steady overall conversion profiles of syngas and solids when the reducer is shortened. Reproduced from ref. [70] with permission from John Wiley and Sons, copyright 2013

selectivity in the CLR. Besides, the gas–solid contacting pattern should be carefully considered and selected for specific CLR applications.

3 Oxygen carrier design

3.1 Reaction principle

The reduction and oxidation of oxygen carriers generally involve the generation and recombination of oxygen ions and vacancies, their diffusion in the bulk phase, and their reaction with adsorbed species on the surface. Transition metal oxides such as NiO and CuO have been widely studied as oxygen carriers, and the reduced metals are also effective catalysts for the conventional reforming processes of various fuels. For example, methane and ethanol reforming could be catalysed by metallic Ni at 700–900 °C and 400–600 °C, respectively, while methanol can allow the reforming process to operate at a relatively lower temperature around 100–300 °C with Cu catalyst. Suitable oxygen carriers would employ active metal for its high reactivity and temperature compatibility with corresponding fuels.

Figure 8 schematically shows the reaction principle of oxygen carriers under a reducing environment. In the first step, the metal–oxygen bonds in oxygen carriers are activated by absorbing thermal energy at high temperatures, resulting in oxygen ions and vacancies as well as electron–hole pairs. This relates to the thermodynamic property or oxygen potential of the metal oxides, as discussed in the previous section. Metal oxides in the CLC and CLR groups of Fig. 4 are the active oxygen carrier components, and their oxidizing capability could determine the fuel conversion and product selectivity. Foreign metals could be used to modify the thermodynamic properties and facilitate redox reactions at low temperatures. The screening and discovery process could be accelerated with computational chemistry methods and high-performance computing systems. For example, Li et al. [96] rationally designed $BaMn_xFe_{1-x}O_{3-\delta}$ oxygen carriers and optimized their redox thermodynamic properties, including equilibrium oxygen partial pressure and E_{vac}, with the assistance of DFT calculations and Ellingham diagrams. The experimental results showed that up to 90% selectivity of syngas and H_2 could be achieved in the reducer and oxidizer, respectively, indicating that $BaMn_xFe_{1-x}O_{3-\delta}$ oxygen carriers are promising for efficient solar-driven CLR process.

In the reducing environment caused by the fuel, the activated oxygen anions diffuse from the bulk phase to the surface under the oxygen chemical potential gradient. At the same time, electrons flow inward to maintain the overall charge neutrality. The ionic diffusion in the bulk phase determines the release and replenishment rate of lattice oxygen. Most oxygen carriers revolve around only a few crystal structure types, such as fluorite and perovskite. In perovskite oxides with more open oxygen sublattices, oxygen vacancies can be created more easily than cation defects. Consequently, perovskite oxides show high lattice oxygen diffusivities, which is suitable for various CLR processes [32, 95, 115–122]. Metal oxides with fluorite structure such as CeO_2 have predominantly oxygen anion defects occupying interstitial sites. The removal of lattice oxygen atoms on ceria could lead to the formation of several phases of the type CeO_{2-x} with a range of possible compositions ($0 \le x \le 0.5$). This feature can be used to form solid solutions with oxygen vacancies by substituting aliovalent ions of the host structure with a higher charge than that of the replacing cation, and has been applied in oxygen carrier development for CLR applications [25, 123, 124]. Thus, specific crystal structure and bulk doping can be used to improve the ionic diffusion rates.

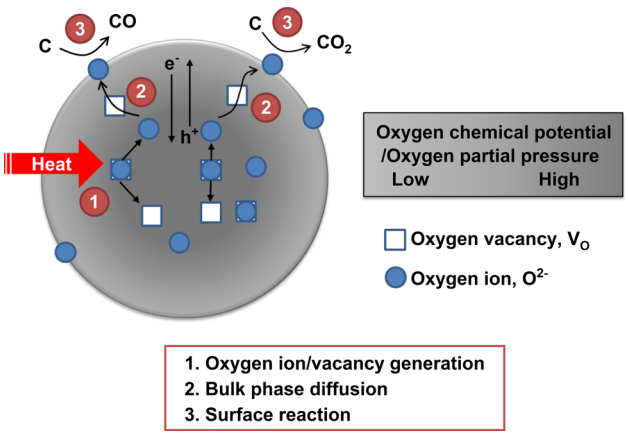

Fig. 8 Reaction principle of oxygen carriers under reducing environment

Surface reactions take place between the adsorbed fuel species and oxygen species diffused from the bulk phase. Catalytic sites could be formed during the reduction of the oxygen carriers or specifically introduced to the surface to promote the reaction kinetics. Fuel conversion and syngas selectivity in the CLR reducer could be improved by controlling the distribution of oxygen supply from the bulk as well as the types of active oxygen species on the surface. It is noted that coke deposition frequently occurs in the reforming process, and if the oxygen supply from the bulk is inadequate, coke could be accumulated on the surface of oxygen carriers and lead to deactivation. While lattice oxygen atoms participate in the oxidation of carbonaceous feedstock, they do not necessarily result in high product selectivity. The selectivity is based on the bond strength between the metal atom and the lattice oxygen atom on the surface. If the metal–oxygen bond is too weak, lattice oxygen can be easily released so that the reactant adsorbed on the surface may be fully oxidized to yield CO_2 and H_2O. If the metal–oxygen bond is too strong, lattice oxygen atoms cannot be released, which could result in a low reactivity. Ideal oxygen carriers with readily mobile lattice oxygen and suitable metal–oxygen bond strength have the potential to be both selective and reactive.

3.2 Effects of the promoters

The CLR process requires oxygen carriers to exhibit both high fuel conversion and high syngas reactivity, along with low cost and high stability at high temperatures. Extensive efforts have been devoted to catalytically modifying the surface for performance improvement. Fan et al. [125] studied the idea of using metal oxide dopant at a very low concentration relative to the total metal oxide oxygen carriers (e.g., < 1%) without yielding phase change to reduce the energy barrier of carbonaceous feedstock activation and hence facilitate carbonaceous feedstock conversion. They modified the Fe_2O_3 oxygen carrier using 1% lanthanum dopant and found that it could enhance redox reactivity while maintaining the high oxygen capacity and recyclability of oxygen carriers. The reactivity of La-doped iron oxide oxygen carriers is higher than that of undoped iron oxide oxygen carriers by 220% for CO reduction reactions and 260% for air regeneration reactions. In addition, 1% La dopant led to a 178% increase in reduction reactivity and a 156% increase in reoxidation reactivity for CH_4 reforming reactions compared to undoped iron oxide. The mechanism for La dopant-based reactivity enhancement stems from the capability of La dopant in lowering the barriers of C–O bond and C–H bond activation during metal oxide redox reactions with carbonaceous fuels. Furthermore, they found that the low concentration aliovalent dopant modification can more significantly improve CH_4 conversion on iron oxide oxygen carriers. Fan et al. [126] doped iron-based oxygen carriers with a small amount of cobalt, and the addition of trace amounts of cobalt significantly increased the activity of the oxygen carriers in the 600–800 °C range, which is beneficial for low-temperature applications of iron-based oxygen carriers. The introduction of cobalt can prompt the formation of oxygen vacancies, which affects the energy barrier of CH_4 reforming on the surface of the oxygen carriers.

In addition to modifying the active sites on the surface/interface to improve the reactivity and selectivity, promoters also can be adopted for modifying the bulk phase structure to improve oxygen vacancy formation and ionic conduction. Chen et al. [127] recently demonstrated that tungsten-based oxygen carriers with nickel modification were effective for the CLR of CH_4. Their results indicated that the oxygen availability, CH_4 conversion, and syngas yield could be significantly increased over $Ni_{0.5}WO_x/Al_2O_3$ compared to WO_3/Al_2O_3. Further investigations showed that there is a strong interaction between surface-grafted nickel species and WO_x species, effectively improving CH_4 activation and the surface reforming reaction. At the same time, nickel was incorporated into the bulk structure of WO_3, which weakened the tungsten–oxygen bond strength and increased the availability of lattice oxygen. As a result, the syngas yield was significantly increased by ~2.7-fold in comparison with unmodified WO_3 oxygen carriers. These findings are a pathway to dramatically modify metal oxide properties using relatively simple fabrication processes, and they significantly impact future chemical looping oxygen carrier design.

Even though much effort has been taken into the modification of oxygen carriers by different approaches, there is still a long way to explore the reaction mechanism more explicitly for CLR applications. The reactions with oxygen carriers involve the generation and transfer of different oxygen species from the bulk phase to the surface and variation of these parameters determines the specific reaction pathway on the surface, thus resulting in different products. By modifying the bonding energy between adsorptive intermediates and metal–oxygen bonds, which are significantly dependent on the distribution and diffusion of various oxygen species, the distribution of products can be modulated.

3.3 Oxygen carrier deactivation

The deactivation of oxygen carriers remains the major problem for CLR applications [128]. In general, the deactivation of oxygen carriers in the CLR process can be analyzed from microscopic and macroscopic aspects. At the microscale, the deactivation of the oxygen carrier is mainly caused by the sintering of active components, thermal inactivation, oxygen carrier poisoning due to contaminant mineral matter in the fuel, carbon deposition and lattice oxygen depletion, which leads to changes of the surface and bulk phase of the oxygen carrier. At the macroscale, deactivation mainly includes changes of textural properties and the decline in mechanical strength.

The high temperature of the CLR process could lead to severe surface sintering of the oxygen carrier, especially the supported oxygen carrier. As a result, the crystal grains of the oxygen carrier grow, and the dispersion of the active component on the surface decreases, thus reducing the surface area of the active component [4, 129]. In addition, sintering could increase the oxygen transmission distance inside the oxygen carrier, causing difficulties in lattice oxygen diffusion. Moreover, the number of active sites of the oxygen carrier is also reduced due to the decrease of lattice imperfection during sintering. Therefore, it is crucial to solve the irreversible sintering of the oxygen carrier. At present, the solution to the sintering problem is mainly realized by optimizing the preparation method and adopting the carrier with high specific surface area and excellent pore structure to obtain the oxygen carrier with smaller grain size while inhibiting grain growth in the reaction process [4, 130–132]. At the same time, the addition of structural promoters could also effectively suppress the sintering of the oxygen carrier.

Thermal inactivation is also a major cause of oxygen carrier deactivation. At high temperatures, the components of oxygen carriers undergo solid-phase reactions to produce substances with poor reactivity and low oxygen storage capacity, and oxygen carriers may also undergo phase transition and phase separation. All these factors could cause a decrease of the activity of the oxygen carrier and eventually lead to inactivation. For example, Al_2O_3 support tends to undergo solid-phase reaction with transition metal oxides at high temperatures [133, 134]. Therefore, when Al_2O_3 is used as the support, it is found that the performance of the oxygen carrier decreases with the increasing number of cycles [135, 136]. Most of the literature attributed the decline in activity to the production of aluminate because aluminate has a lower oxygen storage capacity and reactivity. In addition, due to the formation of aluminate, the metal oxide cannot be completely reduced so that the amount of available oxygen is reduced, resulting in the reduction in conversion and syngas yield. To solve this problem, supports with weak interactions between active components such as $MgAl_2O_4$ spinel can be selected, or strong oxidants such as oxygen can be used to fully oxidize aluminate back to its original form [137–140].

When zirconia is used as the support, the phase change during the high-temperature reaction causes cracks in the structure and issues in the mechanical properties [141]. Zirconia can be stabilized by adding additives such as MgO or CeO_2, thereby solving the problems caused by its phase transition [128, 142]. For phase separation, titanium and iron in the ilmenite structure undergo phase separation. As the reaction progresses, iron oxide gradually accumulates on the surface, while titanium dioxide is gradually enriched in the bulk phase, which affects the cycling stability of the oxygen carrier. The introduction of an Al-based skeleton can solve the phase separation problem of ilmenite-based oxygen carriers [143].

Compared to sintering, carbon deposition is a reversible deactivation because carbon deposition can be eliminated to a certain extent in the oxidation stage. In addition, when CO_2 or steam is selected as the oxidant, CO_2 and carbon deposits can be fully utilized to increase the yield of carbon monoxide. The mechanism, pathway, amount, and composition of carbon deposition vary with oxygen carriers and CLR reactions. However, the specific surface area, pore volume and active center of the oxygen carrier could decrease with the increase of carbon deposition and lead to deactivation of the oxygen carrier. The generation of carbon deposition is mainly caused by the acid center and slow oxygen migration rate in the oxygen carrier. Therefore, in addition to reducing the acid center in the oxygen carrier to reduce carbon deposition, the formation of carbon deposition can also be inhibited by accelerating the transfer of lattice oxygen [144, 145]. The addition of a certain amount of additives, such as adding Sr to the A site of the perovskite oxygen carrier to obtain more oxygen vacancies [118, 146], and adding zirconia with a smaller ion radius to cerium oxide to cause lattice distortion [147, 148], can reduce the activation energy of the diffusion of oxygen ions and is beneficial to the migration and diffusion of lattice oxygen. Therefore, the carbon deposits on the surface can be eliminated in time to avoid deactivation of the oxygen carrier. In addition to modifying the oxygen carrier, the production of carbon deposits can also be suppressed by optimizing the reaction conditions. Adding an appropriate amount of steam or CO_2 to the reactants or immediately entering the oxidation stage after the carbon

deposits are generated can avoid carbon deposits or inhibit the deactivation caused by carbon deposits to a certain extent. A suitable operation pressure is also desired to alleviate the carbon deposition as pressure has a great influence on the deactivation of oxygen carriers. High pressure can lead to fast deactivation by accelerating the carbon deposition on oxygen carriers especially for Ni- and Fe-based ones [149, 150].

The deactivation of the oxygen carrier at the macroscale is mainly caused by the change of the texture characteristics and the decrease in mechanical strength. Both active metal oxides and the support could sinter at high temperatures, causing the change in the texture characteristics of the oxygen carrier. With the increase of temperature and the extension of reaction time, the micropores of the support undergo sintering, which in turn causes an increase in the average pore diameter and decreases in the total porosity and the specific surface area. With the change of the texture characteristics, the contact area of the active components with the reactants decreases, which significantly reduces the performance of the oxygen carrier. When oxides such as CeO_2 are used as the support, the sintering of the support not only affects the macroscopic properties but also reduces the oxygen transport capacity of the support, thereby affecting the overall oxygen transport capacity of the oxygen carrier. To maintain the texture characteristics, a series of preparation methods have been developed and optimized [151]. The abrasion and spalling of the oxygen carrier are closely related to its mechanical strength. For oxygen carriers, the improvement of mechanical strength can be achieved by adding additives and supports or optimizing the preparation method [151].

In addition to the deactivation of the oxygen carrier, the low selectivity of the oxygen carrier to the target product is also a factor affecting its development. Taking chemical looping methane reforming as an example, when oxygen or air is used as the oxidant, the surface oxygen of the oxidized oxygen carrier is restored, and thus, the selectivity of the complete oxidation product is increased, which is undesirable. Therefore, in order to solve this problem, the oxygen carrier can be selectively oxidized by reducing the oxidation time [132] or using a weak oxidant such as CO_2 [152] to restore the oxygen related to partial oxidation, thus increasing the selectivity of the target product. Continuous effort will be devoted to improving the long-term redox stability of oxygen carriers.

4 Oxygen carrier development

4.1 Primary material selection

Oxygen carriers are at the heart of chemical looping process development, which can circulate between two or more reactors/steps and convert raw materials into target products [9]. Since CLR uses oxygen conveyed by the oxygen carrier, they usually consist of metal oxides able to react with fuels such as CH_4. On account of the original purpose of CLR is to avoid the inadequacies of conventional steam reforming, partial oxidation, and autothermal reforming technologies, and to obtain a synthesis gas with a suitable H_2/CO ratio, the oxygen carrier should have a better fuel conversion rate and higher selectivity. In this regard, we can roughly perform a simple screening through the Ellingham diagram. The Ellingham diagram classifies and studies the thermodynamic properties of oxides based on their equilibrium oxygen potentials. The products of metal oxides reacting with the raw materials and their selectivity can be estimated based on their thermodynamic properties from the Ellingham diagram [9]. In addition to the Ellingham diagram, high-throughput thermodynamic screening technology can also be used to screen oxygen carriers [153]. The technology adopts the Gibbs energy descriptor [$G^{\delta}(T)$], which only needs information about the composition, enthalpy of formation and atomic density of the material. The descriptor can be used to predict the Gibbs free energy that reacts with CH_4, thus obtaining the corresponding conversion. Since the prediction method is only sensitive to parameters such as temperature, and the material category has little influence on it, this method can be widely applied to chemical looping processes and has similar accuracy on various materials under equilibrium or near equilibrium situation. Li et al. [154] recently reported the oxygen chemical potentials for over 2000 perovskite oxides were simulated as a function of their oxygen vacancy concentrations and more than 100 materials were predicted to be applicable. Among the potential candidates, intriguingly, "nonobvious". The phase diagram thermodynamic database can be used to computationally study the water conversion capability of metal oxides for chemical looping hydrogen generation [155]. In addition to screening for suitable oxygen carriers, the DFT method was used to screen for dopants, thus providing a fuller understanding of the selection of dopants [156, 157].

Previous studies show that most transition metal oxides agglomerate or sinter rapidly without the addition of additives or supports, resulting in a loss of available metal oxide sites. Considering that the long-term operation of CLR is to realize the industrialization of the process, another requirement is that the oxygen carrier should maintain both physical

and chemical stability over multiple cycles under reaction conditions. In addition, the cost, toxicity, thermal stability, and attrition resistance of the oxygen carrier are also factors to be considered for industrialization. Specific to the requirements of laboratory-scale development for oxygen carriers, we need to maintain a high conversion, a high selectivity of H_2 and CO, and a low selectivity of CO_2 and carbon deposition. For chemical or fuel synthesis purposes, the H_2/CO ratio is better at around 2. In addition, fresh and spent oxygen carriers can be characterized by XRD and TEM to check whether the crystal phase or structure is stable and the variation in the particle size.

Among all transition metals, nickel-, iron-, and cerium-based oxygen carriers are commonly used in the field of CLR (Fig. 9). These oxygen carriers have their own advantages and disadvantages. Ni-based catalysts are the most commonly used catalysts in the traditional methane reforming field, and thus, researchers first consider Ni-based oxygen carriers for CLR. The oxygen carrying capacity of the Ni-based oxygen carrier is excellent, but it faces severe carbon deposits, which could cause the H_2/CO ratio to be much higher than 2. At the same time, Ni-based oxygen carriers can only use air as the oxidant, and cannot be used for chemical looping hydrogen generation. Ni-based oxygen carriers are more expensive and unfriendly to the environment, which is not conducive to further industrialization. Fe-based oxygen carriers have the advantages of a wide range of sources and are environmentally friendly. Currently, a considerable amount of work has been done on the testing and characterization of iron ore. However, Fe-based oxygen carriers have poor activity and are easy to sinter, which results in lower CO selectivity, and reduced Fe could accelerate the methane cracking reaction, resulting in serious carbon deposits.

Based on these requirements and problems, we can summarize the recent progress and challenges in the development of oxygen carriers. Previous studies have focused on solving the problems of reactivity, carbon deposition, sintering, and stability. Taking CH_4 as an example, the chemical bond between carbon and hydrogen atoms in CH_4 is a stable sigma bond, and its chemical properties are relatively inactive. Therefore, CH_4 can participate in fewer reactions than other organic compounds. As a consequence, the high activity of the oxygen carrier is essential for the CLR of CH_4. The reactivity of oxygen carriers generally rests on two parts, one is the theoretical conversion of fuel, and the other is oxygen transport and reaction kinetics. The theoretical conversion rate is mainly determined by the thermodynamic properties of the oxygen carrier. The transport and reaction kinetics are determined by the composition, structure, and texture properties of the oxygen carrier. The texture characteristics include pore volume, specific surface area, and porosity.

Ni-based and copper-based oxygen carriers have good reactivity to raw materials such as CH_4, but the activities of Fe-, Mn-, Co, and Ce-based oxygen carriers are relatively poor. The addition of promoters or supports is considered to contribute to the improvement of activity. For example, the performance of iron oxide doped with 1% La is significantly improved compared with that of pure iron oxide [146]. Three-dimensionally ordered macroporous (3DOM) structures have been widely used in gas–solid reactions because of their uniform pore size (> 50 nm) and well-defined periodic structure, which could facilitate the adsorption and diffusion of reactant molecules. Compared with the nonporous CeO_2–ZrO_2 oxygen carrier, the CH_4 conversion of oxygen carriers with different pore sizes can be increased up to approximately 3.6 times, and the H_2 production rate in the water splitting stage is also increased by 50% thanks to the relatively higher specific surface area, higher concentration of oxygen vacancies, and stronger oxygen mobility [158].

The generation of carbon deposits is one of the most commonly discussed difficulties in reforming catalysts. Taking methane reforming as an example, in the traditional methane reforming field, carbon deposition is mainly considered to

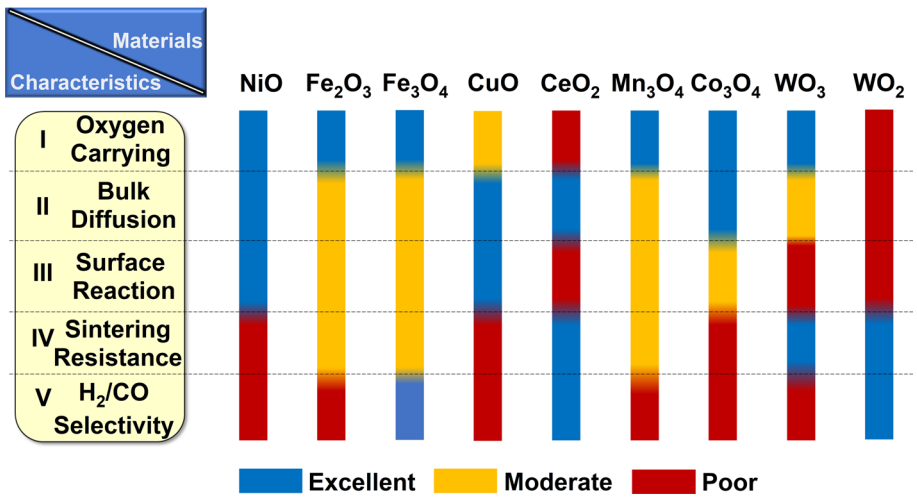

Fig. 9 Oxygen carrying capacity, bulk diffusion, surface reaction, sintering resistance, and H_2/CO selectivity characteristics of Ni-, Fe-, Cu-, Ce-, Mn-, Co and W-based oxygen carriers

be generated by methane cracking, and disproportionation reactions, which are also applicable to the chemical looping process. In the methane reduction stage, the Ni simple substance in the Ni-based oxygen carrier is reduced, which could quickly accelerate carbon deposition.

Generally, for Ni-based oxygen carriers, CO_2 or H_2O is added during the methane reduction stage to suppress carbon deposition or promote carbon deposition elimination. When Ni-based catalysts are used in chemical looping steam reforming, the TPO profiles of the spent Ni catalysts exhibit two CO_2 peaks, which means that there are two types of carbon deposits, one is probably absorbed CH_x or oligomeric carbon that oxidizes at low temperatures (300 °C), and the other is polymeric carbon that oxidizes at higher temperatures. The amount of these two types of carbon deposits has a great relationship with the type of supports [159].

Different from Ni-based oxygen carriers, Fe-based oxygen carriers can be used in chemical looping methane dry reforming and water splitting. The carbon deposits produced during the methane reduction stage can use CO_2 as an oxidant to obtain CO during the oxidation stage. However, the existence of obvious carbon deposits could also affect the proportion of syngas in the methane reduction stage and the activity of the catalyst. At the same time, the generation of carbon deposits also affects its application in chemical looping hydrogen generation and the purity of H_2 in the steam oxidation stage. For Fe-based oxygen carriers, it is generally believed that CH_4 is first adsorbed on the surface of the oxygen carrier, and then activated for dehydrogenation. Next, it is oxidized to CO_2 by oxygen with a strong oxidizing capacity and to CO by oxygen with a moderate oxidizing capacity in the oxygen carrier. With the consumption of lattice oxygen, the supply rate or transmission rate of lattice oxygen cannot match the methane cracking rate, so carbon deposits are generated [160]. The cracking reaction of CH_4 on the surface of the Fe-based oxygen carrier starts as active phase Fe or Fe_3C formed. Meanwhile, the increase in temperature and CH_4 concentration could promote the reduction of Fe-based oxygen, which indirectly promotes the production of carbon deposits.

In addition, the sintering of catalysts under high-temperature reaction conditions is a problem worthy of attention. The changes caused by carbon deposits could be reversible, while sintering is generally irreversible. It can be known through DFT calculations that the CH_4 adsorption energies and CO formation barriers are related to the particle size [130]. Therefore, with the sintering of the oxygen carrier, the particle size becomes larger so that the performance of the oxygen carrier changes significantly. The sintering of the catalyst inevitably affects the lattice oxygen transport rate, which causes the accumulation of carbon deposits. Suppression of catalyst sintering can be achieved by the confinement effects, that is, the use of nanostructures with specific morphology (3DOM, hydrotalcite and SBA-15 structure) to disperse the supported metal particles, thereby significantly improving the anti-sintering performance of the catalyst.

Improving the sintering resistance of the catalyst can also be achieved by adopting supports with large specific surface area or optimizing the preparation method. For copper-based oxygen carriers, the melting point of copper oxide is relatively low, so the sintering problem is a major problem in its development. The $CuO/CuAl_2O_4$ oxygen carrier prepared by the sol–gel method maintained the porous structure, indicating that the sintering could be controlled [161]. The performance of different oxygen carriers applied in the CLR is summarized in Table 3.

4.2 Nickel based oxygen carrier

Compared with noble metal catalysts, Ni-based catalysts can exhibit excellent activity while being inexpensive, so they have been widely used and industrialized in methane steam reforming and dry reforming processes, and have achieved industrialization. With the advent and continuous development of CLR, Ni-based oxygen carriers have also been extensively studied. The supported NiO usually easily loses oxygen and exists in the form of metallic Ni while achieving catalytic function. It is well known that when the temperature is higher than the Hüttig temperature or near the Taman temperature, the sintering rate of metals and metal oxides will be accelerated [207], so the thermal stability of the oxygen carrier can be roughly estimated by these two temperatures. According to the melting point of Ni, the Tammann temperature and Hüttig temperature of metallic Ni are approximately 863 K and 518 K, respectively. However, the temperature of chemical looping steam reforming is usually higher than 923 K, so sintering will always occur during the process. Particle size is an important factor affecting the activity and stability of Ni-based catalysts, so various methods have been used to suppress sintering, thereby weakening the growth of particle size [208].

To improve the sintering resistance of Ni-based oxygen carriers, the first thing that comes to mind is to add structural promoters with a higher Taman temperature and better thermal stability, such as Al_2O_3 [91, 159, 209, 210], ZrO_2 [159, 210, 211], TiO_2 [159], SiO_2 [159, 212], and $MgAl_2O_4$ [137]. Such structural promoters provide a large surface area, which can play a positive role in dispersing Ni particles. At the same time, the interaction between Ni particles and the support also inhibits the migration of Ni particles on its surface, thus exerting anti-sintering effects. For example, Lasa

Table 3 Summary of the performance of different oxygen carriers in chemical looping reforming

Oxygen carrier	Preparation	$T_{reaction}$ (°C)	Fuel	Oxidant	Fuel conversion (%)	H_2/CO selectivity (%)	Refs.
NiO/MCM-41	Modified post-synthesis	650	$C_2H_5OH:H_2O=1:3$	Air	~87	~81/–	[162]
NiO/montmorillonite	Cation-exchange impregnation	650	$C_2H_5OH:H_2O=1:3$	Air	~82	~71/–	[162]
NiO/Al_2O_3	Rising pH coprecipitation	650	$C_2H_5OH:H_2O=1:3$	Air	~79	~56/–	[162]
NiO/Al_2O_3	Co-precipitation	600	Glycerol:$H_2O=1:1.5$	Air/N_2	99	97/46	[91]
$La_{0.8}Ce_{0.1}Ni_{0.4}Ti_{0.6}O_3$	Modified solid state synthesis	570	5% CH_4/He	O_2/He	55	–/> 80	[163]
$LaNiO_3$	Sol–gel	650	$C_2H_5OH:H_2O=1:3$	Air	80	68/–	[164]
$LaNiO_3$/montmorillonite	Sol–gel	650	$C_2H_5OH:H_2O=1:3$	Air	92	80/–	[164]
Ni/CeO_2	Wetness impregnation	800	5% CH_4/He	CO_2/He	95	~96/~96	[165]
Ni/CeO_2–TiO_2	Two-step synthesis	900	1% CH_4/Ar	H_2O/Ar	~100	–/~86	[166]
Ni/CeO_2–TiO_2	Two-step synthesis	900	1% CH_4/Ar	CO_2/Ar	~100	–/~76	[166]
Fe_2O_3/CeO_2	Impregnation	800	5% CH_4/He	CO_2/He	~2	–	[167]
CoO/CeO_2	Impregnation	800	5% CH_4/He	CO_2/He	~76	–	[167]
NiO/Al_2O_3	Co-precipitation	900	5% CH_4/N_2	H_2O, O_2	43	54/33	[168]
Fe_2O_3/Al_2O_3	Co-precipitation	900	5% CH_4/N_2	H_2O, O_2	21	54/53	[168]
$NiO–Fe_2O_3/Al_2O_3$	Co-precipitation	900	5% CH_4/N_2	H_2O, O_2	97	84/28	[168]
Fe_2O_3–MgO/Al_2O_3	Co-precipitation	900	10% CH_4/N_2	H_2O	82	–/96	[169]
$NiFe_2O_4/Al_2O_3$	Sol–gel	900	$CH_4:CO_2=1:1.5$	CO_2/N_2	~97.5	88/88	[170]
Fe_2O_3–$NiO/La_{0.8}Sr_{0.2}FeO_3$	Modified Pechini method	900	25% CH_4/N_2	CO_2, O_2	97	–	[171]
$Fe_{0.88}Ni_{0.12}/CeO_2$	Wetness impregnation	1000	17% CH_4	CO_2	–	> 90/> 90	[172]
$LaFe_{0.9}Ni_{0.1}O_3$	Polystyrene colloidal crystal Templating	850	5% CH_4/N_2	H_2O	90	-	[173]
Fe_2O_3/Ni-modified Al_2O_3	Sol–gel and impregnation	900	$CH_4:CO_2=1:0.38$	O_2/N_2	~90	–/~96	[174]
Fe-Ca/γ-Al_2O_3	Co-impregnation	700	$CH_4:H_2O=1:1.5$	O_2/Ar	100	–	[175]
Y-modified Fe_2O_3/Al_2O_3	Sol–gel	900	5% CH_4/He	O_2/He	~90	~93/~90	[176]
Ce-modified Fe_2O_3/Al_2O_3	Sol–gel and impregnation	900	$CH_4:CO_2=1:0.28$	O_2/N_2	93	–/93	[177]
Fe_2O_3	Sol–gel	1000	25% CH_4/(N_2, He)	Air/(N_2, He)	~35	–	[78]
1% Cu-Fe_2O_3	Sol–gel	1000	25% CH_4/(N_2, He)	Air/(N_2, He)	~40	–	[78]
5% Ca-Fe_2O_3/Al_2O_3	Wetness impregnation	650	$CH_4:H_2O=1:1.5$	–	~94	–	[178]
5% Ce-Fe_2O_3/Al_2O_3	Wetness impregnation	650	$CH_4:H_2O=1:1.5$	–	~92	–	[178]
5% CeO_2-$Fe_2O_3/LaNiO_3$	Citric acid complexation	800	10% CH_4/N_2	H_2O, Air	100	–	[179]
$La_{0.33}Ce_{0.67}$-Fe_2O_3/Al_2O_3	Co-precipitation	800	9% CH_4/He	CO_2/He	~77	–/~10	[180]
$LaFe_3Al_9O_{19}$	Co-precipitation	850	5% CH_4/Ar	CO_2/Ar	81	97/90	[181]
$BaFe_3Al_9O_{19}$	Two-step method	900	5% CH_4/He	O_2/He	86	–/83	[152]
Fe_2TiO_5/Al-based skeleton	–	1000	H_2, CO	Air	> 99	–	[143]
$LaFeO_3$	Sol–gel	900	11% CH_4/He	O_2/Ar	~70	–/> 96	[182]
$LaFeO_3$	Polystyrene colloidal crystal Templating method	850	40% CH_4/N_2	H_2O, Air	~50	–	[183]
$La_{0.7}Sr_{0.3}FeO_3$	Combustion method	850	40% CH_4/N_2	–	~70	~82/~95	[183]

Table 3 (continued)

Oxygen carrier	Preparation	$T_{reaction}$ (°C)	Fuel	Oxidant	Fuel conversion (%)	H_2/CO selectivity (%)	Refs.
$La_{0.7}Sr_{0.3}FeO_3$	Combustion method	800	40% CH_4/N_2	–	~58	–	[118]
$La_{0.5}Sr_{0.5}FeO_3$	Combustion method	800	40% CH_4/N_2	–	~63	–	[118]
$LaFe_{0.7}Mn_{0.3}O_3$	Glycine combustion method	850	40% CH_4/N_2	H_2O, Air	~98	–	[184]
$LaFe_{0.7}Co_{0.3}O_3$	Combustion method	850	40% CH_4/N_2	H_2O/N_2	85	50/43	[116]
$La_{0.85}Sr_{0.15}Fe_{0.95}Al_{0.05}O_{3-\delta}$	Granulation	900	8.6% CH_4/N_2	7.1% H_2O, air	~80	99/99	[185]
$La_{0.6}Sr_{0.4}FeCoO_6$	Micro-emulsion	850	40% CH_4/N_2	H_2O, O_2	~90	~45/~40	[186]
Fe_2O_3@$LaFeO_3$	Modified Pechini method	900	10% CH_4/He	O_2/He	–	64/85	[187]
Fe_2O_3@$La_{0.7}Sr_{0.3}FeO_{3-\delta}$	Modified Pechini method	900	10% CH_4/He	O_2/He	–	84/86	[187]
Fe_2O_3@$SrFeO_3$	Modified Pechini method	900	10% CH_4/He	O_2/He	–	40/64	[187]
Fe_2O_3@$La_{0.8}Sr_{0.2}FeO_{3-\delta}$	Modified Pechini method	900	10% CH_4/He	O_2/He	–	80/87	[188]
Fe_2O_3@SBA-15	–	750	20% CH_4/N_2	–	–	–/~100	[130]
CeO_2–ZrO_2	Co-precipitation	800	CH_4	–	41	80/80	[189]
CeO_2–Fe_2O_3	Chemical precipitation	850	CH_4/N_2	H_2O/N_2	55	~90/~90	[190]
Ce-Fe–O	Co-precipitation	900	CH_4	Air	95	99/99	[191]
Ce-Fe-Zr	Co-precipitation	800	CH_4	Air	64	84/84	[192]
CeO_2–$LaFeO_3$	Sol–gel	850	10% CH_4/N_2	CO_2:H_2O = 1:4.5	–	92/93	[100]
Cu/Zr–Al	Co-precipitation and wet impregnation	650	CH_4:CO_2 = 1:1	O_2/Ar	~99	–	[193]
$Ca_2Fe_2O_5$/MgO	Solid-state synthesis	1000	10% CH_4/Ar	CO_2/N_2	~99	~98/~98	[194]
Cu_2O/$Ca_2Fe_2O_5$	Sol–gel	240	CH_3OH:H_2O = 2:1	Air	~100	–	[195]
Cu–Fe/Al_2O_3	–	900	20% CH_4/He	–	99	–	[196]
Mn_2O_3/Zr-modified Al_2O_3	Co-precipitation and impregnation	650	CH_4:CO_2 = 1:1	O_2/Ar	~98	–	[197]
Rh/$CaMnO_3$	Modified Pechini method	600	10% CH_4/Ar	O_2/Ar	–	98/86	[198]
$BaMn_{0.5}Fe_{0.5}O_3$	Sol–gel	800	CH_4/N_2	H_2O/N_2	95	–/95	[199]
$CoAl_2O_4$	Sol–gel	900	CH_4:CO_2 = 1:1	–	–	~97/~100	[200]
Ca–Co	Co-impregnation	700	CH_4:H_2O = 1:2	O_2/Ar	~98	–	[201]
Ca–Co–Zr	Co-impregnation	700	CH_4:H_2O = 1:2	O_2/Ar	~99	–	[201]
$BaCoO_{3-\delta}$/CeO_2	Sol–gel	860	50% CH_4/N_2	H_2O, Air	–	–/~95	[202]
$Ba_{0.3}Sr_{0.7}CoO_{3-\delta}$/$CeO_2$	Sol–gel	850	50% CH_4/N_2	H_2O, Air	–	–/95	[203]
WO_3/ZrO_2	Wetness impregnation	1000	50% CH_4/N_2	H_2O/N_2	42	–	[204]
WO_3	Co-precipitation	800	17% CH_4/He	O_2/He	11	59/94	[205]
WO_3/Al_2O_3	Co-precipitation	800	17% CH_4/He	O_2/He	22	89/90	[205]
$Ni_{0.5}WO_x$/Al_2O_3	Co-precipitation	800	17% CH_4/He	O_2/He	58	93/91	[205]
WO_3/SiO_2	Impregnation	900	10% CH_4/N_2	O_2/N_2	~29	~73/~73	[206]
$FeWO_x$/SiO_2	Impregnation	900	10% CH_4/N_2	O_2/N_2	62	94/~73	[206]

et al. [209] introduced an Al_2O_3 support for NiO-based oxygen carriers and found that the size of Ni particles stabilized at approximately 50 nm after several cycles, proving that no significant sintering occurred in the extended redox process. Temperature-programmed reduction (TPR) results showed that the interaction between Ni particles and the Al_2O_3 support decreased with increasing Ni loading. In the mean time, Adánez et al. [213] suppressed the sintering of oxygen carriers by changing the types of Al_2O_3 and the preparation methods. The specific surface area of the Ni-based oxygen carrier prepared by using γ-Al_2O_3 and the incipient wet impregnation method after a 50-h test decreased by 65%, while the oxygen carrier adopting the α-Al_2O_3 support and hot incipient wet impregnation method remained substantially unchanged after 100 h of testing [213].

When using Al_2O_3 as the support, the appearance of $NiAl_2O_4$ spinel is inevitable. Although $NiAl_2O_4$ spinel may weaken the sintering of Ni particles, its oxygen carrying capacity and reaction performance are poor compared to NiO. Therefore, $NiAl_2O_4$ [214, 215] and $MgAl_2O_4$ [216, 217] spinels could be directly used as support to suppress the formation of $NiAl_2O_4$ spinel. DFT calculations showed that the adsorption energy of Ni particles on the surface of ZrO_2 is − 4.89 eV and that the oxygen in NiO could bond with Zr atoms on the surface of ZrO_2, which meant that NiO could be easily attached to the surface of ZrO_2, forming a stable oxygen carrier [218]. The E_{vac} of the Ni–Zr oxygen carrier was also calculated at 2.94 eV, and the oxygen carrier activity of ZrO_2 as a support was better than that of the $MgAl_2O_4$ spinel support.

The SBA-16 is also applied to Ni-based oxygen carriers [131]. In order to improve the performance of chemical looping steam methane reforming, Rahimpour et al. [131, 219–221] carried out a series of studies on the application of Ni/SBA-16 oxygen carriers in chemical looping steam methane reforming, and conducted in-depth discussions on the properties of Ni/SBA-16 oxygen carriers and their modification by Ce and Y. With SBA as the support and the addition of Ce as the promoter, the performance of chemical looping steam methane reforming was significantly improved. The confinement effect of SBA and the interaction between Ce and Ni ensured the high dispersion of Ni, while the presence of Ce also stabilized the stability of the SBA skeleton.

The dispersibility of Ni in the supported oxygen carriers varies with the Ni precursor and the preparation method. Therefore, adjusting the type of Ni precursor and preparation method is another strategy method for improving sintering resistance [4]. A layered double hydroxide (LDH) precursor with a specific surface area (60.0 m^2/g) was used to prepare a Ni–Mg–Al–O oxygen carrier, which promoted the dispersion of cations. BET and SEM results showed that the oxygen carrier remained porous after 100 cycles, which proved that its sintering was significantly suppressed. In addition, the addition of Mg formed a solid solution with Ni, and would also inhibit sintering to a certain extent [222].

For supported NiO-based oxygen carriers, sintering and carbon deposition are the main causes of deactivation. However, for $NiFe_2O_4$, it is possible that surface sintering is not the main cause of deactivation. The deactivation of $NiFe_2O_4$ is more likely due to phase segregation or further sintering due to phase segregation, which aggravates the deactivation. Ma et al. [223] found that different phases, such as Ni and Fe_3O_4, appeared during the reduction of $NiFe_2O_4$. As the oxygen carrier was further reduced, FeO and NiFe phases appeared and an Fe-enriched needle-like structure was formed on the surface of $NiFe_2O_4$ after the first cycle. And the phase segregation and deactivation became more serious after that. Ma et al. [224] introduced the CeO_2 into the $NiFe_2O_4$ oxygen carrier to effectively alleviate the phase segregation problem. It was shown that the oxygen vacancy in CeO_2 promoted the mobility of lattice oxygen and thus prevented the phase segregation.

The stability of CH_4 keeps the reaction temperature at a high level, while reactants (ethanol and glycerol) need a lower reaction temperature. Dou et al. [89–91, 162, 225–228] carried out a series of works on the application of nickel-based oxygen carriers in ethanol or glycerol reforming. When Al_2O_3 was used as the support, the CLR had higher glycerol conversion and H_2 yield than conventional reforming [91]. When nickel oxide was supported on montmorillonite, the cation exchange capability and confinement effect of montmorillonite promoted the dispersion of nickel, thereby improving the sintering and coking resistance of the oxygen carrier [90]. At the same time, Dou et al. [227] applied perovskite to CLR, and found that nickel can reversibly pass in and out of the perovskite structure during the process, thereby effectively suppressing the sintering of nickel particles. The addition of calcium and lanthanum promoters effectively increased the reactivity and stability of the oxygen carrier.

The high activity of nickel-based oxygen carriers makes the subsequent carbon deposition problem an obstacle to its development, so it is necessary to better understand the existence of carbon deposition and the corresponding solutions. The morphology or reactivity of carbon deposits in the reforming reaction depends on the specific reaction conditions and the structure of the oxygen carrier. According to the morphology of carbon deposits in previous literature, they can be generally classified into coated carbon and filamentous carbon [229]. They can be further divided into α-carbon (C_α), β-carbon (C_β) corresponding to steaming reforming [230] and α-carbon (C_α), β-carbon (C_β), and γ-carbon (C_γ) corresponding to dry reforming [231] according to the reactivity of carbon deposits.

C_α can be oxidized by CO_2, which is considered to be the carbon deposit that is easier to continue to participate in the reaction to generate CO. C_β and C_γ are the types of carbon deposits that are more difficult to participate in the reaction. C_β may be gradually accumulated and transformed from C_α in the course of the reaction, and C_γ is graphite-like carbon species. C_β and C_γ are generally considered to be the causes of the deactivation of Ni-based catalysts in steam reforming and dry reforming, respectively. Some of the carbon deposits formed on the catalyst surface dissolve in Ni, and the remaining parts remain on the surface. The carbon deposits on the surface contain an orderly structure through dehydrogenation, surface migration and growth, which could encapsulate Ni and cause deactivation. Therefore, it is reasonably inferred that the evolution of the carbon deposit of the Ni-based catalyst, i.e., the initial C_α formation and gradual accumulation of C_α due to gasification imbalance and then transformation to poorly reactive C_β, causes its deactivation gradually.

Specifically, for the oxygen carrier, the reason for carbon deposition is that the Ni particle size is too large, or there are acid sites or carbon deposition nucleation centers on the surface. A large number of studies have been carried out on the causes of carbon accumulation. Certain strategies for enhancing coke resistance in traditional methane reforming are suitable for CLR, but some methods, such as adding additives that enhance O_2 or CO_2 adsorption, might not be suitable for CLR. Highly dispersed Ni nanoparticles with small particle sizes exhibit excellent coke resistance because the Ni particles are small enough to prevent the carbon nanofibers from nucleating on them, and carbon nucleation at the step edges and subsequent growth are also suppressed [232]. Hence, the abovementioned method for improving the dispersion of Ni particles can not only improve the anti-sintering ability of the oxygen carrier but also effectively alleviate the carbon deposition problem of the oxygen carrier.

Immobilizing Ni ions in a stable structure such as perovskite is also a strategy to weaken carbon deposition, as perovskite structures have good oxygen migration capacity and can balance the rate of carbon generation and elimination to a better extent. However, the aggregation of perovskite oxygen carriers during calcination results in their small specific surface area, which limits their application. Li et al. [164] loaded $LaNiO_3$ on the montmorillonite (MMT) support, integrating the strong oxygen migration ability of perovskite with the large specific surface area of MMT. Compared with the unsupported perovskite, $LaNiO_3$/MMT particles had a smaller particle size, and the particle size was mainly distributed between 10 and 20 nm. In the ethanol reforming cyclic test, the activity of $LaNiO_3$/MMT after 10 cycles only decreased by 12.4%, which was much lower than that of $LaNiO_3$.

Metcalfe et al. [163] prepared the Ni-containing perovskite oxygen carrier and controlled the exsolution of nickel particles to optimize the reaction process (Fig. 10). By reduction under hydrogen, an oxygen carrier (Ni-rABO_3) having nickel particles on the surface and within the bulk phase could be obtained. The particle size of the surface particles was larger than that of the bulk particles, and the proportion of the bulk particles was higher. By changing the temperature and treatment time of the oxygen carrier, it was found that the interparticle distance and size of the particles were correspondingly changed. At the same time, the proportion of the bulk particles and the corresponding oxygen capacity increased with increasing treatment time or temperature. For more intuitive analysis, Metcalfe et al. [163] fitted the oxygen uptake measurement with a logistic law and plotted the corresponding oxygen capacity (ζ_G, mol O per mol perovskite) and time constant of oxygen exchange (τ, h^{-1}) in Fig. 10b. It was found that the ζ_G was directly proportional to the bulk nickel content (Ni_B, wt.%), and τ was related to the ratio of the average bulk particle diameter (s, nm) to the average distance between neighboring bulk particles (d, nm).

In order to prove the superiority of Ni-rABO_3, Ni-rABO_3 and Ni/Al_2O_3 were applied to the methane reforming reaction. Ni/Al_2O_3 showed low selectivity for partial oxidation products and high carbon deposition selectivity. In contrast, Ni-rABO_3 exhibited excellent selectivity for partial oxidation products with little carbon deposition. To further prove the importance of the coexistence of surface and bulk particles, samples with only surface or bulk particles were tested and found to be inactive. The operando analysis of oxygen carriers was used to study the mechanism of bulk phases and surface particles (Fig. 10c). When the temperature was approximately 550 °C, CH_4 started to be consumed, corresponding to the reduction of surface nickel oxide particles. Next, the bulk nickel oxide was reduced, and as the bulk nickel oxide was depleted, the perovskite was reduced. The method of obtaining bulk and surface particles through reduction treatment provided important guidance for the development of nickel-based oxygen carriers and perovskite structures.

In addition, the selectivity and anti-carbon capacity of oxygen carriers are also influenced by the properties of the particle. In CLR, support with good oxygen carrying capacity and oxygen mobility can be selected to provide oxygen for the reaction process of Ni particles while supporting. CeO_2 is added to the Ni-based oxygen carrier due to its good sintering resistance and excellent oxygen mobility [165, 167, 233, 234].

In addition to eliminating carbon deposits, chemical looping can be used to utilize the activity of Ni-based oxygen carriers to enable the production of H_2 and CO. Tian et al. [235] achieved H_2 and CO production by passing biogas into the reaction tube containing two catalyst sections. First, in the H_2 production stage, calcium oxide absorbs CO_2 from the

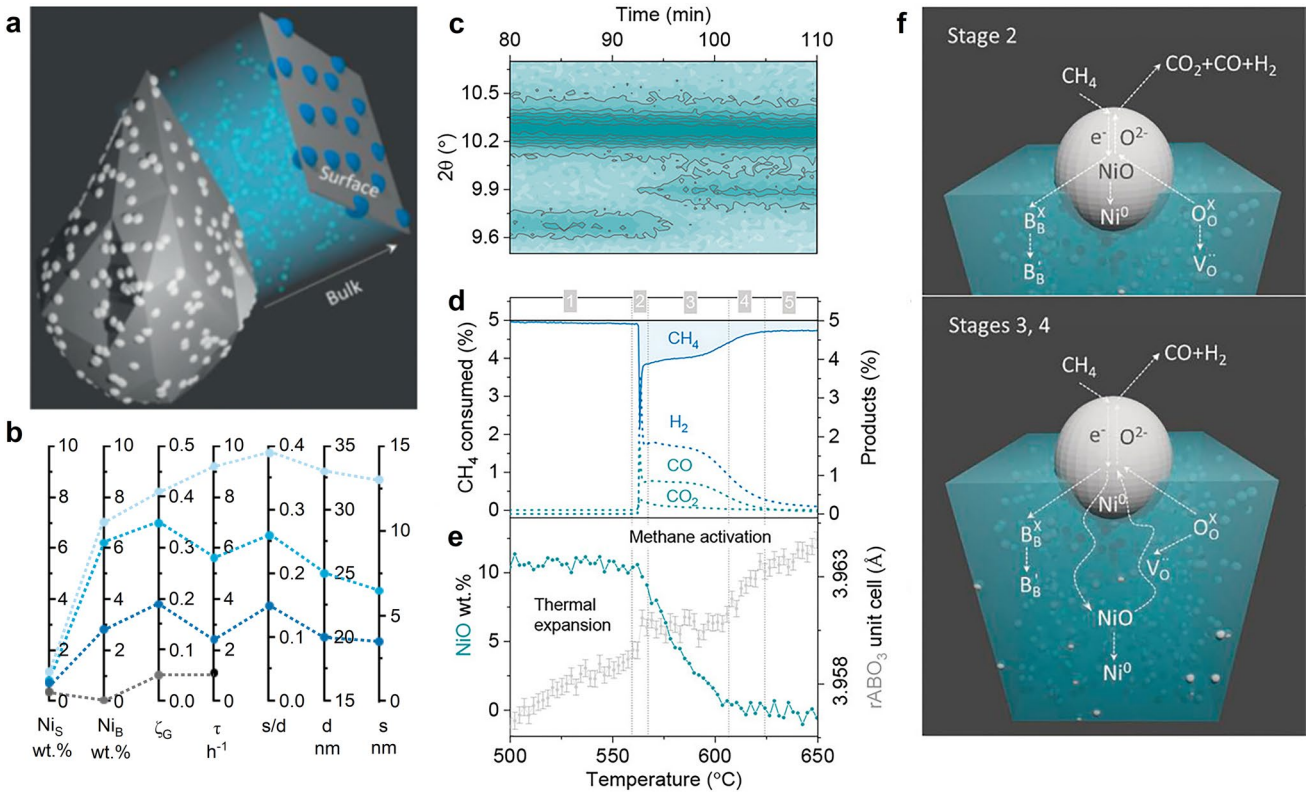

Fig. 10 **a** 3D model of an oxygen carrier particle with nanoparticles dispersed on its surface and within its bulk. **b** Parallel axes plot for the samples reduced at 900 °C for 0 h (dark grey), 10 h (dark blue) and 30 h (blue) and at 1000 °C for 10 h (light blue). **c** XRD data acquired during the TPR under 5% CH_4 of a system with submerged nanoparticles presented as 2D plot, as a function of diffraction angle, time and corresponding temperature; **d** CH_4 consumed and corresponding products produced during the experiment described in **c**. **e** NiO content and perovskite unit cell parameter calculated from **c**. **f** Schematic of CH_4 conversion mechanism corresponding to the main stages identified from **c**. Reproduced from ref. [163] with permission from John Wiley and Sons, copyright 2020

feedstock to produce calcium carbonate, followed by the cracking of methane by the Ni-based oxygen carrier, which produces carbon deposition on the Ni-based oxygen carrier. Then, in the CO production stage, the calcium carbonate in the reaction tube decomposes to produce CO_2, followed by the reaction of carbon on the Ni-based oxygen carrier at the lower end with CO_2 to produce CO. Wang et al. [236] achieved the preparation of H_2 and CO through Ni/La_2O_3 carriers. The H_2 preparation was achieved using the methane cracking ability of Ni, while the carbon accumulation on the catalyst surface reacted with the incoming CO_2 to achieve CO production. These two processes utilize the methane cracking ability of nickel-based catalysts to achieve efficient preparation of H_2 and CO, providing a new idea for the development of nickel-based oxygen carriers.

4.3 Iron based oxygen carrier

Iron is the most commonly used transition metal and the second most abundant metal in the earth's crust. The outer electron configuration of Fe is arranged as 3d64s2 so that it has +3, +2, and zero valence. Because of the different oxidizing abilities displayed during the transition between different valence states of iron oxide and the excellent water or CO_2 dissociation ability of metallic Fe, Fe-based oxygen carriers have been applied in various chemical looping processes with different target products. Because of the various advantages exhibited by Fe-based oxygen carriers, it is a promising candidate for the industrialization of chemical looping processes.

Fe-based oxygen carriers can be generally divided into two categories, namely, synthetic Fe-based oxygen carriers and naturally occurring iron ore-based oxygen carriers. The application of pure iron oxide to the chemical looping process has been previously investigated [237]. Trevisanut et al. [238] applied Fe_3O_4 to chemical looping hydrogen generation and found that the carbon content of the oxygen carrier was controlled to 1% after 20 cycles. However, during the reaction process, iron oxide may be reduced by bioethanol into unstable iron carbide, which can be decomposed into Fe

and carbon, thus promoting the generation and accumulation of carbon deposits with increasing cycle numbers of the redox cycles. Ma et al. [239] studied the morphology and structural changes of iron oxide during the chemical looping reaction. After multiple cycles, it can be found that the surface of the oxygen carrier was sintered and reduced due to the instability of the iron oxide during its conversion. At the same time, the mechanical integrity and strength were decreased due to the continuous migration of Fe ions. Zheng et al. [240] compared the performance of iron oxide and nickel-impregnated iron oxide oxygenate carriers. The CH_4 conversion and H_2 yield of iron oxide alone were low, while the Ni-impregnated oxygen carriers had high H_2 yield, which may be due to the synergistic effect between nickel and iron. The nickel on the surface of the oxygen carrier provides catalytic sites while the iron provides lattice oxygen, which promotes H_2 production. Kidambi et al. [241] prepared Al_2O_3-supported iron oxide oxygen carriers with different Fe_2O_3 loadings. The particle size of iron oxide was found to decrease with the reducing loading of iron oxide, and the particle size of iron oxide with a loading of 100% was 3.3 times larger than that of iron oxide with a loading of 50%.

As mentioned in the section of primary material selection, the performance of the supported iron oxide oxygen carriers is closely related to the particle size of the iron oxide, so it is particularly important to obtain iron oxide particles with a small particle size. High dispersion of iron oxide particles can be achieved by using the SBA-15 support via the confinement effect. Fan et al. [130] successfully synthesized SBA-15 supported iron oxide with high dispersion (Fig. 11). The particle sizes of iron oxide particles confined within SBA-15 (Fe_2O_3@SBA-15) and unsupported iron oxide particles were between 3–5 nm and 50–100 nm, respectively. After redox cycles, the particle size of the Fe_2O_3@SBA-15 oxygen carrier increased by 5–8 nm, while the particle diameter of the unsupported Fe_2O_3 was between 1 and 10 μm. DFT calculations showed that the CH_4 adsorption energies and CO formation barriers were related to the particle size. The Fe_2O_3@SBA-15

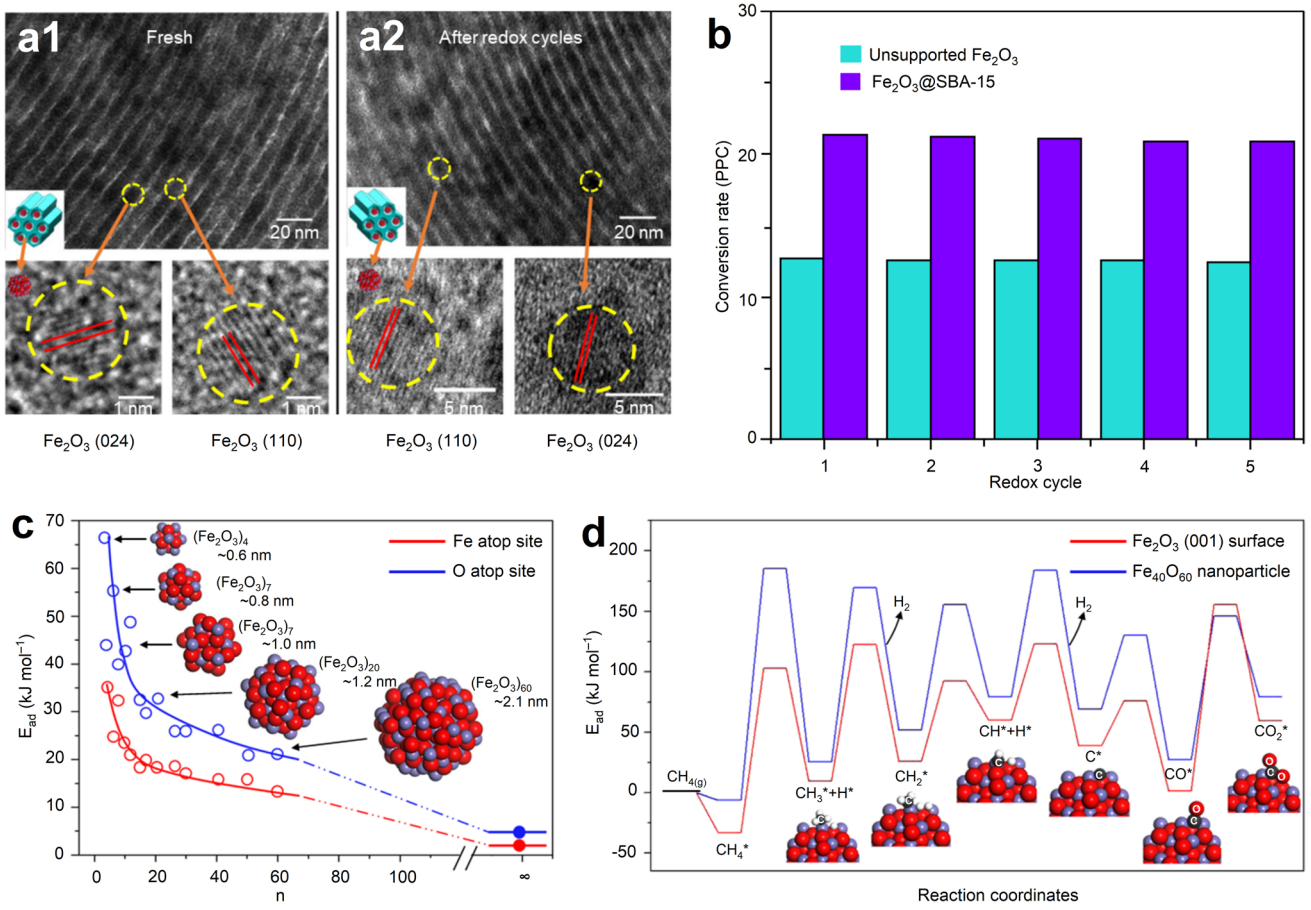

Fig. 11 **a** Morphological characteristics of Fe_2O_3@SBA-15: **a1** Fresh Fe_2O_3@SBA-15 and HR-TEM images of two typical Fe_2O_3 nanoparticles, **a2** Fe_2O_3@SBA-15 after 75 redox cycles and HR-TEM images of two typical Fe_2O_3 nanoparticles. **b** Conversion rate of Fe_2O_3@SBA-15 and bulk Fe_2O_3 during redox at 800 °C. **c** Calculated energies of CH_4 adsorption. E_{ad} (kJ mol^{-1}), on the Fe atop site and O atop site of $(Fe_2O_3)_n$ nanoparticles as a function of n. **d** Energy profile of CH_4 partial oxidation on $Fe_{40}O_{60}$ nanoparticle and Fe_2O_3 (001) surface. Reproduced from ref. [130] with permission from Springer Nature, copyright 2019

oxygen carrier achieved nearly 100% CO selectivity at low temperatures, and the conversion rate was approximately 1.69 times than that of unsupported Fe_2O_3.

Since the oxygen transmission rate and the subsequent reaction performance are also closely related to the particle size, iron oxide is generally supported on a support or restricted in a composite oxide. Therefore, synthetic Fe-based oxygen carriers are mainly divided into supported and composite oxide oxygen carriers. The metal dispersion degree and anti-sintering capacity were the two most concerned factors for supported oxygen carriers, and strategies like changing the supports and dopants were employed to conduct surface or bulk phase modification. For composite oxide oxygen carriers, taking perovskite as an example, the performance can be optimized by replacing the metal at the A and B sites. The natural ore oxygen carriers are mainly hematite and ilmenite [242]. Natural ore generally needs to be calcined at high temperature before being applied to the chemical looping process. Although the main component of the ore is Fe-based oxides, the properties of ores may vary due to changes in other components caused by different ore origins [242].

For supported oxygen carriers, the most commonly used supports are SiO_2 and Al_2O_3. SiO_2 has a poor dispersion effect on iron oxide during the reaction process, and reacts irreversibly with iron oxide to form iron silicate, so it is less commonly used [243]. Al_2O_3 as a support can better disperse iron oxide and improve the sintering resistance of the oxygen carrier [244]. Fe_2O_3/Al_2O_3 oxygen carriers have been widely used in chemical looping methane reforming and alcohol reforming. Kang et al. [174] used the Fe_2O_3/Al_2O_3 oxygen carrier in the chemical looping dry reforming process. In the 20 cycles test at 900 °C, the CH_4 conversion and the CO selectivity were all above 95% and remained stable. Meanwhile, the H_2/CO ratio of the oxygen carrier was approximately 2.2, indicating that the carbon deposition was not significant. Qin et al. [245] successfully applied Fe_2O_3/Al_2O_3 oxygen carriers in chemical looping reforming of ethanol-containing organic wastewater. When the ethanol concentration was 5% and the reaction temperature was 800 °C, the carbon conversion and syngas yield of the oxygen carrier were 100% and 3.325 L/g, respectively. However, it was found in the experiment that Al_2O_3 went through a solid phase reaction with Fe_2O_3 during the cycle to produce spinel. The effect of $FeAl_2O_4$ spinel is contradictory because its formation can reduce the sintering of oxygen carriers while reducing the storage capacity of Fe_2O_3 [246]. Yüzbasi et al. [247] prepared Al_2O_3-supported iron oxide oxygen carriers with a loading of 80% by the sol–gel method and used three different Fe salts as Fe precursors. XRD characterization revealed that the $FeAl_2O_4$ spinel only existed in the oxygen carrier using ferric chloride as a precursor. In addition, although the oxygen carrier using ferric chloride as a precursor possessed no advantage compared with the other two precursors in the performance test, its performance remained stable in 15 cycles. Compared to the other two oxygen carriers, this oxygen carrier had the largest proportion of spinel, which played a role in preventing the oxygen carrier from sintering during the reaction, thus leading to its good stability.

The existence of $FeAl_2O_4$ spinel is more significant for CLC. First, in thermodynamics, when Fe_2O_3 reacts with CH_4 at 900 °C to produce Fe^{2+}, CO_2, and H_2O, the Gibbs free energy of Fe_2O_3 to $FeAl_2O_4$ is 1.5 times less than that of Fe_2O_3 to FeO, suggesting that the addition of Al_2O_3 thermally results in more oxygen conversion in CLC. Second, it is currently believed that only Fe_2O_3 to Fe_3O_4 produces high purity CO_2. According to the thermodynamic calculation by HSC chemistry software, it can be known that at 900 °C, the addition of Al_2O_3 causes the oxidation products to have an impact on the reduction of Fe_3O_4 by CH_4 to FeO, making it more inclined to produce CO_2. Finally, the presence of $FeAl_2O_4$ spinel also means that Fe_2O_3 is well dispersed on Al_2O_3 because the reduction of specific surface area caused by sintering could prevent Fe_2O_3 and Al_2O_3 from contacting closely, thus significantly reducing the amount of spinel produced in the reduction process. Wang et al. [248] added different proportions of silicon to the Al_2O_3 support to enhance the sintering resistance of the oxygen carrier. XRD characterization showed that the presence of silica inhibited the conversion of γ-Al_2O_3 to α-Al_2O_3 to ensure the stability of the specific surface area, and a large amount of $FeAl_2O_4$ spinel was produced during the reduction process. The best-performing sample decreased its oxygen transfer capacity by only 6% after sixty cycles, indicating that it had good cycle stability. However, in the process of chemical looping hydrogen generation or dry reforming, the oxidation ability of water or CO_2 was thermodynamically not strong enough to oxidize the Fe^{2+} in $FeAl_2O_4$ spinel back to Fe^{3+}, which meant that the yield of CO or H_2 was decreased.

The formation of $FeAl_2O_4$ spinel can be prevented by the rational design of oxygen carriers. Hafizi et al. [249] added 5% Mg to the Al_2O_3-supported iron oxide oxygen carrier, where the presence of $MgAl_2O_4$ spinel could be found in the prepared oxygen carrier without the presence of $FeAl_2O_4$ spinel. Meanwhile, the proportion of $FeAl_2O_4$ spinel in the oxygen carrier after 15 cycles decreased significantly. In addition to suppressing the formation of spinel by adding Mg, Mg–Al spinel support can also be used directly [138, 140, 243]. In order to maximize the production of CO, Buelens et al. [139] developed a super-dry reforming method, which adopted $Fe_2O_3/MgAl_2O_4$ as an oxygen carrier, Ni/$MgAl_2O_4$ as a reforming catalyst, and CaO/Al_2O_3 as a CO_2 sorbent. Unlike other chemical looping processes that directly pass O_2, H_2O or CO_2 to oxidize the oxygen carriers, this process used CaO/Al_2O_3 to achieve the storage of CO_2 in the reduction stage

and released CO_2 to oxidize the oxygen carrier in the oxidation stage. The yield of CO is also maximized while achieving the in situ removal of CO_2. Through long-term cycle tests, it was found that the $Fe_2O_3/MgAl_2O_4$ oxygen carrier possessed good cycle stability and obtained a high space–time yield of CO. Yttrium was also added to Al_2O_3-loaded iron oxide to form a uniform garnet structure with Fe and Al when the ratio of Y_2O_3 to Fe_2O_3 was 1.5 [176]. Moreover, according to the [57] Fe Mössbauer spectra, it was found that the sintering was significantly alleviated with the addition of Y because iron oxide with low amount of yttrium doping had a smaller particle size than that without doping. With the increase of doping amount and the activation of oxygen carriers, more Fe^{3+} was found to enter the garnet structure. The CO production of the oxygen carrier also improved with increasing doping amount. On the basis of the DFT calculation, the reason why the garnet structure was highly selective for CO was that the E_{vac} of the oxygen carrier doped with yttrium was approximately 41% higher than that of the non-doped oxygen carrier.

Fe_2O_3/Al_2O_3 oxygen carriers also face problems (carbon deposition, sintering, and poor reactivity) during the CLR process. The addition of metallic Ni can effectively alleviate the problem of poor reactivity of iron oxide oxygen carriers. Huang et al. [168] added an equal proportion of NiO to the Fe_2O_3/Al_2O_3 oxygen carrier, and found that the conversion of CH_4 is up to 3.75 times higher than that of the pure iron oxide oxygen carrier, and the CO_2 selectivity was also reduced by 81%. Kang et al. [174] also obtained the Ni-entrapped Fe_2O_3/Al_2O_3 oxygen carrier by the sol–gel method. The addition of 1% Ni increased the interaction between the metal and the support, which significantly improved the CO selectivity and reduced the H_2/CO ratio. There were two main origins of carbon deposition on the Fe_2O_3/Al_2O_3 oxygen carrier, one was that the limited oxygen transport capacity and oxygen migration capacity of iron oxide could not remove carbon deposition in time and the other was that Al_2O_3 was an acidic support, which promoted the generation of carbon deposition. Therefore, the elimination of carbon deposition is considered from these two aspects. Carbon deposition due to the acidity of the support was mitigated by adding a certain proportion of alkali metals. Through DFT calculations, Feng et al. [250] found that lithium, sodium, and potassium alkali metals tended to stay on the surface of the oxygen carrier. Because alkali metal owned a lower valence state than Fe, the introduction of alkali metal lowered the E_{vac} on the surface, making oxygen carriers more active. Zhu et al. [144] added K_2CO_3 to the Fe_2O_3/Al_2O_3 oxygen carrier and applied it to chemical looping hydrogen generation. Performance tests showed that the K_2CO_3-doped Fe_2O_3/Al_2O_3 oxygen carrier did not show significant carbon deposits at a CH_4 concentration of 40% and remained stable, while carbon deposits of the undoped Fe_2O_3/Al_2O_3 oxygen carrier increased significantly over time. The purity of H_2 in the steam oxidation stage was also improved due to the addition of K_2CO_3. CeO_2 with good oxygen migration ability and oxygen storage ability was also added to the Fe_2O_3/Al_2O_3 oxygen carrier to inhibit the formation of carbon deposits. $CeAlO_3$, $Al_3Fe_5O_{12}$, and $AlFeO_3$ were formed by adding 5% CeO_2 to the iron oxide oxygen carrier through the sol–gel method, and $CeAlO_3$ activated and decomposed CO_2, thereby providing active surface oxygen for carbon deposition elimination [145]. At the same time, the addition of CeO_2 generated more oxygen vacancies to promote the transport of lattice oxygen. The thermogravimetric analyzer test suggested that the coke-resistant ability of the CeO_2-doped Fe_2O_3/Al_2O_3 oxygen carrier was enhanced. Meanwhile, in the fixed-bed test, the purities of H_2 and carbon-containing substances in the steam oxidation stage were 100% and 0, respectively, which proved that no carbon deposit was generated in the reduction stage. Kang et al. [177] prepared the ceria-enhanced Fe_2O_3/Al_2O_3 mesoporous oxygen carrier with a large specific surface area and used it for chemical looping dry reforming. Due to the large specific surface area, the reaction gas was in close contact with CeO_2. Therefore, compared with the Fe_2O_3/Al_2O_3 oxygen carrier prepared by the wetness impregnation method, the H_2/CO ratio and average carbon deposit decreased by 28% and 63%, respectively. In the preparation of catalysts, inert carriers are mostly used, and oxygen carriers are no exception. However, Zeng et al. [251] believed that the addition of Al_2O_3 and other inert materials diluted the active components, which made carbon deposition and other problems more serious, and that the addition of ion-conducting supports promoted the transport of oxygen from the bulk phase to the surface. Indeed, the addition of the gadolinium-doped cerium oxides (GDC) support allowed the oxygen carrier to achieve maximum conversion at a lower temperature and in a shorter time than pure Fe_2O_3 and Fe_2O_3/Al_2O_3. Zeng et al. [252] conducted long-cycle tests on $Fe_2O_3/Gd_{0.3}Ce_{1.7}O_{2-\delta}$ and found that the oxygen carrier maintained good activity for 30 cycles. Also, it was shown that oxygen ion conductivity is the rate-determining step of the process. Therefore, the introduction of $Gd_{0.3}Ce_{1.7}O_{2-\delta}$ support enhanced the oxygen ion conductivity of the oxygen carrier, which is the reason for the good reactivity of the oxygen carrier.

During the CLC process, the addition of La_2O_3 can significantly inhibit the phase separation of the iron oxide oxygen carrier, which makes the oxygen carrier show good reactivity and stability. Tang et al. [180] combined the advantages of La_2O_3 and CeO_2 and added them together to the iron oxide oxygen carrier. XRD characterization showed that $LaFeO_3$ and $CeFeO_3$ formed during the reaction process and that the dispersion of iron oxide was improved due to the addition of La and Ce. The formation of $LaFeO_3$ perovskite enabled lattice oxygen to be quickly transferred from the bulk phase

to the surface, while the formation of $CeFeO_3$ allowed more oxygen vacancies in the oxygen carrier, thus increasing the oxygen migration capacity. Through the cycling test, it was found that although the Fe_2O_3/Al_2O_3 carrier possessed the highest CO selectivity in the first cycle, it rapidly decreased, and the carbon deposition increased significantly. For the oxygen carrier doped with La, it maintained good stability in 10 cycles, which proved that the addition of La increased the stability of the oxygen carrier. When CeO_2 or Zr/La-modified CeO_2 was used as a support for an Fe-based oxygen carrier, the oxygen carrier exhibited good chemical looping performance [253–255]. When Zr-doped CeO_2 was used as a support, no CO_x was found in the steam oxidation stage in the chemical looping hydrogen generation, and the presence of Zr also prevented the migration of Fe ions, thereby improving the sintering resistance of the oxygen carrier [253]. Xiong et al. [256] further modified the CeO_2 support, thus contributing to the formation of oxygen vacancies in the carrier, which further affected the oxygen ion conductivity. Meanwhile, the introduction of lanthanum and gallium promoted the formation of oxygen vacancies and inhibited the outward migration of iron ions to a certain extent.

Researchers are more concerned about how the oxygen carrier changes during the chemical looping reforming process, so the advantages of in situ characterization in determining the reduction path become more prominent. Müller et al. [257] found that the reduction path of Fe_2O_3/ZrO_2 through in situ XANES and ex suit XRD was consistent with the existing literature. Fe_2O_3 followed the path of Fe_3O_4, FeO and Fe, and the process from FeO to Fe was the slowest. Zhou et al. [258] also studied the reduction process and the effect of reduced Fe species in chemical looping dry reforming of methane. Similarly, Fe_2O_3 was reduced to Fe_3O_4 at the earlier stage of the reaction, converting CH_4 to CO_2. However, the small amount of CO_2 would inhibit the subsequent partial oxidation of methane to syngas. Introduction of reduced catalyst with low Fe valent could increase syngas production and it seemed that these reduced pieces, e.g., Fe^0, could consume CO_2 with its ability in catalysing the dry reforming, alleviating inhibition effect of CO_2 generated as result of full CH_4 oxidation by Fe_2O_3 to Fe_3O_4, and facilitating syngas generation. When Cu was added to the iron oxide oxygen carrier, Cu existed in the form of $CuFe_2O_4$ in the oxygen carrier. The reduction of $CuFe_2O_4$ and Fe_2O_3 in the oxygen carrier occurred synchronously, and $CuFe_2O_4$ was reduced to Cu and Fe_3O_4. In addition, the addition of Cu accelerated the reduction of Fe_2O_3 to Fe_3O_4, and although there was no change in the reduction path of Fe_2O_3, the overlap between the two intermediates of Fe_3O_4 and FeO was smaller, indicating that the conversion of Fe_3O_4 to FeO was faster. Compared with the undoped one, the doping of Cu made the oxygen carrier complete reduction in fewer pulses, which proved that the addition of Cu changed the reduction path of the original oxygen carrier and obviously promoted the oxygen carrier. X-ray absorption spectroscopy (XAS) characterizations can not only judge the reduction path but also understand the atomic coordination environment and surface disorder degree of the oxygen carrier. Müller et al. [259] revealed the effect of pH on the preparation process more clearly with the aid of XAS characterizations. XANES results showed that pH could affect the local coordination environment of Fe atoms on the oxygen carrier, and the octahedral environment of iron atoms became more distorted as the pH decreased. At the same time, EXAFS characterization indicated that the degree of disorder on the surface also increased with decreasing pH. This high degree of disorder was attributed to the insertion of Fe^{3+} into ZrO_2.

In order to judge more intuitively the oxygen conductivity of the oxygen carrier and provide more direct evidence for oxygen ion conduction, electrochemical testing methods are introduced into the oxygen carrier characterization process to show the oxygen ion conductivity of the oxygen carrier [251, 259]. Electrochemical impedance spectroscopy (EIS) and electrical conductivity relaxation (ECR) measurements are representative electrochemical tests that are commonly used in button batteries and solid oxide fuel cells, and can obtain the conductivity of the tested materials.

The addition of the support generally plays a role in dispersing the active components, but the ECR test shows its more important significance. The addition of ZrO_2 support to the Fe_2O_3 oxygen carrier increased the conductivity of the oxygen carrier, and significantly reduced the activation energy of ion transport, meaning that ZrO_2 enhanced the solid diffusion of oxygen anions and electrons in the oxygen carrier [259]. For the EIS test of oxygen carriers, the conductivity can be divided into two parts, one is generated by oxygen ions and the other is generated by electrons. From the experimental results, compared with the conductivity of oxygen ions, the conductivity of electrons was negligible, indicating that the conductivity of oxide ions was dominant. Moreover, it was found that the addition of ion-conducting supports significantly increased the conductivity of oxygen carriers, providing theoretical support for the adoption of perovskite and GDC materials with good ion conduction [251]. In addition to revealing the role of the carrier, the ECR test is used to detect the effect of doping. Gong et al. [260] adopted ECR to obtain the oxygen bulk diffusion coefficient and surface exchange coefficient of the Ce-doped perovskite oxygen carrier, and found that the doping of cerium reduces the activation energy for lattice oxygen migration. In order to clarify the reason for the increase in conductivity caused by doping, Gong et al. [261] conducted an in-depth discussion and found that with the addition of Ce, the degree of distortion of the FeO_6 octahedral increased, which might be the reason for its conductivity change.

In order to understand the phase change of Fe_2O_3-$La_{0.7}Sr_{0.3}FeO_3$ during cycling, in situ XRD characterization was adopted. Ex situ XRD showed that the oxygen carrier was composed of $La_{0.7}Sr_{0.3}FeO_3$ and $SrFe_{12}O_{19}$ before the reduction began [262]. At the beginning of the reduction, perovskite was found to shift to a low angle by in situ XRD, accompanied by the disappearance of $SrFe_{12}O_{19}$ and the appearance of Fe. After several scans, the Ruddlesden–Popper (RP) structure also appeared, and finally, La_2O_3 and a small amount of SrO appeared. After water oxidation, it was found that the initial state was not fully restored, which meant that the redox cycle was not completely reversible, and the composite material was in a dynamic change process. Multilength X-ray computed tomography (X-ray CT) was performed in order to observe the overall change in the oxygen carrier more intuitively. Therefore, the surface and phase images of the oxygen carrier were visually observed, and the phase and pore structure distribution of the oxygen carrier in the dynamic change process were also obtained from the images, which provided a possibility for better observation of the changes of the oxygen carrier in the cycling process.

Fe-based composite oxide oxygen carriers are oxygen carriers with specific structures, mainly including spinel ferrite, ilmenite, and perovskite. The effect of mechanical mixing of two metal oxides is often the sum of the activities of the individual metal oxides. The difference between composite oxides and mechanical mixing is that the added components can improve the catalyst's activity by stabilizing the catalyst structure, changing the catalyst electronic structure, and forming defects on the surface. At the same time, composite oxides are mostly nonstoichiometric compounds with defects in the crystal structure. Therefore, they exhibit excellent oxygen and electron transfer behaviors in oxidation–reduction reactions.

Spinel composite oxides have been used for a long time in the complete and selective oxidation of hydrocarbons because of their low cost, environmental friendliness, high temperature resistance, and stable chemical properties. Zeng et al. [263] prepared Co–Mn co-doped iron-based spinel oxygen carriers and applied the oxygen carriers to the chemical looping CO_2 splitting process. The test results showed that the $Mn_{0.2}Co_{0.8}Fe_2O_4$ oxygen carrier exhibited the CO yield comparable to perovskite oxygen carriers at 650 °C, proving the feasibility of the spinel oxygen carrier application. Huang et al. [264] conducted a detailed exploration of the reaction mechanism of spinel oxygen carriers by in situ XPS. They found that the reaction process was all carried out on the surface of the oxygen carrier, so the concentration gradient drove the gradual transfer of lattice oxygen from the bulk phase to the surface. Evdou et al. [265] tested the performance of spinel ferrites with different A-sites in chemical looping, and found that the performance and stability of oxygen carriers change significantly with various A-site metals. The $CuFe_2O_4$ oxygen carrier maintained stability while exhibiting the highest CH_4 reactivity and the largest amount of lattice oxygen involved in the reaction. Compared to $CuFe_2O_4$, the initial reactivities of $NiFe_2O_4$ and $ZnFe_2O_4$ were moderate, and their deactivation was obvious in five cycles, but the causes of Ni and Zn iron spinel deactivation were different. XRD characterization of the oxygen carriers after redox cycles showed that $ZnFe_2O_4$ was decomposed into iron oxide and metallic Zn, while $NiFe_2O_4$ showed no phase separation. There were aggregates of zinc in $ZnFe_2O_4$ after cycling, and the $NiFe_2O_4$ after cycling showed obvious sintering according to the SEM images. However, SEM–EDS showed that Ni and Fe simple substances of $NiFe_2O_4$ were evenly distributed, and the ratio of Ni/Fe was 1/2, proving that the cause of deactivation was sintering rather than phase separation.

Solving phase separation and sintering issues is the focus of future research on spinel oxygen carriers. Huang et al. [266] investigated the application of $NiFe_2O_4$ oxygen carrier in chemical looping hydrogen generation. Since Ni was thermodynamically impossible to decompose water, it was found in the TGA test that the H_2 production capacity gradually weakened with the addition of Ni. At the same time, it was found in fixed bed experiments that the H_2 production of Fe_2O_3 and $NiFe_2O_4$ decreased with decreasing reduction time, but spinel reached a deeper reduction degree than iron oxide in a short time due to its strong oxidation capability. Therefore, when the reduction time was shortened to 12 min, the H_2 yield of spinel exceeded that of iron oxide, illustrating that spinel was suitable for chemical looping hydrogen generation. However, Fe was separated in the form of iron oxide after a number of cycles, causing the spinel structure to be destroyed. Lee et al. [267] experimentally found that spinel-loaded oxygenates not only face the problem of phase separation, but also have the problems of surface grain aggregation and surface densification with the increasing number of cycles. These problems were effectively solved by introducing Al into the spinel to form a solid solution between the spinel and Al, which is beneficial for the long-term use of spinel oxygen carriers.

As mentioned earlier, $NiFe_2O_4$ spinel faces sintering problems, so Al_2O_3 is added to promote the dispersion of Ni and Fe to suppress sintering and phase separation. Compared with pure $NiFe_2O_4$ spinel, the addition of Al_2O_3 made only a small amount of iron oxide appear in the oxygen carrier after five cycles, and the H_2 yield remained stable for 20 cycles. The reason why Al_2O_3 enhanced the anti-sintering ability was that its uniform distribution on the surface of the oxygen carrier made the direct contact of adjacent Ni–Fe particles difficult, thus increasing the stability. At the same time, although Ni was thermodynamically incapable of being oxidized by steam, the strong phase action of Fe–Ni in

$NiFe_2O_4/Al_2O_3$ enabled part of the Ni to recover in the form of Fe–O–Ni under the steam atmosphere and then existed in $Ni_{0.4}Fe_{2.6}O_4$. On the basis of the Al_2O_3 support, Ma et al. [268] applied CeO_2, ZrO_2, and $CeZrO_2$ supports to $NiFe_2O_4$ spinel oxygen carriers. When ZrO_2 and $CeZrO_2$ were used as supports, oxygen carriers suffered serious phase separation and sintering problems. However, the $NiFe_2O_4/CeO_2$ oxygen carrier improved the oxygen migration ability while maintaining good cycle stability without phase separation.

Naturally occurring ilmenite has shown good performance in CLC. Fan et al. [269] applied it to CLR, and fully analyzed the morphological changes of ilmenite during the reaction. According to the SEM characterization results, the Ti–Fe composite oxide formed nanobelts on the surface after oxidation treatment at 700 °C, and the oxygen carrier became porous with increasing cycle number. The DFT calculation results showed that the formation of surface nanobelts mainly composed of iron oxide was due to the fact that the energy barrier of Fe ions migrating to the surface was smaller than that of Ti ions. At the same time, $FeTiO_3$ had a lower E_{vac} than Fe_2O_3, which made it easier to form a porous structure on the surface after cycling. The porous structure of ilmenite worsened its mechanical properties, and the formation of nanobelts also promoted phase separation. In order to alleviate the problems of mechanical properties and phase separation of ilmenite, Fan et al. [143] adopted an Al-based skeleton to the preparation of oxygen carriers. The existence of the Al-based skeleton enabled the oxygen carrier to maintain good activity and stability under 3000 cycles.

Perovskite has gained prominence in three-way catalysis, complete oxidation of hydrocarbons, and fuel cells due to the variability of its constituent elements, valence states, stoichiometric ratios, and oxygen vacancies [270]. The defects in perovskite are mainly oxygen vacancies, which can not only promote the transport of lattice oxygen but also assist the activation of many reactions, so perovskite can be well applied in chemical looping. La-perovskite is the most widely used perovskite-type oxygen carrier in CLR. Mihai et al. [132] applied $LaFeO_3$ perovskite to chemical looping methane partial oxidation, and investigated the influence of the particle size and oxygen content of the oxygen carrier on the reaction process and kinetics. XRD characterization revealed that the particle size of the oxygen carrier changed with the complex agent selected during the preparation process, which in turn affected the cycling stability of the oxygen carrier. By analyzing the performance of the oxygen carrier, it was found that the recovery time for the oxygen carrier in the oxidation stage was much less than the reaction time in the reduction stage. Based on performance data, Mihai et al. [132] proposed that the types of methane oxidation products were closely related to the coordination environment of Fe, and the coordination environment changed dynamically during the redox process. During the reaction, the types of Fe could be roughly divided into three categories according to their coordination environment, and different types of iron correspond to different product distributions. For example, iron highly coordinated with oxygen atoms might be the active site responsible for complete oxidation, and iron with highly coordinated oxygen vacancies may be responsible for carbon deposition. UV–vis characterization showed that the absorption edge energy of the oxygen carrier with small particle size was larger, which meant a high resistance for O removal from the perovskite. Meanwhile, the method of controlling the surface oxygen concentration by controlling the oxidation time was adopted to optimize the performance. It was found that when the oxidation time was 95 s, almost pure syngas was obtained. However, due to incomplete oxidation, the H_2/CO ratio and carbon deposition increased. Chen et al. [271] carried out a detailed study on the coordination environment of iron in perovskites. They found that the reduction process of the oxygen carrier is divided into three stages, and the coordination environment of iron in the perovskite is different in these three stages. And the coordination environment of iron, that is, the concentration of oxygen vacancies, changes the energy barrier for complete oxidation of methane. Therefore, the transition of the oxygen carrier from an oxygen-rich surface to a surface dominated by oxygen vacancies implies a transition from complete oxidation of methane to selective oxidation.

For perovskites used in the chemical looping process, it is generally to use different metals to replace the A or B positions. According to the principle of electrical neutrality, perovskites formed by replacing similar A or B ions with similar ions can not only change the original oxidation state and coordination state of A or B but also cause defects in the structure, especially the concentration of oxygen vacancies, to change significantly. For $LaFeO_3$ perovskite, the modification of the A-site mainly uses Sr or Ce, while the modification of the B-site mainly uses transition metal elements. He et al. [118] replaced the A and B sites of $LaFeO_3$ perovskite, and found that when a part of La was replaced by Sr, the oxygen vacancies of the oxygen carrier were increased and the decomposition of CH_4 was suppressed, so the performance of the oxygen carrier was significantly improved. When 30% of Fe was replaced by Co, the oxygen-donation ability, anti-coking performance, and H_2 generation capacity of the oxygen carrier were all improved, and it remained stable for 20 cycles [116]. Introduced Ni species in $LaNi_{0.07}Fe_{0.93}O_{3-x}$ were well dispersed on the surface of $LaFeO_3$ and could play a catalytic role in adsorbing and activating CH_4 during the reduction process as revealed through experimental investigation and DFT calculations, resulting in enhanced activity and lowered reaction temperature for syngas and H_2 generation. The reduced Ni species generated in the reduction step could also promote the splitting of H_2O to H_2 at relatively low

temperatures. The formation of H_2 started at 302 ℃, which was about 70 ℃ lower than that of reduced pure $LaFeO_3$ and the improved performance was able to remain after 50 successive redox cycles [272]. Li et al. [273] adopted Ce and Ni to dope the A- and B-site of $LaFeO_3$ perovskite, respectively, and investigated the effect of calcination temperature on the reaction performance of the oxygen carriers. The experimental results showed that with the increase of the calcination temperature, the nickel gradually migrated to the surface of the oxygen carrier, thus making the oxygen carrier more prone to carbon accumulation, so that the low calcination temperature may be more favorable for the $LaFeO_3$ perovskite to improve the anti-carbon performance. Wang et al. [274] modulated the A-site of $La_{1-x}Sr_xFe_{0.8}Al_{0.2}O_3$ oxygen carriers to improve the oxygen content of the oxygen carriers. The experimental results show that after the oxygen carriers were reduced by CH_4, the modulation of the A-site causes the rapid formation of Fe^0 and RP structure oxide. The RP structure oxide has good oxygen transport properties, so the perovskite and RP structure oxide transferred lattice oxygen rapidly to the Fe^0, thus suppressing the generation of carbon deposits.

For the suppression of carbon deposition, in addition to modifying the oxygen carrier to accelerate the transmission of lattice oxygen, it can also be achieved by adjusting the reduced properties of the oxygen carrier, such as forming an alloy. It can also avoid the contact of simple metal substances with the reactants through physical isolation, which avoids the formation of carbon deposits in space. The reason for the carbon deposition on the iron-based oxygen carrier is the appearance of Fe^0. Wang et al. [275] introduced Sn in barium iron perovskite so that the Fe–Sn alloy instead of Fe^0 was in contact with the reducing atmosphere to achieve this purpose. Wang et al. [276] introduced Al into iron-based perovskites so that the oxygen carrier formed a core–shell structure during the reduction process. The formation of core–shell structure after reduction was clearly observed through HRTEM and EDS mapping. The formation of the core–shell structure was attributed to strong metal-support interactions, and the core–shell structure prevented elemental iron from directly contacting CH_4, thus inhibiting the generation of carbon deposits. The addition of Al achieved the in situ coating of elemental iron, and the resulting double perovskite shell also had good lattice oxygen conductivity. XANES and Mössbauer characterization revealed that Al-doped samples had a higher proportion of Fe^{4+} and a lower proportion of oxygen vacancies, indicating that the addition of Al suppressed the generation of oxygen vacancies. DFT calculations showed that Sr and Al co-doped samples could produce two types of oxygen vacancies, namely, Fe-O_{Vac} and Al-O_{Vac}. The E_{vac} of Fe-O_{Vac} was lower than that of Al-O_{Vac}, indicating that the addition of Al inhibited the formation of oxygen vacancies, thus effectively alleviating the production of methane overoxidation.

In addition to La-perovskite, Zhang et al. [277, 278] studied the application of $SrFe_{3-\delta}$ perovskite in CLR (Fig. 12). Instead of directly using perovskite as the oxygen carrier, Zhang et al. [277] dispersed $SrFe_{3-\delta}$ perovskite into the CaO dispersing medium to form nanocomposites. By shortening the oxidation time, the average conversion of CH_4 reached 90%, and the conversion of CO_2 in the oxidation stage was maintained at 100%. At the same time, Zhang et al. [278] dispersed perovskite into CaO·MnO, and found that manganese oxide reacted with carbon deposits at high temperatures, which effectively suppressed the carbon deposit selectivity. On this basis, Zhang et al. [279] also used chlorine dopants for $SrFeO_{3-\delta}$-CaO to improve the performance. The introduction of chlorine promotes the cracking of methane in the reduction process, so that the conversion of CH_4 and CO_2 can reach up to 98% and 100%, respectively, with high carbon efficiency.

In addition to spinel, ilmenite, and perovskite composite oxide oxygen carriers discussed in the previous sections, hexaaluminate structure oxygen carriers have also received close attention due to their structural specificity and high temperature stability [152, 280, 281]. After the Fe-based oxygen carrier is reduced by CH_4 and reoxidized with air, electrophilic O^{2-} or O^- species are enriched on the surface, thereby reducing the overall CO selectivity. In order to solve this problem, Wang et al. [152] adopted a similar method mentioned in the previous section to control the regeneration extent of oxygen carriers. For the Ba-hexaaluminate oxygen carrier, the oxidation time was shortened, which increased the selectivity of CO by 43% during the methane reduction stage [152]. They further discussed the active sites of methane oxidation and the reason for the increase in selectivity, i.e., Fe^{3+} in Al(1), Al(2), and Al(3) sites of $BaFe_3Al_9O_{19}$ oxygen carrier, which were beneficial to the combustion of methane to generate CO_2, were reduced, and the amount of Fe^{2+} and Fe^0, which were responsible for CO generation, was increased. Wang et al. [181] further studied the La-hexaaluminate oxygen carrier, and found that O_6-Fe^{3+} (Oh) in the $LaFe_3Al_9O_{19}$ oxygen carrier had a high activity to completely oxidize methane in the magnetite structure of oxygen carrier activity, while O_5-Fe^{3+} (Tr) and O_4-Fe^{3+} (Th) in the $LaFe_3Al_9O_{19}$ oxygen carrier selectively oxidized methane to syngas. Interestingly, when CO_2 was used as an oxidant, CO_2 only selectively oxidized O_5-Fe^{3+} (Tr) and O_4-Fe^{3+} (Th), which effectively improved the selectivity of syngas and made effective use of CO_2. Substituting part of Fe with other metals in $BaFe_3Al_9O_{19}$ was further studied to optimize the performance of oxygen carriers [282]. Bimetallic $BaFe_2MAl_9O_{19}$ (M = Mn, Ni, and Co) only crystallized in β-Al_2O_3 hexaaluminate due to the existence of Mn, Ni, and Co, with + 2 valence state, and the β-Al_2O_3 structure remained during the CH_4 reduction step. It was found the CO_2 regenerated $BaFe_2CoAl_9O_{19}$ oxygen

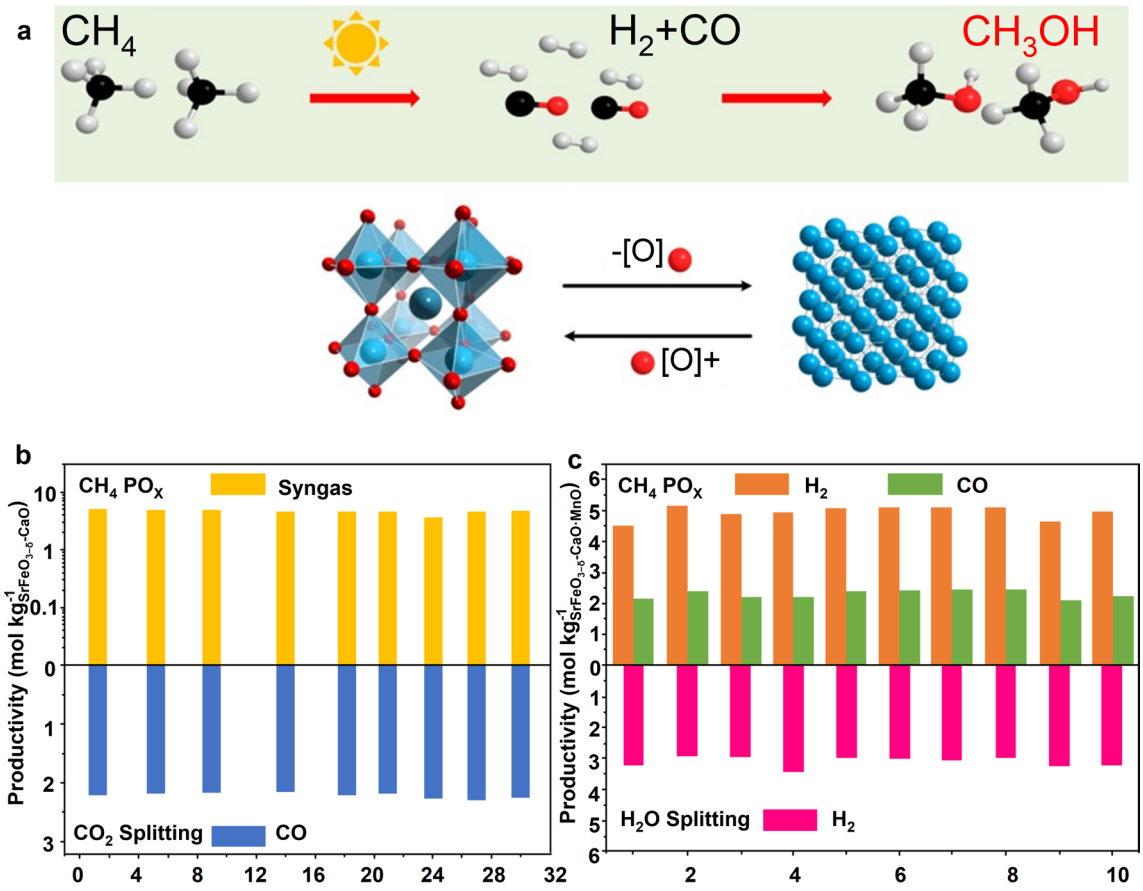

Fig. 12 **a** Coproduction of H_2/CO and CH_3OH from CH_4 and H_2O/CO_2 by chemical looping reforming. Reproduced from ref. [278] with permission from the American Chemical Society, copyright 2019. **b** Redox stability of $SrFeO_{3-\delta}$-CaO at 980 °C during the chemical looping dry reforming process. Reproduced from ref. [277] with permission from the American Association for the Advancement of Science, copyright 2017. **c** Redox stability of $SrFeO_{3-\delta}$/CaO·MnO at 900 °C during the chemical looping steam reforming process. Reproduced from ref. [278] with permission from the American Chemical Society, copyright 2019

carriers exhibited improved reactivity and cyclic stability for CO_2 utilization and syngas generation with high CH_4 conversion, high syngas yield and desirable H_2/CO ratio (~ 2). The performance improvement was attributed to the enhanced oxygen-donation ability and the preservation of hexaaluminate phase during successive CH_4/CO_2 redox cycles. The performance of the oxygen carrier is closely related to the crystal structure of the oxygen carrier, and the necessary calcination temperature guarantees the formation of the target crystal phase, as is the La-Fe-Al hexaaluminate oxygen carrier [281]. When the calcination temperature did not reach the crystal phase formation temperature, the oxygen carriers were mainly iron oxide and perovskite. With increasing calcination temperature to 1100 °C, the crystal structure of the oxygen carrier was hexaaluminate, and there were no impurities. By testing oxygen carriers with different calcination temperatures, it was found that there was a clear difference, which showed that the performance of the hexaaluminate oxygen carrier was related to its crystal structure rather than composition. The hexaaluminate oxygen carrier also has a relatively special property that it can still maintain the original crystal structure after reduction. By comparing the XRD of the fresh oxygen carrier with the reduced oxygen carrier, the XRD peak of the reduced oxygen carrier shifted to a low angle due to the reduction of iron, but it still maintained the MP structure. This property was due to the charge compensation mechanism of hexaaluminate. At the same time, this charge compensation mechanism will also be evident when Al is replaced by different metals [280]. XPS revealed that the doped Mn, Ni and Co metals all existed in the form of divalent ions, so that compared with the undoped oxygen carriers, the XRD results of these doped oxygen carriers were mainly β-Al_2O_3 because the ideal valence state of large cations in β-Al_2O_3 was 1.5 and that in MP was 2.4. In most articles, the general focus is on the chemical properties of the oxygen carrier, and the physical properties are only concerned with the specific surface area and the like, but the mechanical properties of the oxygen carrier are also extremely important to it. Good mechanical properties are

the prerequisite to ensure the normal operation of the oxygen carrier. The mechanical properties of hexaaluminate oxygen carriers doped with different metals were tested, and it was found that the mechanical properties were also related to the doped metals.

The advantages of low price and wide sources of iron ores have made the wide applications of Fe-based oxygen carriers more feasible. At present, iron ores have been used in various chemical looping processes, with ilmenite as one successful example for CLC. Lu et al. [283] applied ilmenite and nickel-impregnated ilmenite to the CLR process, and the iron species in ilmenite was also gradually reduced from Fe^{3+} to Fe^0 during the reduction process. And when nickel was introduced, the oxygen carrier was reduced to form Ni or Ni–Fe so that syngas was prepared in the presence of CO_2. Different from the introduction of transition metal oxides, Gu et al. [284] modified natural iron ore with rare earth metals, and found that the introduction of CeO_2 and La_2O_3 both promoted the reactivity of iron ore, and no carbon deposits were found during the reduction process. The introduction of La_2O_3 causes the formation of $LaFeO_3$ after the oxygen carrier is oxidized, which is beneficial to the H_2 production. Lu et al. [285] used magnetite for chemical looping methane reforming and explored the changes of magnetite during the reaction. TGA tests showed that magnetite required a longer induction period to obtain better performance, which was probably related to the dense structure of magnetite. And the presence of only a small amount of CO_2 during the performance test indicated that magnetite oxidized methane to syngas with high selectivity. XRD characterization showed that the crystal phases of magnetite after the reaction were basically the same as those after calcination, which proved the stability of iron ore during the reaction. Further study was conducted and it was found that the temperature of the reduction as well as reoxidation process exerted a great influence on the reactivity and purity of H_2 [286]. Increasing temperature from 800 to 1000 ℃ was beneficial to the reduction of iron oxide which took part in methane activation, and controlling the reoxidation temperature under 650 ℃ would eliminate the effect of carbon impurities (C and Fe_3C) generated during the reduction process on the purity of H_2. When the reoxidation was higher than 650 ℃, the steam would react with carbon deposit to form CO and CO_2, resulting in lower purity of H_2. Besides, pre-treatment of iron ore was responsible for performance improvement. Iron ore generally needs to be calcined at high temperatures to remove moisture and volatiles before engagement in redox cycles. At the same time, metal hydroxides and carbonates are decomposed, and stable metal oxides are formed after calcination. Therefore, the H_2 yield in the steam oxidation stage of the calcined oxygen carrier was slightly improved compared with that of the original oxygen carrier [285]. Li et al. [287] concluded that ultrasonic treatment also leads to the enhancement of the performance of iron ore, the reason being that ultrasonic action promotes the interaction between the active fractions in iron ore and between the active fractions and the inert material, thus increasing the activity of iron ore. It was also found that during the reduction process of magnetite, the reduction occurs first at the boundary between the active fraction and the inert material, and then gradually spreads to the surrounding area.

Hematite has good activity and stability in the process of methane chemical looping combustion [288], and Gu et al. [289] applied it for CLR and modified it with sunflower straw ash. The results proved that the H_2 yield of the modified iron ore is increased by approximately 1.1 times, and has a better stability. The reason for the good performance was that the sunflower straw ash contained a certain proportion of potassium carbonate, and the addition of potassium carbonate weakened the Fe–O bond. In addition to CH_4, hematite has also been used in the process of producing H_2 from vegetable oil with desirable performance [290]. Although iron ore has achieved promising results in the application of CLR, problems (low reactivity, sintering, agglomeration and changes in mechanical properties) caused by cycling have also occurred in the process. Huang et al. [291] used hematite for biomass to syngas, and found that the presence of hematite increased the gas yield and carbon conversion by approximately 41%. However, as the number of cycles increased, hematite sintering and abrasion became serious problems. Therefore, the application of iron ore in the chemical looping process needs further research on these aspects.

Although the supported oxygen carrier is more convenient to prepare, it is correspondingly faced with more serious sintering and carbon deposition problems, and the activity of iron oxide needs to be further improved. Although composite oxide oxygen carriers can combine the effects of multiple metals, they also face the disadvantages of poor oxygen storage capacity and structural decomposition. Its application needs further research to obtain oxygen carriers with high activity and selectivity. For naturally occurring iron ore-based oxygen carriers, subsequent research should focus on inhibiting sintering and agglomeration, and improving mechanical properties.

4.4 Copper based oxygen carrier

Lewis and Gillil proposed to use the redox cycle between CuO and Cu_2O for producing food grade CO_2, which is a typical example of CLOU [48, 292–294]. The equilibrium oxygen partial pressure with CuO could be as high as

0.01 bar at 900 °C, which is much higher than that of other types of oxygen carriers and could dramatically promote the carbonaceous fuel gasification and combustion process. Cu-based oxygen carriers have the advantages of high reactivity, high oxygen storage capacity, and low price [133, 136]. However, the sintering problem under high-temperature reaction conditions is one of the main reasons limiting its future development in the field of CLR. The literature shows that the reactivity with CH_4 of Cu-based oxygen carriers, although less than that of Ni-based oxygen carriers, was stronger than that of Fe-based and Mn-based oxygen carriers, which proves its potential for development [295]. Therefore, solving the sintering problem of Cu-based oxygen carriers has been the main direction of its further development in chemical looping applications. Both supports and promoters have been tested to alleviate the sintering problem. The addition of inert supports such as Al_2O_3 [133, 296–298], TiO_2 [133, 297, 299], and $MgAl_2O_4$ [300] can slow down the sintering problem of copper oxide, but the addition of Al_2O_3, an acidic support, leads to the aggravation of carbon deposition [301]. As a result, Alirezaei et al. [193] incorporated ZrO_2 into Al_2O_3, which promoted the dispersion of copper oxide and adjusted the mechanical properties of oxygen carriers. Such modification also effectively suppressed carbon deposits, with the maximum reduction of carbon accumulation by approximately 94%. Instead of alleviating the sintering problem at high reaction temperature, it is an alternative to enhanced oxygen transport capacity of Cu-based oxygen carriers under a lower temperature with alkaline metal oxides, e.g., MgO. Researchers tested the impact of alkaline earth metal oxides, i.e., Mg and Ca, as well as the alkali metal oxides, Na and K oxides, on the enhancement of oxygen uncoupling at lower temperatures. A series of CuO oxygen carriers with 5 wt% of alkali oxides addition were synthesised and studied with thermogravimetric analyzer regarding the oxygen uncoupling behaviour. The results showed that MgO had a positive effect while Na_2O and K_2O showed an opposite trend and CaO did not show sensible change on the uncoupling rate at temperature lower than 850 ℃. The clear enhancement of MgO addition was ascribed to its ability to enhance the chemical stability that allows steady oxygen uncoupling [294].

The relatively lower reforming temperature of alcohols can alleviate the sintering problem of copper-based oxygen carriers to some extent. Besides, the excellent performance of Cu–Zn–Al catalysts in traditional alcohol reforming processes for H_2 generation has inspired the exploration of Cu-based oxygen carriers in chemical looping alcohol reforming. For the as-proposed chemical looping oxidative steam reforming of methanol, the $Ca_2Fe_2O_5$ was utilized to support copper oxide to tune the redox activity and achieve a relatively stable catalytic activity. The lattice oxygen concentration is one of the dominant factors determining the methanol conversion pathways and a pathway from formaldehyde intermediate to methyl-formate intermediate was observed with decreasing lattice oxygen concentration by in situ drifts characterization. The introduction of $Ca_2Fe_2O_5$ was aimed at regulating the lattice oxygen's redox activity and mobility, achieving the homogenous release of lattice oxygen. Also, the active copper species were also kept at an appropriate oxidation state to provide compatible active oxygen species for methanol oxidative reforming. The Cu_2O–Cu looping was accomplished by regulating the reaction temperature and airflow rate, and this proposed lower-valence looping could prevent the excessive oxidation of methanol. During the performance tests, the copper-based catalyst, Cu_2O–$Ca_2Fe_2O_5$, showed high catalytic activity with a H_2 production rate of 37.6 μmol H_2/($g_{catalyst}$·s) under a temperature of 240 °C, as well as an acceptable redox durability within 60 cyclic tests [93]. Wang [113] loaded copper oxide on Al_2O_3 and used it for ethanol reforming. It was found that the oxygen released by copper oxide promoted the elimination of carbon deposition, and the carbon deposition gradually decreased with the increase of copper oxide when the reaction temperature reached 500 °C. Instead of avoiding carbon deposition, to generate high-purity H_2 with a low concentration of CO, the bi-functional material CuO–MgO was adopted for sorption-enhanced steam methanol reforming. CuO served as an active catalytic site for methanol reforming to H_2 and CO_2, and CO_2 was removed by MgO sorbent with high-purity H_2. Also, it was found that the appropriate amount of Cu^{2+} entering in MgO lattice could enlarge CO_2 adsorption capacity and enhance CO_2 desorption. Simultaneously, Cu species were significantly dispersed and stabilized due to the existence of MgO [195]. On this basis, sorption-enhanced chemical-looping oxidative steaming reforming of methanol was further proposed and simulated with the Cu–Mg based bifunctional catalyst. In the study, copper species existed in oxidized state and underwent a reduction process in the fuel reactor. Hence, the gradually reduced CuO provided not only catalytic site but lattice oxygen while Mg-based sorbent continued to go through CO_2 adsorption and desorption reactions. The simulation results revealed that CuO and MgO could shift the equilibrium of the WGS reaction and suppress CO generation. And the proposed process achieved auto-thermal operation after operation parameters such as water to methanol ratio and temperature of reactors being analysed and optimized [111, 194]. With further addition of Ga_2O_3, the catalyst showed strong resistance to particle sintering and agglomeration as the particle size of Cu showed no conspicuous change as evidenced by XRD and TEM characterization after cycles [112]. Without severe sintering problem under a relatively

lower alcohol reforming temperature, it could be anticipated that the integration of chemical looping and SER could be a promising strategy to address the carbon deposition issue and achieve high-purity H_2 production from alchols [195]. Fundamental and applied research on copper oxide for low-temperature reforming deserves further effort.

4.5 Cerium based oxygen carrier

CeO_2 is a typical representative of the oxygen carrier of fluorite structure. It has been extensively studied in the reactions of CO oxidation, CO_2 hydrogenation, and reforming of methane and alcohols, and has also been successfully applied in three-way catalysts [302, 303]. The rapid generation and elimination of oxygen vacancies in CeO_2 makes it a suitable oxygen carrier material [304]. CeO_2 was originally used as an oxygen storage material in automotive three-way catalysts, and the first generation of commercial CeO_2 oxygen storage materials came out in 1989 [305]. The role of CeO_2 is to make the three-way catalyst adapt to different working conditions through the reversible transformation between Ce^{4+} and Ce^{3+}. At the same time, it can also promote metal dispersion, enhance support stability, and facilitate water gas shift and steam reforming reactions. The role of CeO_2 in this process is similar to that of oxygen carriers in CLR. Then, Otsuka et al. [306] applied CeO_2 catalyst to the field of methane oxidation and successfully obtained a synthesis gas with a H_2/CO ratio of 2. The successful application of CeO_2 in three-way catalysts and methane oxidation has made it promising for CLR. For CeO_2, the good oxygen storage capacity and oxygen migration ability render CeO_2 a good choice as dopant or support for oxygen carriers, but when it is used as an oxygen carrier alone, its poor reactivity, low reduction degree, and sintering problems at high temperatures are exposed.

In the three-way catalyst, ZrO_2 was added to CeO_2 to improve the stability and oxygen storage capacity. Although the reactivity of ZrO_2 is not good, temperature programmed reduction and other characterizations show that CeO_2 doped with ZrO_2 improves the oxygen storage capacity, stability, and reducibility of CeO_2 [147]. Therefore, for cerium-based oxygen carriers, ZrO_2 is typically considered to be added to CeO_2. Otsuka et al. [307] conducted methane reforming test on CeO_2 doped with different proportions of ZrO_2. The results show that when the doping amount of ZrO_2 was 20%, the yield of H_2 and CO was approximately 1.7 times that of pure CeO_2, indicating that the addition of ZrO_2 significantly enhanced the reactivity of CeO_2. On this basis, Zheng et al. [148] prepared CeO_2-ZrO_2 oxygen carriers with a porous structure at different calcination temperatures. 3DOM structures have been shown to be more likely to form under low-temperature calcination and to enhance the reducibility and activity of CeO_2–ZrO_2 oxygen carriers. Performance tests showed that the low-temperature calcined oxygen carrier had the highest CH_4 conversion and H_2 yield, and maintained an ordered structure after multiple cycles. Meanwhile, Raman characterization revealed higher I_{603}/I_{463} ratios of porous CeO_2–ZrO_2 solid solution compared to nonporous samples, indicating that the porous samples had a higher concentration of oxygen vacancies. Furthermore, the concentration of oxygen vacancies decreased with increasing pore size, proving the effect of pore structure on the oxygen vacancy concentration and reactivity of the CeO_2–ZrO_2 oxygen carrier [158].

Directly supporting CeO_2 on a support having a 3DOM structure is also an alternative. Macroporous $LaFeO_3$ loaded with CeO_2 is prepared with the aim of combining the advantages of CeO_2 and $LaFeO_3$ perovskite to obtain an oxygen carrier with excellent performance, as well as providing a new way to combine Ce-based and Fe-based oxygen carriers [99]. TEM images showed that CeO_2 with particle sizes of 2–3 nm was evenly dispersed on the $LaFeO_3$ perovskite. Meanwhile, the activity tests showed that the performance of the oxygen carrier remained stable in 30 cycles and that the crystal phase of the oxygen carrier did not change after multiple cycles. Simultaneously, after CeO_2 was supported on the $LaFeO_3$ perovskite, the reducibility of the oxygen carrier was significantly improved. Fe in the perovskite was inclined to Fe^{2+} with the interaction of CeO_2 and the perovskite. Doping with a small amount of Fe causes more oxygen vacancies in CeO_2 while forming a solid solution, which helps improve the activity and stability of CeO_2. Concerning the development of Ce–Fe oxygen carriers, Li et al. [142] and Zhu et al. [308] have elaborated on it in detail, which is not described here. In addition to doping CeO_2, analogous to the presence of noble metals in the three-way catalysts, transition metals such as Ni, Fe and Co with suitable catalytic ability can be added to CeO_2 to improve its reactivity [86, 114, 133, 167, 174, 309–311]. Ni has a high methane activation capacity, and its introduction into CeO_2 greatly increased the reactivity so that the conversion of CH_4 was maintained at 95% with 100% syngas selectivity at 800 °C during the 60 cycles test [165].

Different from doping or loading metals with CeO_2, Wang et al. [312] introduced tin oxide applied in the oxygen ion conductor to achieve water splitting through the circulation between CeO_2–SnO_2 and $Ce_2Sn_2O_7$ pyrochlore. Compared with the nonstoichiometric cycle of pure CeO_2, CeO_2 and SnO_2 were used to generate pyrochlore reversibly, which achieved the goal of Ce^{4+} to trivalent cerium, thereby increasing the reduction degree of CeO_2. On the basis of the $Ce_2Sn_2O_7$ pyrochlore. Wang et al. [166] further explored pyrochlore-type oxides, catalyzed the reaction by using Ni on the surface, and provided lattice oxygen through the reversible cycle of CeO_2–TiO_2 and $Ce_2Ti_2O_7$ pyrochlore (Fig. 13).

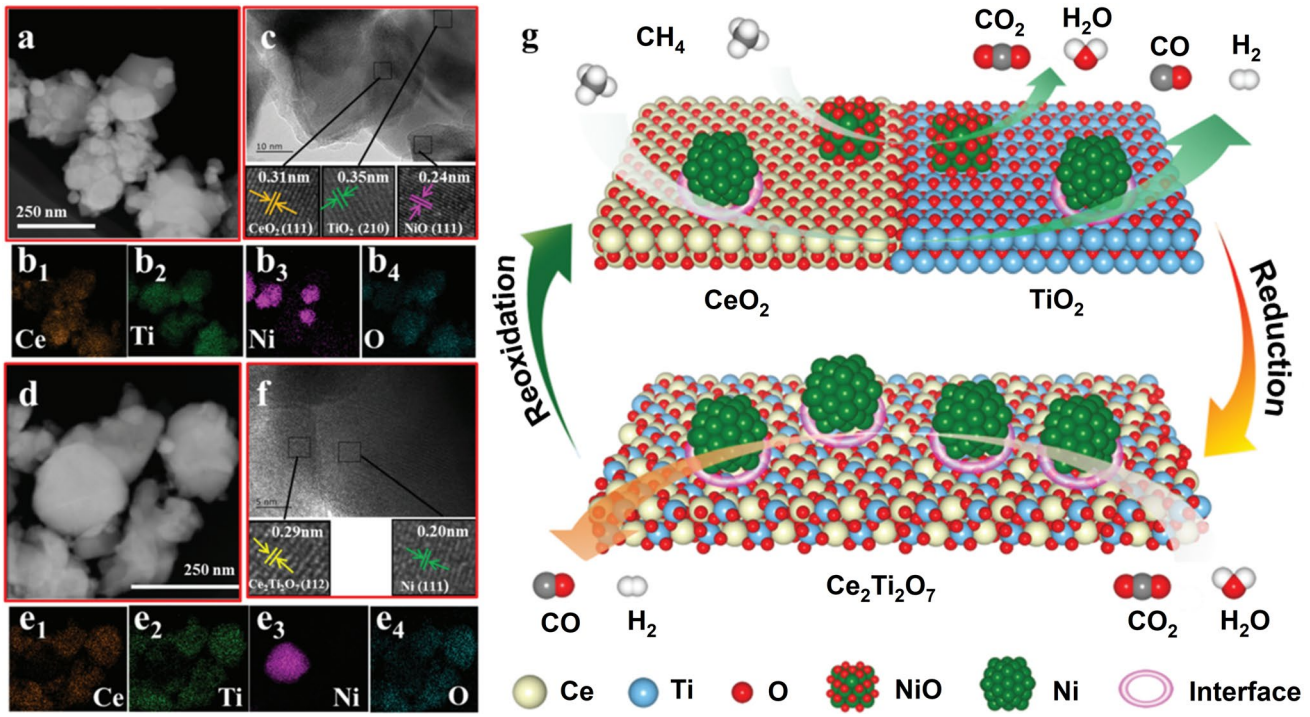

Fig. 13 **a** STEM image, **b1**–**b4** the corresponding element-mapping images and **c** HRTEM images of as-synthesized 5Ni/CeO_2–TiO_2. **d** STEM image, **e1**–**e4** the corresponding element-mapping images and **f** HRTEM images of 5Ni/CeO_2–TiO_2 after the CH_4 reduction half cycle. **g** Schematic of the reaction mechanism for chemical looping steam reforming of methane and chemical looping dry reforming of methane processes over the 5Ni/CeO_2–TiO_2 oxygen carrier. Reproduced from ref. [166] with permission from the Royal Society of Chemistry, copyright 2019

The synergistic effect between the surface metal and the oxide support significantly increased the yield of CO and H_2. High-resolution transmission electron microscopy (HRTEM) and scanning transmission electron microscopy combined with energy-dispersive X-ray spectroscopy (STEM-EDX) results showed that in the fresh and circulating oxygen carriers, NiO was supported on CeO_2 and TiO_2, but the CeO_2 and TiO_2 were not uniformly mixed. However, after the oxygen carrier was reduced by methane, the distribution of Ce and Ti was uniform, and the lattice fringes were consistent with pyrochlore, which proved the reversible cycle of CeO_2–TiO_2 and $Ce_2Ti_2O_7$ pyrochlore. According to DFT calculations, the E_{vac} of Ti-doped CeO_2 was lower than that of pure CeO_2 or TiO_2. The introduction of TiO_2 weakened the Ce–O bond and promoted the oxygen migration ability of CeO_2. At the same time, calculations showed that the addition of Ni and the corresponding metal-support interface also promoted methane activation and dissociation of H_2O or CO_2. By combining the reversible transformation of CeO_2–TiO_2 and a specific structural oxide, the catalytic effect of the metal was also fully exerted while Ce^{4+} was converted to Ce^{3+}, which provided a new design idea for Ce-based oxygen carriers.

4.6 Other oxygen carrier

Mn-based oxygen carriers not only have the advantages of low price and environmental friendliness like Fe-based oxygen carriers but also have various valence states (+2, +3, and +4). Johansson pointed out that the reactivity order of transition metal-based oxygen carriers with CH_4 was Ni > Cu > Mn > Fe, while the crushing strength was opposite, and many studies on Mn-based oxygen carriers have been carried out [295]. Although Mn has many valence states, the available valence states for practical use are very few because MnO_2 and Mn_2O_3 decompose at 460 and 820 °C, respectively [313]. At the same time, MnO is difficult to be reduced even at elevated temperatures. Therefore, for Mn-based oxygen carriers, the transformation of Mn_3O_4 to MnO is typically used to achieve the target product. Supported Mn_3O_4 oxygen carriers are mainly used in the CLC process, and the irreversible salts produced by the reaction between manganese oxide and commonly used supports are the main reason for their limited development. By applying Mn_3O_4 oxygen carriers with different supports to the CLC process, it is found that although Mn_3O_4/ZrO_2 faces structural crack problems due to the phase transition of ZrO_2, the weak interaction between Mn_3O_4 and ZrO_2

makes the oxygen carrier possess high activity and good resistance to carbon deposition [141, 314–316]. For CLR, Zr-modified Al_2O_3 also performed well as a support for Mn-based oxygen carriers [197]. Through XRD characterization, it was found that Zr was possibly inserted into Al_2O_3 or highly dispersed on Al_2O_3 and that the formation of $MnAl_2O_4$ spinel was restricted. At the same time, by adding CO_2 in the same proportion as CH_4 at the reduction stage, the conversion of CH_4 in the 16 cycles of the optimal oxygen carrier at 650 °C was above 95%, and the carbon deposition was reduced by approximately 50%.

In addition to changing the supports, the introduction of promoters could improve the performance of Mn-based oxygen carriers. Bazhenova et al. [317] theoretically explained and analyzed the influence of Fe doping on Mn_2O_3 at the atomic level by DFT calculations. Since Fe–O bonds were more stable than Mn–O bonds, the addition of Fe made the oxides more stable and changed the electronic structure of the oxides. At the same time, E_{vac} increased with the addition of Fe atoms, and the diffusion barrier changed with the concentration and distribution of Fe atoms. Although a series of explorations have been made on the application of manganese-based oxygen carriers in CLR, it has low selectivity to syngas and needs to increase the reactivity. Shen et al. [318] applied B-substituted $LaMn_{1-x}B_xO_{3+\delta}$ (B = Fe, Co and Ni) perovskites to the chemical looping steam reforming process and investigated the effect of different B-substitutions on the reactivity of oxygen carriers. The experimental results showed that different B-site substitutions promoted the oxygen release rate of $LaMnO_3$ to a certain extent, with the most obvious effect of nickel. However, nickel-doped oxygen carriers have the problem of carbon accumulation. Meanwhile, Fe and Co substitutions provide more active sites for the reaction, matching the bulk phase lattice oxygen migration rate, so the oxygen carriers show good performance. On this basis, Shen et al. [319] doped the A and B sites of $LaMnO_3$ perovskite with Sr and Co. The introduction of Sr promoted the migration of lattice oxygen through the generation of oxygen vacancies, while Co in the B-site could provide active sites for the reaction, so that the surface reaction and bulk phase lattice oxygen migration were well matched and the oxygen carrier showed good reaction performance. Research also showed introduction of Cu to B-site was featured with improved performance on carbon formation resistance. Catalysts with various amount of Cu showed different trend for H_2 productivity and resistance for carbon deposition. With increasing Cu content, H_2 productivity saw a rise at first and then dropped, while the amount of carbon deposition displayed a steady upward trend. An appropriate substitution of Cu for La was beneficial for promoting H_2 productivity and reducing carbon deposition and it was attributed to the enhanced reducibility and changes of oxygen species obtained from H_2-TPR and CH_4-TPR. [320]. One should also be aware that the amount of doping metal as well as calcination temperature are essential optimization parameters. Yang et al. [321] prepared two series of Fe-doped $LaMnO_3$ oxygen carriers calcined at temperatures ranging from 700 to 850 ℃. The series of $La_{0.85}MnFe_{0.15}O_3$ showed better structural and porous properties, and samples exhibiting higher CH_4 conversion and syngas productivity were with a higher concentration of oxygen vacancies and better oxygen mobility. For both series, $La_{0.85}MnFe_{0.15}O_3$ and $LaMn_{0.9}Fe_{0.1}O_3$, different calcined temperature resulted in the shift and intensity of reduction peaks in H_2-TPR and CH_4-TPR results, which implied the reducibility degree and oxygen mobility. It was found that two samples, $La_{0.85}MnFe_{0.15}O_3$ and $LaMn_{0.9}Fe_{0.1}O_3$, with calcination temperature at 800 ℃, presented ideal ratios of H_2/CO in the isothermal reaction and larger amount of H_2 during the water splitting step.

The applications of cobalt oxide in chemical looping reported in the literature are mainly as an auxiliary agent to increase the activity and stability of oxygen carriers, including inhibiting the interaction between metal and Al_2O_3 support, increasing the dispersion of metal to enhance the activity of oxygen carriers, and forming alloys with metal to suppress sintering [126, 313]. Although the oxygen carrying capacity of Co_3O_4 is much higher than that of NiO, Fe_2O_3, Mn_2O_3 and CuO, there are relatively few reports on Co_3O_4-based oxygen carriers. Leaving aside its high price, Co_3O_4 is less active at low temperatures. Its decomposition at 890 °C also limits the increase of reaction temperature because the CoO produced after decomposition has poor reactivity to reactants such as CH_4, and its reaction with supports (Al_2O_3, TiO_2, and MgO) is also considered to be one of the reasons for the degradation of oxygen carriers' performance [134]. With concerns on the reoxidation of cobalt in the cycling process and the reactivity, the development of cobalt oxide oxygen carriers is limited [322]. A deeper understanding of the phase and surface properties that influence the particle stability and reactivity of Co_3O_4 during the reaction could help promote its application in chemical looping. On the basis of optimizing the properties of unsupported Co_3O_4 oxygen carriers, Alalwan et al. [323] carried out a detailed study of the changes in the surface and bulk properties during the reaction process and proposed that the interface between the metal and metal oxide might be helpful to improve Co-based oxygen carriers. The Oxygen carrier was reduced through the path of Co_3O_4 to CoO and finally to Co, and its performance was enhanced with increasing temperature and decreasing space velocity in the test temperature and gas hourly space velocity range. Importantly, it was found through XRD and XPS characterization showed that the reduction process of CoO to Co followed the nucleation and nuclei growth

mechanism within the particle bulk. It was mainly because of the lower cohesive energy of oxygen atoms at the interface of these phases that CoO and Co mixtures had better performance.

The aluminate or titanate produced through the reaction between cobalt oxide and support during the reduction stage can also be directly used as the oxygen carrier. Wong et al. [200] and Rios et al. [324] took advantage of the stability of aluminates and titanates in Co-based oxygen carriers, and directly applied $CoAl_2O_4$ and Co_2TiO_4 oxygen carriers to chemical looping dry reforming and partial oxidation, respectively. They found through performance tests that although there were some deficiencies in the two oxygen carriers, the results proved the possibility of their applications in CLR. Perovskite structure has also been used in Co-based oxygen carriers due to their excellent high-temperature stability and oxygen migration ability [202, 203, 325, 326]. $BaCoO_{3-\delta}/CeO_2$ and $Ba_{1-x}Sr_xCoO_{3-\delta}/CeO_2$ oxygen carriers were used in chemical looping steam methane reforming to investigate the effect of support and A-site doping on the properties of Co-based perovskite oxygen carriers [202, 203]. Compared with the $BaCoO_{3-\delta}$ oxygen carrier, the addition of CeO_2 increased the syngas and H_2 yields. During the reduction process, CeO_2 mainly played two roles: one was to form $BaCeO_3$ with the consumption of $BaCoO_{3-\delta}$, and the other was to provide oxygen for methane partial oxidation while being reduced to $CeO_{1.675}$. Both of these processes promoted the production of syngas, and the presence of $CeO_{1.675}$ also increased the production of H_2 in the steam oxidation stage. After Sr doping, the A-site metal interacted with CeO_2 to reversibly form $BaCeO_3$ and $SrCeO_3$, which was beneficial for the production of syngas and H_2.

Lee et al. [327] applied B-site substituted $LaCo_{0.6}B_{0.4}O_3$ (B = Fe, Mn, Ni) oxygen carriers to the chemical looping steam reforming process and investigated the effects of different B-site substitutions on the performance of oxygen carriers. The experimental results showed that the introduction of iron promoted the oxidation of the oxygen carrier by steam and promoted the migration of lattice oxygen from the bulk phase to the surface oxygen vacancies, so that the $LaCo_{0.6}Fe_{0.4}O_3$ oxygen carrier has good reactivity and cyclic stability. Previous studies have shown that Co and Mn-based oxygen carriers are promising candidates, however, their corresponding oxygen partial pressure is more suitable for full oxidation applications, and how to tune their structures and properties for CLR remains challenging.

Tungsten oxides are located in the partial oxidation zone of the Ellingham diagram in Fig. 1, which proves that it is thermodynamically feasible to obtain syngas under a chemical looping fashion. The polyvalent state of WO_3 and its high melting point make it suitable for application in the field of chemical looping. Compared with Fe_2O_3, SnO_2, V_2O_5, and MoO_2 oxide, the methane reforming test in a fixed bed at 900 °C found that WO_3 had the highest CO selectivity and the lowest CO_2 selectivity [328]. Both calculations and experiments have proven that W-based oxygen carriers are potential candidates, but the main reasons for the lack of related research are their poor activity and the problem of carbon deposition. To solve these problems, researchers have conducted in-depth studies on the effects of supports and promoters on activity and stability. The activity of WO_3 on supports (Al_2O_3, SiO_2, and ZrO_2) was tested, and it was found that the performance of WO_3/ZrO_2 was significantly improved [204, 329]. Further research was carried out on WO_3/ZrO_2, and it was found that WO_3 would also be reduced by the syngas produced in the methane reforming stage and that the proportion of H_2 reduction would be greater [330]. Chen et al. [205] introduced NiO to modify WO_3 and improve its reactivity. Bulk doped Ni weakened the strength of the W–O bond to increase the oxygen transfer rate, and surface Ni form reduction was used as the active site for the catalytic methane reaction. The reaction mechanism of WO_3 with CH_4 was obtained through XRD and other characterizations. WO_3–$WO_{2.96}$ and $WO_{2.96}$–$WO_{2.72}$ were responsible for full oxidation, and $WO_{2.72}$–WO_2 and WO_2–W were responsible for partial oxidation. Methane cracking and carbon deposition were caused by metallic Ni and W. The modification of the surface and bulk made its performance much better than that of pure WO_3. However, its performance and structure gradually changed during ten cycles, which needed further improvement on the stability. In order to improve the activity of the tungsten oxide oxygen carrier and maintain the structural stability of the oxygen carrier during cycling, Liu et al. [206] prepared the Fe_yWO_x/SiO_2 oxygen carrier and applied it to CLR. The addition of iron greatly improved the performance of the oxygen carrier, and during the reduction process, the strong interaction between iron and tungsten resulted in the formation of the iron-tungsten alloy so that no phase separation occurred, ensuring structural stability. The TPR characterization showed that the reduction temperature of tungsten oxide decreased with the addition of iron, which proved that the addition of iron weakened the W–O bond and made tungsten oxide contribute more oxygen to participate in the reaction. The existence of the form also improves its selectivity. Iron existed in the form of Fe^{2+} in the oxygen carrier, which was also beneficial to the improvement of selectivity. The addition of iron to tungsten oxide provided a new strategy for the development of tungsten oxide oxygen carriers.

With the gradual maturity of the chemical looping reforming process, composite metal oxides are currently the mainstream development trend. After extensive literature review and analysis of the XRD data of the oxygen carrier after reduction, it was found that the composite metal oxide can be classified not only according to the active component but also according to its reduced state. The reduced state of the composite metal oxide can be roughly divided into the

following six categories. The first type is the solid solution formed after the reduction of oxygen carriers, mainly including Ce–Fe oxygen carriers [191]. The second type is the alloy formed after reduction, including Ni–Fe oxygen carriers [168] and spinel oxygen carriers [266], as well as $BaFe_{1-x}Sn_xO_{3-\delta}$ perovskite [275]. The third type is phase separation after reduction, and the phase separation can be further subdivided into two cases. One case is that the initial state can be recovered after oxidation, which mainly includes perovskite and double perovskite oxygen carriers, and a small part of spinel oxygen carriers [183, 184, 186, 199, 268, 331]. Another case is that the initial state cannot be recovered after oxidation, mainly including Ni-W and Fe-Ti oxygen carriers [33, 143, 205]. The fourth type is the composite metal oxide formed after the reduction of oxygen carriers, mainly including $CeO_{2-x}SnO_2/Ce_2Sn_2O_7$, CeO_2–$TiO_2/Ce_2Ti_2O_7$, $Ba_{1-x}Sr_xCoO_{3-\delta}/CeO_2$ and $BaCoO_{3-\delta}/CeO_2$ oxygen carriers [166, 202, 203, 312]. The fifth type is the elemental form after reduction, which $La_{0.8}Ce_{0.1}Ni_{0.4}Ti_{0.6}O_3$, Fe_2O_3-$CaTi_{0.85}Fe_{0.15}O_3$, and $La_{0.5}Ca_{0.4}Ni_{0.2}Ti_{0.8}O_{3-\gamma}$ oxygen carriers are typical representatives of this type [163, 332, 333]. This type of oxygen carrier will appear simple substances after reduction, but the main frames that are equivalent to the dispersion media remain unchanged. The last type is the oxygen carrier that retains the crystal structure after reduction. This type of oxygen carrier can still maintain the original crystal structure after the loss of oxygen, which is relatively rare, mainly including $LaFe_3Al_9O_{19}$ hexaaluminate oxygen carriers [152, 181, 280, 281, 282]. Although some studies do not show XRD characterization of the oxygen carrier after reduction, which makes some studies cannot be classified better, most of the classifications are currently representative. And for the oxygen carriers that do not show XRD characterization after reduction, it can be judged according to the type of its active material. For example, if the NiO oxygen carrier is doped with iron, an alloy may be formed during the reduction process [168]. The reduction state of the oxygen carrier is classified according to the representative oxygen carrier, but there are exceptions. For example, most of the perovskites undergo phase separation after reduction, but $BaFe_{1-x}Sn_xO_{3-\delta}$ perovskite forms an alloy [275]. Most of the spinel oxygen carriers form alloys after reduction, but $Mn_{0.5}Fe_{0.5}(FeAl)O_x$ undergoes phase separation [334]. The states of the oxygen carriers after reduction are not only to better distinguish the oxygen carrier, but also to predict the performance of the oxygen carriers. This classification can give researchers a general research direction before conducting literature research, for example, the performance advantages of oxygen carriers may be attributed to the formation of forming alloys or solid solutions after reduction. For example, most perovskite oxygen carriers can be restored to the original crystal phase, so the cycle stability is better. Although composite metal oxides can be classified according to the reduced state, at present, there is a lack of research on the mechanism of their different performance after reduction, and further research on the reduced state is needed.

5 Conclusions and perspectives

Conventional carbonaceous fuel reforming processes are both capital and energy intensive due to the lengthy unit operations. The chemical looping reforming process integrates the reforming reaction and gas–gas separation in one unit operation via the redox cycle of metal oxide-based oxygen carriers, which could potentially evolve as an affordable, clean and efficient alternative for syngas production. The overall reactions of CLR systems are the same as conventional reforming or partial oxidation processes. The rational design of the CLR reactor system could decouple these reactions with the circulation of effective oxygen carriers, and directly produce high-quality syngas (high CO/H_2 concentrations and desirable ratios) without the need for air separation and/or acid gas removal units. The CLR process is also advantageous in terms of exergy efficiency via recuperating the low-grade heat while producing more high-grade heat with the redox operation scheme.

Historical development has shown the evolution of oxygen carriers from naturally occurring ores to synthesized materials, and the development trend of reactor system from fixed bed batch mode operation to continuous circulating fluidized bed reactor design. The high cost in the scaling-up and engineering of high-temperature reactors and the incomprehension in the design and development of oxygen carriers are the main causes for the slow development of these early CLR processes.

The basic schemes of various CLR processes are summarized. The two-reactor autothermal CLR scheme decouples the overall reaction of POX or ATR in two reactors. Endothermic CLR schemes require specific considerations on reactor design with external heating. The super-dry reforming scheme can directly obtain high CO yield from greenhouse gases CH_4 and CO_2. Three-reactor autothermal CLR schemes have also been developed to directly produce high purity H_2 with in situ CO_2 capture. Such scheme integrates CLC to provide heat for the reforming reaction, thus avoiding external heating. The design and operation of three interconnected reactors requires systematic approach. Issues that need to

be further addressed include the simultaneous handling of looping particles, oxygen carrier reactivity and recyclability, heat transfer and solid/gas leakage among the reactors.

The syngas selectivity in a CLR process could be affected by many factors, including reaction stoichiometry, thermodynamic equilibrium, surface reaction path and reactor system configuration. The overall reaction stoichiometry determines the syngas selectivity and H_2:CO ratio as well as the heat balance based on the fuel and oxidant input. The performance of oxygen carriers, typically metal oxides, can be estimated based on their equilibrium oxygen potential at high temperatures. The oxygen potential of various metal oxides could be studied and categorized with ease via the Ellingham diagram or the oxygen partial pressure diagram. Metal oxides in the CLR group can be used for syngas production from various carbonaceous fuels, which can thermodynamically ensure the stable production of high purity syngas while minimizing carbon deposition. Thermodynamic analysis can guide the selection of active components and estimate the syngas selectivity in CLR system.

The reactor system design also plays a critical role in determining the chemical looping process performance. Fixed bed, fluidized bed and moving bed are widely tested operation modes for the reducer. Fixed bed reactors can handle gaseous fuel but require frequent gas switching at high temperatures, which is not suitable for large-scale operation. In addition, the poor heat transfer between gas and solids in the fixed bed reactor could cause hot spots that further lead to sintering and deactivation of oxygen carriers. Therefore, the gas–solid contacting pattern should be carefully considered for the reducer design. The mixed flow pattern mainly occurs in the single-stage fluidized bed reactor, while the countercurrent and cocurrent flow patterns could be achieved in a moving bed or a series of interconnected fluidized bed system. Various fluidized bed configurations, such as bubbling-, turbulent- and spout-fluidized bed operations, have been applied to provide good mixing characteristics and uniform heat transfer in CLC applications. Two CLR processes have been developed using iron-based moving bed reactor system. The cocurrent moving bed reducer design can help achieve high-quality syngas production because the moving bed reducer does not suffer a reduced shale gas conversion and/or undesirable syngas composition due to gas channelling and back mixing of particles with different oxidation states. The countercurrent moving bed design could maximize both fuel gas and iron oxide conversions, which have been proven by various models.

The reaction principle of oxygen carriers generally involves the generation and recombination of oxygen ions and vacancies, their diffusion in the bulk phase, and their reaction with adsorbed species on the surface. Oxygen carriers can be designed to control the rate of lattice oxygen delivery to the surface catalytic site. This facility permits balancing the rate of oxidation and reduction of the catalyst. The properties of the oxygen carrier can be modified to improve its catalytic function as well as to regulate the rate of the diffusion of reactants in the oxygen carriers in order to minimize byproduct generation. The application of catalytically active oxygen carriers has the potential to drastically increase the yield of the reaction products.

The deactivation of oxygen carriers remains the major problem for CLR applications and researchers have made tremendous efforts to solve the problems of sintering, carbon deposition and poor selectivity of oxygen carriers. Supported oxygen carriers and composite oxide oxygen carriers are currently common types of oxygen carriers. Supported oxygen carriers are vastly used in industrial processes, but inevitably, they face severe sintering and other problems. For composite oxide oxygen carriers, perovskite oxygen carriers are the most widely studied type, and their excellent structure leads to high syngas selectivity. Perovskite oxygen carriers, however, have the problem of poor oxygen storage capacity. Various supports, promoters and preparation methods have been adopted to optimize CLR performance of supported and composite oxide oxygen carriers. The development of oxygen carriers will continue toward the understanding and utilization of bimetal- and polymetal-based oxygen carriers. Nevertheless, alleviating the sintering problem and maintaining the stability of oxygen carries by focusing on the modification merely can be challenging at high temperatures. Closer consideration to lowering the reforming temperature with changing feedstocks is an alternative and the development of low-temperature reforming has been encouraged for the CLR process. The development of bio-oil/alcohol reforming is suggested for low-temperature CLR applications, which reduces the difficulties in maintaining the physical and chemical properties of oxygen carriers and engineering the associated reactor system.

At present, research on the reaction mechanism involved in the CLR process is still a challenge. The general explanation of the reaction process is only made by comparing experimental performance or ordinary characterization methods, and there is no detailed exploration of the reaction mechanism in the reaction process. The understanding of the CLR reaction process needs to be further deepened in combination with catalytic science in order to achieve a clear reaction mechanism and develop new processes. The application of thermodynamics and DFT calculations in the screening and theoretical research of oxygen carriers is particularly critical. The combination of characterization techniques on local structure and DFT calculation could provide a deeper understanding of the oxygen carrier while assisting the

experimental research. The difference between the performance of the oxygen carriers and the selectivity of the products is explained theoretically by the analysis of the E_{vac} and the energy barrier of the reaction involved in the process. However, the dynamic nature of the oxygen carrier reaction and the large number of atoms involved have also brought challenges to DFT calculations.

With the significant progress made recently in reactor system and oxygen carrier development, CLR technology has great potential to achieve clean, efficient and cost-effective utilization of carbonaceous fuels.

Acknowledgements This work was supported by the National Key R&D Program of China (2018YFE111100) and National Science Foundation of China (21908162, U1663224) for financial support.

Author contributions LZ and AT conceived the project. HZ, XJ and YG constructed the framework of the manuscript and summarized the literature. All the authors were involved in writing the manuscript. All authors read and approved the final manuscript.

Declarations

Competing interests There are no competing interests to declare.

References

1. EIA U. Annual energy outlook 2022. Washington: U.S. Energy Information Administration; 2022.
2. Adanez J, Abad A, Garcia-Labiano F. Progress in chemical-looping combustion and reforming technologies. Prog Energy Combust Sci. 2012;38:215–82.
3. Bui M, Adjiman CS, Bardow A. Carbon capture and storage (CCS): the way forward. Energy Environ Sci. 2018;11:1062–176.
4. Li S, Gong J. Strategies for improving the performance and stability of Ni-based catalysts for reforming reactions. Chem Soc Rev. 2014;43:7245–56.
5. Fan L-S. Chemical looping partial oxidation: gasification, reforming, and chemical syntheses. Cambridge: Cambridge University Press; 2017.
6. Masson-Delmotte V, Zhai P, Pörtner H-O. Global warming of 1.5 ℃, An IPCC Special Report on the impacts of global warming of 1.5 ℃. Geneva: IPCC; 2018.
7. Gielen D, Gorini R, Leme R. World energy transitions outlook: 1.5 ℃ pathway. Abu Dhabi: International Renewable Energy Agency; 2021.
8. Yi Q, Li W, Feng J. Carbon cycle in advanced coal chemical engineering. Chem Soc Rev. 2015;44:5409–45.
9. Zeng L, Cheng Z, Fan JA. Metal oxide redox chemistry for chemical looping processes. Nat Rev Chem. 2018;2:349–64.
10. Buelens LC, Poelman H, Marin GB. 110th anniversary: carbon dioxide and chemical looping: current research trends. Ind Eng Chem Res. 2019;58:16235–57.
11. Zhu X, Imtiaz Q, Donat F. Chemical looping beyond combustion—a perspective. Energy Environ Sci. 2020;13:772–804.
12. Fan L-S. Chemical looping systems for fossil energy conversions. Hoboken: Wiley; 2010.
13. Leion H, Mattisson T, Lyngfelt A. Solid fuels in chemical-looping combustion. Int J Greenh Gas Control. 2008;2:180–93.
14. Adánez J, Abad A, Mendiara T. Chemical looping combustion of solid fuels. Prog Energy Combust Sci. 2018;65:6–66.
15. Rao AB, Rubin ES. A technical, economic, and environmental assessment of amine-based CO_2 capture technology for power plant greenhouse gas control. Environ Sci Technol. 2002;36:4467–75.
16. Song T, Shen L. Review of reactor for chemical looping combustion of solid fuels. Int J Greenh Gas Control. 2018;76:92–110.
17. Rajabi M, Mehrpooya M, Haibo Z. Chemical looping technology in CHP (combined heat and power) and CCHP (combined cooling heating and power) systems: a critical review. Appl Energy. 2019;253: 113544.
18. Kapetaki Z. Carbon capture utilisation and storage technology development report 2020. Luxembourg: Publications Office of the European Union; 2020.
19. Lyngfelt A, Leckner B, Mattisson T. A fluidized-bed combustion process with inherent CO_2 separation; application of chemical-looping combustion. Chem Eng Sci. 2001;56:3101–13.
20. Tabacco D, Innarella C, Bruno C. Theoretical and numerical investigation on flameless combustion. Combust Sci Technol. 2002;174:1.
21. Connell D, Dunkerley M. Systems analysis of the coal direct chemical looping process for coal-based electricity production with in situ carbon dioxide capture. Clearwater: The 36th International Technical Conference on Clean Coal & Fuel Systems; 2011.
22. Ge H, Guo W, Shen L. Experimental investigation on biomass gasification using chemical looping in a batch reactor and a continuous dual reactor. Chem Eng J. 2016;286:689–700.

23. Guo Q, Cheng Y, Liu Y. Coal chemical looping gasification for syngas generation using an iron-based oxygen carrier. Ind Eng Chem Res. 2014;53:78–86.
24. Huang Z, Zhang Y, Fu J. Chemical looping gasification of biomass char using iron ore as an oxygen carrier. Int J Hydrog Energy. 2016;41:17871–83.
25. Muhich C, Steinfeld A. Principles of doping ceria for the solar thermochemical redox splitting of H_2O and CO_2. J Mater Chem A. 2017;5:15578–90.
26. Rao CNR, Dey S. Solar thermochemical splitting of water to generate hydrogen. PNAS. 2017;114:13385.
27. Sun Z, Liu H, Bai H. The crucial role of deoxygenation in syngas refinement and carbon dioxide utilization during chemical looping-based biomass gasification. Chem Eng J. 2022;428: 132068.
28. Bhavsar S, Veser G. Chemical looping beyond combustion: production of synthesis gas via chemical looping partial oxidation of methane. RSC Adv. 2014;4:47254–67.
29. Thursfield A, Murugan A, Franca R. Chemical looping and oxygen permeable ceramic membranes for hydrogen production—a review. Energy Environ Sci. 2012;5:7421–59.
30. Hosseini D, Abdala PM, Donat F. Bifunctional core-shell architecture allows stable H_2 production utilizing CH_4 and CO_2 in a catalytic chemical looping process. Appl Catal B. 2019;258: 117946.
31. Bhavsar S, Najera M, Solunke R. Chemical looping: to combustion and beyond. Catal Today. 2014;228:96–105.
32. He F, Li F. Perovskite promoted iron oxide for hybrid water-splitting and syngas generation with exceptional conversion. Energy Environ Sci. 2015;8:535–9.
33. Luo S, Zeng L, Xu D. Shale gas-to-syngas chemical looping process for stable shale gas conversion to high purity syngas with a H2:CO ratio of 2:1. Energy Environ Sci. 2014;7:4104–17.
34. Hsieh T-L, Xu D, Zhang Y. 250 kWth high pressure pilot demonstration of the syngas chemical looping system for high purity H_2 production with CO_2 capture. Appl Energy. 2018;230:1660–72.
35. Kathe MV, Empfield A, Na J. Hydrogen production from natural gas using an iron-based chemical looping technology: thermodynamic simulations and process system analysis. Appl Energy. 2016;165:183–201.
36. Zeng L, Tong A, Kathe M. Iron oxide looping for natural gas conversion in a countercurrent moving bed reactor. Appl Energy. 2015;157:338–47.
37. Fan L-S, Zeng L, Luo S. Chemical-looping technology platform. AIChE J. 2015;61:2–22.
38. Ishida M, Zheng D, Akehata T. Evaluation of a chemical-looping-combustion power-generation system by graphic exergy analysis. Energy. 1987;12:147–54.
39. Anheden M, Svedberg G. Exergy analysis of chemical-looping combustion systems. Energy Convers Manag. 1998;39:1967–80.
40. Fan L-S, Li F. Chemical looping technology and its fossil energy conversion applications. Ind Eng Chem Res. 2010;49:10200–11.
41. Zhang F, Zhu L, Rao D. The evaluation of a methane autothermal chemical looping reforming experiment based on exergy analysis. RSC Adv. 2019;9:22032–44.
42. Howard L. Process for the production of hydrogen. US Patent 1,078,686. 1913.
43. Reed H, Berg C. Hydrogen process. US Patent 2,635,947. 1953.
44. Lewis WK, Gilliland ER. Production of pure carbon dioxide. US Patent 2,665,971. 1954.
45. Lewis WK, Gilliland ER, Sweeney MP. Gasification of carbon, metal oxides in a fluidized powder bed. Chem Eng Prog. 1951;47:251–6.
46. Lewis WK, Gilliland ER. Conversion of hydrocarbons with suspended catalyst. US Patent 2,498,088. 1950.
47. Lewis WK, Gilliland ER, Reed WA. Reaction of methane with copper oxide in a fluidized bed. Ind Eng Chem Res. 1949;41:1227–37.
48. Lewis WK, Gilliland ER, McBride GT. Gasification of carbon by carbon dioxide in fluidized powder bed. Ind Eng Chem. 1949;41:1213–26.
49. Institute of Gas Technology. Development of the steam-iron process for hydrogen production. United States: IGT; 1979.
50. Otsuka K, Wang Y, Sunada E. Direct partial oxidation of methane to synthesis gas by cerium oxide. J Catal. 1998;175:152–60.
51. Kašpar J, Fornasiero P, Graziani M. Use of CeO_2-based oxides in the three-way catalysis. Catal Today. 1999;50:285–98.
52. Salazar-Villalpando MD, Berry DA, Cugini A. Role of lattice oxygen in the partial oxidation of methane over Rh/zirconia-doped ceria. Isotopic studies. Int J Hydrog Energy. 2010;35:1998–2003.
53. Cl M, Bw E, Kc W. Efficient generation of H_2 by splitting water with an isothermal redox cycle. Science. 2013;341:540–2.
54. Halmann M, Frei A, Steinfeld A. Thermo-neutral production of metals and hydrogen or methanol by the combined reduction of the oxides of zinc or iron with partial oxidation of hydrocarbons. Energy. 2002;27:1069–84.
55. Steinfeld A, Kuhn P. High-temperature solar thermochemistry: production of iron and synthesis gas by Fe_3O_4-reduction with methane. Energy. 1993;18:239–49.
56. Lyngfelt A, Thunman H. Carbon dioxide capture for storage in deep geologic formations—results from the CO_2 capture project, volume 1—capture and separation of carbon dioxide from combustion sources. Amsterdam: Elsevier Science; 2005. p. 625–46.
57. Lyngfelt PMCLA. Chemical-looping combustion of solid fuels—design and operation of a 100 kW unit with bituminous coal. Int J Greenh Gas Control. 2013;15:150–62.
58. Leion H, Mattisson T, Lyngfelt A. Use of ores and industrial products as oxygen carriers in chemical-looping combustion. Energy Fuels. 2009;23:2307–15.
59. Lyngfelt A, Johansson M, Mattisson T. Chemical-looping combustion—status of development. Sweden: Chalmers University of Technology; 2008.
60. Berguerand N, Lyngfelt A. The use of petroleum coke as fuel in a 10 KWth chemical-looping combustor. Int J Greenh Gas Control. 2008;2:169–79.
61. Berguerand N, Lyngfelt A. Design and operation of a 10 KWth chemical-looping combustor for solid fuels—testing with South African coal. Fuel. 2008;87:2713–26.
62. Schmitz M, Linderholm C. Chemical looping combustion of biomass in 10- and 100-kW pilots—analysis of conversion and lifetime using a sintered manganese ore. Fuel. 2018;231:73–84.
63. Gogolev I, Linderholm C, Gall D. Chemical-looping combustion in a 100 kW unit using a mixture of synthetic and natural oxygen carriers—operational results and fate of biomass fuel alkali. Int J Greenh Gas Control. 2019;88:371–82.

64. Hildor F, Mattisson T, Leion H. Steel converter slag as an oxygen carrier in a 12 MWth CFB boiler—ash interaction and material evolution. Int J Greenh Gas Control. 2019;88:321–31.
65. Ströhle J, Orth M, Epple B. Design and operation of a 1 MWth chemical looping plant. Appl Energy. 2014;113:1490–5.
66. Ohlemüller P, Reitz M, Ströhle J. Investigation of chemical looping combustion of natural gas at 1 MWth scale. Proc Combust Inst. 2019;37:4353–60.
67. Ohlemüller P, Ströhle J, Epple B. Chemical looping combustion of hard coal and torrefied biomass in a 1MWth pilot plant. Int J Greenh Gas Control. 2017;65:149–59.
68. Chen H, Cheng M, Liu L. Coal-fired chemical looping combustion coupled with a high-efficiency annular carbon stripper. Int J Greenh Gas Control. 2020;93: 102889.
69. Feng X, Shen L, Wang L. Effect of baffle on hydrodynamics in the air reactor of dual circulating fluidized bed for chemical looping process. Powder Technol. 2018;340:88–98.
70. Zhou Q, Zeng L, Fan L-S. Syngas chemical looping process: dynamic modeling of a moving-bed reducer. AIChE J. 2013;59:3432–43.
71. Tong A, Zeng L, Kathe MV. Application of the moving-bed chemical looping process for high methane conversion. Energy Fuels. 2013;27:4119–28.
72. Sridhar D, Tong A, Kim H. Syngas chemical looping process: design and construction of a 25 kW th subpilot unit. Energy Fuels. 2012;26:2292–302.
73. Fan L-S, Zeng L, Wang W. Chemical looping processes for CO_2 capture and carbonaceous fuel conversion—prospect and opportunity. Energy Environ Sci. 2012;5:7254–80.
74. Li F, Zeng L, Velazquez-Vargas LG. Syngas chemical looping gasification process: bench-scale studies and reactor simulations. AIChE J. 2009. https://doi.org/10.1002/aic.12093.
75. Li F, Kim H, Sridhar D. Syngas chemical looping gasification process: oxygen carrier particle selection and performance. Energy Fuels. 2009;23:4182–9.
76. Li F, Fan L-S. Clean coal conversion processes—progress and challenges. Energy Environ Sci. 2008;1:248–67.
77. Wang D, Fan L-S. Bulk coarse particle arching phenomena in a moving bed with fine particle presence. AIChE J. 2014;60:881–92.
78. Qin L, Guo M, Liu Y. Enhanced methane conversion in chemical looping partial oxidation systems using a copper doping modification. Appl Catal B. 2018;235:143–9.
79. Li D, Xu R, Li X. Chemical looping conversion of gaseous and liquid fuels for chemical production: a review. Energy Fuels. 2020;34:5381–413.
80. Osman M, Khan MN, Zaabout A. Review of pressurized chemical looping processes for power generation and chemical production with integrated CO_2 capture. Fuel Process Technol. 2021;214: 106684.
81. Wang W, Cao Y. A combined thermodynamic and experimental study on chemical-looping ethanol reforming with carbon dioxide capture for hydrogen generation. Int J Energy Res. 2013;37:25–34.
82. Pimenidou P, Rickett G, Dupont V. Chemical looping reforming of waste cooking oil in packed bed reactor. Bioresour Technol. 2010;101:6389–97.
83. Zafar Q, Mattisson T, Gevert B. Integrated hydrogen and power production with CO_2 capture using chemical-looping reformingredox reactivity of particles of CuO, Mn_2O_3, NiO, and Fe_2O_3 Using SiO_2 as a support. Ind Eng Chem Res. 2005;44:3485–96.
84. Jerndal E, Mattisson T, Lyngfelt A. Investigation of different NiO/$NiAl_2O_4$ particles as oxygen carriers for chemical-looping combustion. Energy Fuels. 2009;23:665–76.
85. Rydén M, Lyngfelt A, Mattisson T. Synthesis gas generation by chemical-looping reforming in a continuously operating laboratory reactor. Fuel. 2006;85:1631–41.
86. He F, Wei Y, Li H. Synthesis gas generation by chemical-looping reforming using Ce-based oxygen carriers modified with Fe, Cu, and Mn oxides. Energy Fuels. 2009;23:2095–102.
87. Xu T, Jiang C, Wang X. Bio-oil chemical looping reforming coupled with water splitting for hydrogen and syngas coproduction: effect of supports on the performance of Ni-Fe bimetallic oxygen carriers. Energy Convers Manag. 2021;244: 114512.
88. Jiang B, Li L, Zhang Q. Chemical looping reforming of glycerol for continuous H_2 production by moving-bed reactors: simulation and experiment. Energy Fuels. 2020;34:1841–50.
89. Jiang B, Li L, Bian Z. Hydrogen generation from chemical looping reforming of glycerol by Ce-doped nickel phyllosilicate nanotube oxygen carriers. Fuel. 2018;222:185–92.
90. Jiang B, Dou B, Wang K. Hydrogen production by chemical looping steam reforming of ethanol using NiO/montmorillonite oxygen carriers in a fixed-bed reactor. Chem Eng J. 2016;298:96–106.
91. Jiang B, Dou B, Song Y. Hydrogen production from chemical looping steam reforming of glycerol by Ni-based oxygen carrier in a fixed-bed reactor. Chem Eng J. 2015;280:459–67.
92. Dou B, Song Y, Wang C. Hydrogen production by enhanced-sorption chemical looping steam reforming of glycerol in moving-bed reactors. Appl Energy. 2014;130:342–9.
93. Sun Z, Zhang XH, Li HF. Chemical looping oxidative steam reforming of methanol: a new pathway for auto-thermal conversion. Appl Catal B. 2020. https://doi.org/10.1016/j.apcatb.2020.118758.
94. Muhich CL, Evanko BW, Weston KC. Efficient generation of H_2 by splitting water with an isothermal redox cycle. Science. 2013;341:540.
95. Zhang J, Haribal V, Li F. Perovskite nanocomposites as effective CO_2-splitting agents in a cyclic redox scheme. Sci Adv. 2017. https://doi.org/10.1126/sciadv.1701184.
96. Haribal VP, He F, Mishra A. Iron-doped $BaMnO_3$ for hybrid water splitting and syngas generation. Chemsuschem. 2017;10:3402–8.
97. Li K, Wang H, Wei Y. Syngas production from methane and air via a redox process using Ce–Fe mixed oxides as oxygen carriers. Appl Catal B. 2010;97:361–72.
98. Zhu X, Zhang M, Li K. Chemical-looping water splitting over ceria-modified iron oxide: performance evolution and element migration during redox cycling. Chem Eng Sci. 2018;179:92–103.
99. Zheng Y, Li K, Wang H. Designed oxygen carriers from macroporous $LaFeO_3$ supported CeO_2 for chemical-looping reforming of methane. Appl Catal B. 2017;202:51–63.

100. Chen Y, Zhu X, Li K. Chemical looping Co-splitting of H_2O–CO_2 for efficient generation of syngas. ACS Sustain Chem Eng. 2019;7:15452–62.
101. Buelens LC, Galvita VV, Poelman H. Super-dry reforming of methane intensifies CO_2 utilization via Le Chatelier's principle. Science. 2016. https://doi.org/10.1126/science.aah7161.
102. Pimenidou P, Rickett G, Dupont V. High purity H_2 by sorption-enhanced chemical looping reforming of waste cooking oil in a packed bed reactor. Bioresour Technol. 2010;101:9279–86.
103. Zeng PC, Dou BL, Zhang H. Chemical looping steam reforming of ethanol without and with in-situ CO_2 capture. Int J Hydrog Energy. 2022;47:6552–68.
104. Hafizi A, Rahimpour MR, Hassanajili S. High purity hydrogen production via sorption enhanced chemical looping reforming: application of $22Fe_2O_3/MgAl_2O_4$ and $22Fe_2O_3/Al_2O_3$ as oxygen carriers and cerium promoted CaO as CO_2 sorbent. Appl Energy. 2016;169:629–41.
105. Hafizi A, Rahimpour MR, Heravi M. Experimental investigation of improved calcium-based CO_2 sorbent and Co_3O_4/SiO_2 oxygen carrier for clean production of hydrogen in sorption-enhanced chemical looping reforming. Int J Hydrog Energy. 2019;44:17863–77.
106. Xie P, Yu S, Ouyang L. Extracting high-purity hydrogen via sodium looping-based formic acid dehydrogenation. Int J Hydrog Energy. 2022;47:11164–76.
107. Zeng L, Kathe MV, Chung EY. Some remarks on direct solid fuel combustion using chemical looping processes. Curr Opin Chem Eng. 2012;1:290–5.
108. Imtiaz Q, Hosseini D, Müller CR. Review of oxygen carriers for chemical looping with oxygen uncoupling (CLOU): thermodynamics, material development, and synthesis. Energy Technol. 2013;1:633–47.
109. Zhao H, Tian X, Ma J. Development of tailor-made oxygen carriers and reactors for chemical looping processes at Huazhong University of Science & Technology. Int J Greenhouse Gas Control. 2020;93: 102898.
110. Hara Y, Sakawa M, Kondo S-I. Mathematical model of the shaft furnace for reduction of iron ore pellet. Tetsu to Hagane. 1976;62:315–23.
111. Zeng L, Wei D, Toan S. Sorption-enhanced chemical looping oxidative steam reforming of methanol for on-board hydrogen supply. Green Energy Environ. 2020. https://doi.org/10.1016/j.gee.2020.08.011.
112. Sun Z, Liu J, Zhang R. Fabricating Ga doped and MgO embedded nanomaterials for sorption-enhanced steam reforming of methanol. J Mater Chem A. 2022. https://doi.org/10.1039/D1TA10306G.
113. Wang W. Thermodynamic and experimental aspects on chemical looping reforming of ethanol for hydrogen production using a Cu-based oxygen carrier. Int J Energy Res. 2014;38:1192–200.
114. Soykal II, Sohn H, Ozkan US. Effect of support particle size in steam reforming of ethanol over Co/CeO_2 catalysts. ACS Catal. 2012;2:2335–48.
115. Zhao K, Zheng A, Li H. Exploration of the mechanism of chemical looping steam methane reforming using double perovskite-type oxides $La_{1.6}Sr_{0.4}FeCoO_6$. Appl Catal B. 2017;219:672–82.
116. Zhao K, He F, Huang Z. Perovskite-type oxides $LaFe_1-xCo_xO_3$ for chemical looping steam methane reforming to syngas and hydrogen co-production. Appl Energy. 2016;168:193–203.
117. Bork AH, Kubicek M, Struzik M. Perovskite $La_{0.6}Sr_{0.4}Cr_{1-x}Co_xO_{3-\delta}$ solid solutions for solar-thermochemical fuel production: strategies to lower the operation temperature. J Mater Chem A. 2015;3:15546–57.
118. He F, Li X, Zhao K. The use of $La_{1-x}Sr_xFeO_3$ perovskite-type oxides as oxygen carriers in chemical-looping reforming of methane. Fuel. 2013;108:465–73.
119. Nalbandian L, Evdou A, Zaspalis V. $La_{1-x}Sr_xM_yFe_1-yO_{3-\delta}$ perovskites as oxygen-carrier materials for chemical-looping reforming. Int J Hydrog Energy. 2011;36:6657–70.
120. Mihai O, Chen D, Holmen A. catalytic consequence of oxygen of lanthanum ferrite perovskite in chemical looping reforming of methane. Ind Eng Chem Res. 2011;50:2613–21.
121. Rydén M, Lyngfelt A, Mattisson T. Novel oxygen-carrier materials for chemical-looping combustion and chemical-looping reforming; $La_xSr_{1-x}Fe_yCo_{1-y}O_{3-\delta}$ perovskites and mixed-metal oxides of NiO, Fe_2O_3 and Mn_3O_4. Int J Greenh Gas Control. 2008;2:21–36.
122. Dai XP, Li RJ, Yu CC. Unsteady-state direct partial oxidation of methane to synthesis gas in a fixed-bed reactor using $AFeO_3$ (A = La, Nd, Eu) perovskite-type oxides as oxygen storage. J Phys Chem B. 2006;110:22525–31.
123. Paier J, Penschke C, Sauer J. Oxygen defects and surface chemistry of ceria: quantum chemical studies compared to experiment. Chem Rev. 2013;113:3949–85.
124. Andersson DA, Simak SI, Skorodumova NV. Optimization of ionic conductivity in doped ceria. Proc Natl Acad Sci USA. 2006;103:3518–21.
125. Qin L, Cheng Z, Guo M. Impact of 1% lanthanum dopant on carbonaceous fuel redox reactions with an iron-based oxygen carrier in chemical looping processes. ACS Energy Lett. 2017;2:70–4.
126. Guo M, Cheng Z, Liu Y. Cobalt doping modification for enhanced methane conversion at low temperature in chemical looping reforming systems. Catal Today. 2019. https://doi.org/10.1016/j.cattod.2019.06.016.
127. Chen S, Zeng L, Tian H. Enhanced lattice oxygen reactivity over Ni modified WO3-based redox catalysts for chemical looping partial oxidation of methane. ACS Catal. 2017. https://doi.org/10.1021/acscatal.7b00436.
128. Tang M, Xu L, Fan M. Progress in oxygen carrier development of methane-based chemical-looping reforming: a review. Appl Energy. 2015;151:143–56.
129. Park J-N, Zhang P, Hu Y-S. Synthesis and characterization of sintering-resistant silica-encapsulated Fe_3O_4 magnetic nanoparticles active for oxidation and chemical looping combustion. Nanotechnology. 2010;21: 225708.
130. Liu Y, Qin L, Cheng Z. Near 100% CO selectivity in nanoscaled iron-based oxygen carriers for chemical looping methane partial oxidation. Nat Commun. 2019;10:1–6.
131. Meshksar M, Daneshmand-Jahromi S, Rahimpour M. Synthesis and characterization of cerium promoted Ni/SBA-16 oxygen carrier in cyclic chemical looping steam methane reforming. J Taiwan Inst Chem Eng. 2017;76:73–82.
132. Mihai O, Chen D, Holmen A. Chemical looping methane partial oxidation: the effect of the crystal size and O content of $LaFeO_3$. J Catal. 2012;293:175–85.
133. Tijani MM, Aqsha A, Mahinpey N. Synthesis and study of metal-based oxygen carriers (Cu Co, Fe, Ni) and their interaction with supported metal oxides (Al_2O_3, CeO_2, TiO_2, ZrO_2) in a chemical looping combustion system. Energy. 2017;138:873–82.
134. Karimi E, Forutan H, Saidi M. Experimental study of chemical-looping reforming in a fixed-bed reactor: performance investigation of different oxygen carriers on Al_2O_3 and TiO_2 support. Energy Fuels. 2014;28:2811–20.

135. Mattisson T, Järdnäs A, Lyngfelt A. Reactivity of some metal oxides supported on alumina with alternating methane and oxygen application for chemical-looping combustion. Energy Fuels. 2003;17:643–51.
136. Forutan H, Karimi E, Hafizi A. Expert representation chemical looping reforming: a comparative study of Fe, Mn, Co and Cu as oxygen carriers supported on Al_2O_3. J Ind Eng Chem. 2015;21:900–11.
137. Moulijn JA, Van Diepen A, Kapteijn F. Catalyst deactivation: is it predictable?: What to do? Appl Catal A. 2001;212:3–16.
138. Zeng D-W, Peng S, Chen C. Nanostructured $Fe_2O_3/MgAl_2O_4$ material prepared by colloidal crystal templated sol–gel method for chemical looping with hydrogen storage. Int J Hydrogen Energy. 2016;41:22711–21.
139. Buelens LC, Galvita VV, Poelman H. Super-dry reforming of methane intensifies CO_2 utilization via Le Chatelier's principle. Science. 2016;354:449–52.
140. Hu J, Chen S, Xiang W. Sintering and agglomeration of Fe_2O_3-$MgAl_2O_4$ oxygen carriers with different Fe_2O_3 loadings in chemical looping processes. Fuel. 2020;265: 116983.
141. Johansson M, Mattisson T, Lyngfelt A. Investigation of Mn_3O_4 with stabilized ZrO_2 for chemical-looping combustion. Chem Eng Res Des. 2006;84:807–18.
142. Li D, Xu R, Gu Z. Chemical-looping conversion of methane: a review. Energy Technol. 2019. https://doi.org/10.1002/ente.201900925.
143. Chung C, Qin L, Shah V. Chemically and physically robust, commercially-viable iron-based composite oxygen carriers sustainable over 3000 redox cycles at high temperatures for chemical looping applications. Energy Environ Sci. 2017;10:2318–23.
144. Zhu M, Chen S, Ma S. Carbon formation on iron-based oxygen carriers during CH_4 reduction period in chemical looping hydrogen generation process. Chem Eng J. 2017;325:322–31.
145. Sun S, Zhao M, Cai L. Performance of CeO_2-modified iron-based oxygen carrier in the chemical looping hydrogen generation process. Energy Fuels. 2015;29:7612–21.
146. Huang Z, Deng Z, Chen D. Thermodynamic analysis and kinetic investigations on biomass char chemical looping gasification using Fe-Ni bimetallic oxygen carrier. Energy. 2017;141:1836–44.
147. Daturi M, Finocchio E, Binet C. Reduction of high surface area CeO_2–ZrO_2 mixed oxides. J Phys Chem B. 2000;104:9186–94.
148. Zheng Y, Wei Y, Li K. Chemical-looping steam methane reforming over macroporous CeO_2–ZrO_2 solid solution: effect of calcination temperature. Int J Hydrog Energy. 2014;39:13361–8.
149. Tomishige K, Himeno Y, Matsuo Y. Catalytic performance and carbon deposition behavior of a NiO–MgO solid solution in methane reforming with carbon dioxide under pressurized conditions. Ind Eng Chem Res. 2000;39:1891–7.
150. Hu J, Galvita VV, Poelman H. Pressure-induced deactivation of core-shell nanomaterials for catalyst-assisted chemical looping. Appl Catal B. 2019;247:86–99.
151. Fan L-S. Chemical looping systems for fossil energy conversions. Hoboken: Wiley; 2011.
152. Shen Q, Huang F, Tian M. Effect of regeneration period on the selectivity of synthesis gas of Ba-Hexaaluminates in chemical looping partial oxidation of methane. ACS Catal. 2018;9:722–31.
153. Singstock NR, Bartel CJ, Holder AM. High-throughput analysis of materials for chemical looping processes. Adv Energy Mater. 2020;10:2000685.
154. Wang X, Gao Y, Krzystowczyk E. High-throughput oxygen chemical potential engineering of perovskite oxides for chemical looping applications. Energy Environ Sci. 2022;15:1512–28.
155. Rojas J, Haribal V, Jung I-H. Computational discovery of metal oxides for chemical looping hydrogen production. Cell Rep Phys Sci. 2021;2: 100362.
156. Chen Y-Y, Guo M, Kim M. Predictive screening and validation on chemical looping oxygen carrier activation by tuning electronic structures via transition metal dopants. Chem Eng J. 2021;406: 126729.
157. Feng Y, Wang N, Guo X. Dopant screening of modified Fe_2O_3 oxygen carriers in chemical looping hydrogen production. Fuel. 2020;262: 116489.
158. Zheng Y, Li K, Wang H. Enhanced activity of CeO_2–ZrO_2 solid solutions for chemical-looping reforming of methane via tuning the macroporous structure. Energy Fuels. 2016;30:638–47.
159. Antzara A, Heracleous E, Silvester L. Activity study of NiO-based oxygen carriers in chemical looping steam methane reforming. Catal Today. 2016;272:32–41.
160. Cheng Z, Qin L, Guo M. Oxygen vacancy promoted methane partial oxidation over iron oxide oxygen carriers in the chemical looping process. Phys Chem Chem Phys. 2016;18:32418–28.
161. Mei D, Zhao H, Ma Z. Using the Sol–Gel-derived $CuO/CuAl_2O_4$ oxygen carrier in chemical looping with oxygen uncoupling for three typical coals. Energy Fuels. 2013;27:2723–31.
162. Dou B, Zhang H, Cui G. Hydrogen production and reduction of Ni-based oxygen carriers during chemical looping steam reforming of ethanol in a fixed-bed reactor. Int J Hydrogen Energy. 2017;42:26217–30.
163. Kousi K, Neagu D, Bekris L. Endogenous nanoparticles strain perovskite host lattice providing oxygen capacity and driving oxygen exchange and CH_4 conversion to syngas. Angew Chem. 2020;132:2531–40.
164. Li L, Song Y, Jiang B. A novel oxygen carrier for chemical looping reforming: $LaNiO_3$ perovskite supported on montmorillonite. Energy. 2017;131:58–66.
165. Löfberg A, Guerrero-Caballero J, Kane T. Ni/CeO_2 based catalysts as oxygen vectors for the chemical looping dry reforming of methane for syngas production. Appl Catal B. 2017;212:159–74.
166. Ruan C, Huang Z-Q, Lin J. Synergy of the catalytic activation on Ni and the CeO_2–$TiO_2/Ce_2Ti_2O_7$ stoichiometric redox cycle for dramatically enhanced solar fuel production. Energy Environ Sci. 2019;12:767–79.
167. Guerrero-Caballero J, Kane T, Haidar N. Ni Co, Fe supported on Ceria and Zr doped Ceria as oxygen carriers for chemical looping dry reforming of methane. Catal Today. 2019;333:251–8.
168. Huang J, Liu W, Yang Y. High-performance Ni–Fe redox catalysts for selective CH_4 to syngas conversion via chemical looping. ACS Catal. 2018;8:1748–56.
169. Hu J, Li HB, Chen SY. Enhanced Fe_2O_3/Al_2O_3 oxygen carriers for chemical looping steam reforming of methane with different Mg ratios. Ind Eng Chem Res. 2022;61:1022–31.

170. Kim Y, Lim HS, Lee M. Ni-Fe-Al mixed oxide for combined dry reforming and decomposition of methane with CO_2 utilization. Catal Today. 2021;368:86–95.
171. Lim HS, Kang D, Lee JW. Phase transition of Fe_2O_3–NiO to $NiFe_2O_4$ in perovskite catalytic particles for enhanced methane chemical looping reforming-decomposition with CO_2 conversion. Appl Catal B. 2017;202:175–83.
172. More A, Bhavsar S, Veser G. Iron–nickel alloys for carbon dioxide activation by chemical looping dry reforming of methane. Energy Technol. 2016;4:1147–57.
173. Shen Y, Zhao K, He F. The structure-reactivity relationships of using three-dimensionally ordered macroporous $LaFe_{1-x}Ni_xO_3$ perovskites for chemical-looping steam methane reforming. J Energy Inst. 2019;92:239–46.
174. Kang D, Lim HS, Lee M. Syngas production on a Ni-enhanced Fe_2O_3/Al_2O_3 oxygen carrier via chemical looping partial oxidation with dry reforming of methane. Appl Energy. 2018;211:174–86.
175. Hafizi A, Rahimpour M, Hassanajili S. Calcium promoted Fe/Al_2O_3 oxygen carrier for hydrogen production via cyclic chemical looping steam methane reforming process. Int J Hydrogen Energy. 2015;40:16159–68.
176. Kang Y, Tian M, Huang C. Improving syngas selectivity of Fe_2O_3/Al_2O_3 with Yttrium modification in chemical looping methane conversion. ACS Catal. 2019;9:8373–82.
177. Kang D, Lee M, Lim HS. Chemical looping partial oxidation of methane with CO_2 utilization on the ceria-enhanced mesoporous Fe_2O_3 oxygen carrier. Fuel. 2018;215:787–98.
178. Hafizi A, Rahimpour M, Hassanajili S. Hydrogen production via chemical looping steam methane reforming process: effect of cerium and calcium promoters on the performance of Fe_2O_3/Al_2O_3 oxygen carrier. Appl Energy. 2016;165:685–94.
179. Liang H. Study on the effect of CeO_2 on $Fe_2O_3/LaNiO_3$ as the oxygen carrier applied in chemical-looping hydrogen generation. Int J Hydrog Energy. 2015;40:13338–43.
180. Tang M, Liu K, Roddick DM. Enhanced lattice oxygen reactivity over Fe_2O_3/Al_2O_3 redox catalyst for chemical-looping dry (CO2) reforming of CH_4: Synergistic La-Ce effect. J Catal. 2018;368:38–52.
181. Zhu Y, Liu W, Sun X. La-hexaaluminate for synthesis gas generation by chemical looping partial oxidation of methane using CO_2 as sole oxidant. AIChE J. 2018;64:550–63.
182. Dai X, Cheng J, Li Z. Reduction kinetics of lanthanum ferrite perovskite for the production of synthesis gas by chemical-looping methane reforming. Chem Eng Sci. 2016;153:236–45.
183. Zhao K, He F, Huang Z. Three-dimensionally ordered macroporous $LaFeO_3$ perovskites for chemical-looping steam reforming of methane. Int J Hydrog Energy. 2014;39:3243–52.
184. Zhao K, He F, Huang Z. Perovskite-type $LaFe_{1-x}Mn_xO_3$ (x= 0, 0.3, 0.5, 0.7, 1.0) oxygen carriers for chemical-looping steam methane reforming: oxidation activity and resistance to carbon formation. Korean J Chem Eng. 2017;34:1651–60.
185. Donat F, Muller CR. CO_2-free conversion of CH_4 to syngas using chemical looping. Appl Catal B. 2020. https://doi.org/10.1016/j.apcatb.2020.119328.
186. Zhao K, Li L, Zheng A. Synergistic improvements in stability and performance of the double perovskite-type oxides $La_{2-x}Sr_xFeCoO_6$ for chemical looping steam methane reforming. Appl Energy. 2017;197:393–404.
187. Neal L, Shafiefarhood A, Li F. Effect of core and shell compositions on MeOx@ $La_ySr_{1-y}FeO_3$ core–shell redox catalysts for chemical looping reforming of methane. Appl Energy. 2015;157:391–8.
188. Neal LM, Shafiefarhood A, Li F. Dynamic methane partial oxidation using a Fe_2O_3@ $La_{0.8}Sr_{0.2}FeO_{3-\delta}$ core–shell redox catalyst in the absence of gaseous oxygen. ACS Catal. 2014;4:3560–9.
189. Li K, Wang H, Wei Y. Direct conversion of methane to synthesis gas using lattice oxygen of CeO_2–Fe_2O_3 complex oxides. Chem Eng J. 2010;156:512–8.
190. Zhu X, Wei Y, Wang H. Ce–Fe oxygen carriers for chemical-looping steam methane reforming. Int J Hydrog Energy. 2013;38:4492–501.
191. Yonggang W, Hua W, Kongzhai L. Ce-Fe-O mixed oxide as oxygen carrier for the direct partial oxidation of methane to syngas. J Rare Earths. 2010;28:560–5.
192. Li K, Wang H, Wei Y. Partial oxidation of methane to syngas with air by lattice oxygen transfer over ZrO_2-modified Ce–Fe mixed oxides. Chem Eng J. 2011;173:574–82.
193. Alirezaei I, Hafizi A, Rahimpour M. Application of zirconium modified Cu-based oxygen carrier in chemical looping reforming. J CO2 Util. 2016;14:112–21.
194. Shah V, Cheng Z, Baser DS. Highly selective production of syngas from chemical looping reforming of methane with CO_2 utilization on MgO-supported calcium ferrite redox materials. Appl Energy. 2021. https://doi.org/10.1016/j.apenergy.2020.116111.
195. Sun Z, Zhang X, Li H. Chemical looping oxidative steam reforming of methanol: a new pathway for auto-thermal conversion. Appl Catal B. 2020;269: 118758.
196. Nadgouda SG, Guo M, Tong A. High purity syngas and hydrogen coproduction using copper-iron oxygen carriers in chemical looping reforming process. Appl Energy. 2019;235:1415–26.
197. Alirezaei I, Hafizi A, Rahimpour M. Syngas production in chemical looping reforming process over ZrO_2 promoted Mn-based catalyst. J CO2 Util. 2018;23:105–16.
198. Shafiefarhood A, Zhang J, Neal LM. Rh-promoted mixed oxides for "low-temperature" methane partial oxidation in the absence of gaseous oxidants. J Mater Chem A. 2017;5:11930–9.
199. Mishra A, Galinsky N, He F. Perovskite-structured $AMn_xB_{1-x}O_3$ (A= Ca or Ba; B= Fe or Ni) redox catalysts for partial oxidation of methane. Catal Sci Technol. 2016;6:4535–44.
200. Wong YJ, Koh MK, Khavarian M. Investigation on cobalt aluminate as an oxygen carrier catalyst for dry reforming of methane. Int J Hydrog Energy. 2017;42:28363–76.
201. Akbari-Emadabadi S, Rahimpour M, Hafizi A. Production of hydrogen-rich syngas using Zr modified Ca-Co bifunctional catalyst-sorbent in chemical looping steam methane reforming. Appl Energy. 2017;206:51–62.
202. Ding H, Xu Y, Luo C. A novel composite perovskite-based material for chemical-looping steam methane reforming to hydrogen and syngas. Energy Convers Manag. 2018;171:12–9.

203. Ding H, Luo C, Li X. Development of BaSrCo-based perovskite for chemical-looping steam methane reforming: a study on synergistic effects of A-site elements and CeO_2 support. Fuel. 2019;253:311–9.
204. Kodama T, Shimizu T, Satoh T. Stepwise production of CO-rich syngas and hydrogen via methane reforming by a WO_3-redox catalyst. Energy. 2003;28:1055–68.
205. Chen S, Zeng L, Tian H. Enhanced lattice oxygen reactivity over Ni-modified WO_3-based redox catalysts for chemical looping partial oxidation of methane. ACS Catal. 2017;7:3548–59.
206. Liu R, Pei C, Zhang X. Chemical looping partial oxidation over $FeWO_x/SiO_2$ catalysts. Chin J Catal. 2020;41:1140–51.
207. Trimm DL. Catalyst deactivation. In: Bartholomew CH, Butt JB, editors. Studies in surface science and catalysis, vol. 68. Amsterdam: Elsevier; 1991. p. 29–51.
208. Hou Z, Gao J, Guo J. Deactivation of Ni catalysts during methane autothermal reforming with CO_2 and O_2 in a fluidized-bed reactor. J Catal. 2007;250:331–41.
209. Sedor KE, Hossain MM, de Lasa HI. Reactivity and stability of Ni/Al_2O_3 oxygen carrier for chemical-looping combustion (CLC). Chem Eng Sci. 2008;63:2994–3007.
210. Silvester L, Antzara A, Boskovic G. NiO supported on Al_2O_3 and ZrO_2 oxygen carriers for chemical looping steam methane reforming. Int J Hydrogen Energy. 2015;40:7490–501.
211. Rydén M, Johansson M, Lyngfelt A. NiO supported on $Mg–ZrO_2$ as oxygen carrier for chemical-looping combustion and chemical-looping reforming. Energy Environ Sci. 2009;2:970–81.
212. Baudouin D, Rodemerck U, Krumeich F. Particle size effect in the low temperature reforming of methane by carbon dioxide on silica-supported Ni nanoparticles. J Catal. 2013;297:27–34.
213. Dueso C, Ortiz M, Abad A. Reduction and oxidation kinetics of nickel-based oxygen-carriers for chemical-looping combustion and chemical-looping reforming. Chem Eng J. 2012;188:142–54.
214. Chiron F-X, Patience GS, Rifflart S. Hydrogen production through chemical looping using $NiO/NiAl_2O_4$ as oxygen carrier. Chem Eng Sci. 2011;66:6324–30.
215. Sun Y, Jiang E, Xu X. Supplied oxygen properties of $NiO/NiAl_2O_4$ in chemical looping Re-forming of biomass pyrolysis gas: the influence of synthesis method. ACS Sustain Chem Eng. 2018;6:14660–8.
216. Zafar Q, Mattisson T, Gevert B. Redox investigation of some oxides of transition-state metals Ni, Cu, Fe, and Mn supported on SiO_2 and $MgAl_2O_4$. Energy Fuels. 2006;20:34–44.
217. Medeiros RLBA, Macedo HP, Figueredo GP. Study of the reactivity by pulse of CH_4 over NiO/Fe-doped $MgAl_2O_4$ oxygen carriers for hydrogen production. Int J Hydrog Energy. 2017;42:24823–9.
218. Feng Y, Wang N, Guo X. Influence mechanism of supports on the reactivity of Ni-based oxygen carriers for chemical looping reforming: A DFT study. Fuel. 2018;229:88–94.
219. Daneshmand-Jahromi S, Meshksar M, Hafizi A. Synthesis, characterization and application of Ni-based oxygen carrier supported on novel yttrium-incorporated SBA-16 for efficient hydrogen production via chemical looping steam methane reforming. J Taiwan Inst Chem Eng. 2018;89:129–39.
220. Daneshmand-Jahromi S, Rahimpour MR, Meshksar M. Hydrogen production from cyclic chemical looping steam methane reforming over yttrium promoted Ni/SBA-16 oxygen carrier. Catalysts. 2017;7:286.
221. Meshksar M, Rahimpour MR, Daneshmand-Jahromi S. Synthesis and application of cerium-incorporated SBA-16 supported Ni-based oxygen carrier in cyclic chemical looping steam methane reforming. Catalysts. 2018;8:18.
222. Huang J, Liu W, Yang Y. Phase interactions in Mg-Ni-Al-O oxygen carriers for chemical looping applications. Chem Eng J. 2017;326:470–6.
223. Ma Z, Zhang S, Lu Y. Phase segregation mechanism of $NiFe_2O_4$ oxygen carrier in chemical looping process. Int J Energy Res. 2021;45:3305–14.
224. Ma Z, Zhang S, Xiao R. Inhibited phase segregation to enhance the redox performance of $NiFe_2O_4$ via CeO_2 modification in the chemical looping process. Energy Fuels. 2020;34:6178–85.
225. Jiang B, Li L, Bian Z. Chemical looping glycerol reforming for hydrogen production by Ni@ ZrO_2 nanocomposite oxygen carriers. Int J Hydrog Energy. 2018;43:13200–11.
226. Zhang Q, Li L, Jiang B. An intelligent oxygen carrier of $La_{2-x}Sr_xNiO_{4-\lambda}$ for hydrogen production by chemical looping reforming of ethanol. Int J Hydrog Energy. 2017;42:17102–11.
227. Zhang Q, Li L, Jiang B. Hydrogen by chemical looping reforming of ethanol: the effect of promoters on $La_{2-x}M_xNiO_{4-\lambda}$ (M=Ca, Sr and Ce) oxygen carriers. Chem Eng Sci. 2017;174:259–67.
228. Wang K, Dou B, Jiang B. Effect of support on hydrogen production from chemical looping steam reforming of ethanol over Ni-based oxygen carriers. Int J Hydrog Energy. 2016;41:17334–47.
229. Abild-Pedersen F, Nørskov JK, Rostrup-Nielsen JR. Mechanisms for catalytic carbon nanofiber growth studied by ab initio density functional theory calculations. Phys Rev B. 2006;73: 115419.
230. Trimm DL. Catalysts for the control of coking during steam reforming. Catal Today. 1999;49:3–10.
231. Guo J, Lou H, Zheng X. The deposition of coke from methane on a $Ni/MgAl_2O_4$ catalyst. Carbon. 2007;45:1314–21.
232. Peng H, Zhang X, Zhang L. One-pot facile fabrication of multiple nickel nanoparticles confined in microporous silica giving a multiple-Cores@Shell structure as a highly efficient catalyst for methane dry reforming. ChemCatChem. 2017;9:127–36.
233. Li L, Jiang B, Tang D. Hydrogen production from chemical looping reforming of ethanol using Ni/CeO_2 nanorod oxygen carrier. Catalysts. 2018;8:257.
234. Han Y, Tian M, Wang C. Highly active and anticoke Ni/CeO_2 with ultralow ni loading in chemical looping dry reforming via the strong metal-support interaction. ACS Sustain Chem Eng. 2021;9:17276–88.
235. Tian S, Yang X, Chen X. Catalytic calcium-looping reforming of biogas: a novel strategy to produce syngas with improved H_2/CO molar ratios. J Clean Prod. 2020;270: 122504.
236. Kang Y, Han Y, Wei C. A novel carbon cycle process assisted by Ni/La2O3 catalyst for enhanced thermochemical CO_2 splitting. J Energy Chem. 2021;61:297–303.

237. Kale GR, Kulkarni BD, Bharadwaj K. Chemical looping reforming of ethanol for syngas generation: a theoretical investigation. Int J Energy Res. 2013;37:645–56.
238. Trevisanut C, Bosselet F, Cavani F. A study of surface and structural changes of magnetite cycling material during chemical looping for hydrogen production from bio-ethanol. Catal Sci Technol. 2015;5:1280–9.
239. Ma Z, Xiao R, Chen L. Redox reaction induced morphology and microstructure evolution of iron oxide in chemical looping process. Energy Convers Manag. 2018;168:288–95.
240. Zheng Y, Marek EJ, Scott SA. H_2 production from a plasma-assisted chemical looping system from the partial oxidation of CH_4 at mild temperatures. Chem Eng J. 2020;379: 122197.
241. Kidambi PR, Cleeton JP, Scott SA. Interaction of iron oxide with alumina in a composite oxygen carrier during the production of hydrogen by chemical looping. Energy fuels. 2012;26:603–17.
242. Yu Z, Yang Y, Yang S. Iron-based oxygen carriers in chemical looping conversions: a review. Carbon Resour Convers. 2019;2:23–34.
243. Ma S, Chen S, Soomro A. Effects of supports on hydrogen production and carbon deposition of Fe-based oxygen carriers in chemical looping hydrogen generation. Int J Hydrog Energy. 2017;42:11006–16.
244. Chiu P-C, Ku Y, Wu Y-L. Characterization and evaluation of prepared Fe_2O_3/Al_2O_3 oxygen carriers for chemical looping process. Aerosol Air Qual Res. 2014;14:981–90.
245. Qin W, Wang J, Luo L. Chemical looping reforming of ethanol-containing organic wastewater for high ratio H_2/CO syngas with iron-based oxygen carrier. Int J Hydrog Energy. 2018;43:12985–98.
246. Rihko-Struckmann LK, Datta P, Wenzel M. Hydrogen and carbon monoxide production by chemical looping over iron-aluminium oxides. Energy Technol. 2016;4:304–13.
247. Yüzbasi NS, Kierzkowska A, Müller C. Development of Fe_2O_3-based, Al_2O_3-stabilized oxygen carriers using sol-gel technique for H_2 production via chemical looping. Energy Procedia. 2017;114:436–45.
248. Kang Y, Tian M, Wang Y. Silica modified alumina as supports of Fe_2O_3 with high performance in chemical looping combustion of methane. ACS Sustain Chem Eng. 2018;6:12884–92.
249. Hafizi A, Rahimpour M, Hassanajili S. Hydrogen production by chemical looping steam reforming of methane over Mg promoted iron oxygen carrier: optimization using design of experiments. J Taiwan Inst Chem Eng. 2016;62:140–9.
250. Feng Y, Wang N, Guo X. Density functional theory study on improved reactivity of alkali-doped Fe_2O_3 oxygen carriers for chemical looping hydrogen production. Fuel. 2019;236:1057–64.
251. Zeng D, Kang F, Qiu Y. Iron oxides with gadolinium-doped cerium oxides as active supports for chemical looping hydrogen production. Chem Eng J. 2020;396: 125153.
252. Zeng D, Qiu Y, Ma L. Tuning the support properties toward higher CO_2 conversion during a chemical looping scheme. Environ Sci Technol. 2020;54:12467–75.
253. Ma S, Li M, Wang G. Effects of Zr doping on Fe_2O_3/CeO_2 oxygen carrier in chemical looping hydrogen generation. Chem Eng J. 2018;346:712–25.
254. Bhavsar S, Isenberg N, More A. Lanthana-doped ceria as active support for oxygen carriers in chemical looping combustion. Appl Energy. 2016;168:236–47.
255. Díaz-Pérez MA, Moya J, Serrano-Ruiz JC. Interplay of support chemistry and reaction conditions on copper catalyzed methanol steam reforming. Ind Eng Chem Res. 2018;57:15268–79.
256. Xiong Y, Zhao J, Zheng Z. Modified CeO_2 as active support for iron oxides to enhance chemical looping hydrogen generation performance. Int J Hydrog Energy. 2020;45:32995–3006.
257. Yüzbasi NS, Abdala PM, Imtiaz Q. The effect of copper on the redox behaviour of iron oxide for chemical-looping hydrogen production probed by in situ X-ray absorption spectroscopy. Phys Chem Chem Phys. 2018;20:12736–45.
258. Zhou ZH, Deng GS, Li L. Chemical looping co-conversion of CH_4 and CO_2 using Fe_2O_3/Al_2O_3 pellets as both oxygen carrier and catalyst in a fluidized bed reactor. Chem Eng J. 2022. https://doi.org/10.1016/j.cej.2021.132133.
259. Yüzbasi NS, Kierzkowska AM, Imtiaz Q. ZrO_2-supported Fe_2O_3 for chemical-looping-based hydrogen production: effect of pH on its structure and performance as probed by X-ray absorption spectroscopy and electrical conductivity measurements. J Phys Chem C. 2016;120:18977–85.
260. Zhang X, Su Y, Pei C. Chemical looping steam reforming of methane over Ce-doped perovskites. Chem Eng Sci. 2020;223: 115707.
261. Zhang X, Pei C, Chang X. FeO_6 octahedral distortion activates lattice oxygen in perovskite ferrite for methane partial oxidation coupled with CO_2 splitting. J Am Chem Soc. 2020;142:11540–9.
262. Neagu D, Papaioannou EI, Tjaden B. Tracking the evolution of a single composite particle during redox cycling for application in H_2 production. Sci Rep. 2020;10:5266.
263. Qiu Y, Ma L, Li M. Copper and cobalt co-doped ferrites as effective agents for chemical looping CO_2 splitting. Chem Eng J. 2020;387: 124150.
264. Huang Z, Gao N, Lin Y. Exploring the migration and transformation of lattice oxygen during chemical looping with $NiFe_2O_4$ oxygen carrier. Chem Eng J. 2022;429: 132064.
265. Evdou A, Zaspalis V, Nalbandian L. Ferrites as redox catalysts for chemical looping processes. Fuel. 2016;165:367–78.
266. Huang Z, Deng Z, Chen D. Exploration of reaction mechanisms on hydrogen production through chemical looping steam reforming using $NiFe_2O_4$ oxygen carrier. ACS Sustain Chem Eng. 2019;7:11621–32.
267. Kim Y, Lim HS, Lee M. Enhanced morphological preservation and redox activity in Al-incorporated $NiFe_2O_4$ for chemical looping hydrogen production. ACS Sustain Chem Eng. 2021;9:14800–10.
268. Ma Z, Zeng D, Zhang S. Effect of supports on the redox performance of $NiFe_2O_4$ in a chemical looping process. Energy Technol. 2019;7:1900374.
269. Qin L, Cheng Z, Fan JA. Nanostructure formation mechanism and ion diffusion in iron–titanium composite materials with chemical looping redox reactions. J Mater Chem A. 2015;3:11302–12.
270. Zhu X, Li K, Neal L. Perovskites as geo-inspired oxygen storage materials for chemical looping and three-way catalysis: a perspective. ACS Catal. 2018;8:8213–36.

271. Yang J, Bjørgum E, Chang H. On the ensemble requirement of fully selective chemical looping methane partial oxidation over La-Fe-based perovskites. Appl Catal B. 2022;301: 120788.
272. Long Y, Yang K, Gu Z. Hydrogen generation from water splitting over polyfunctional perovskite oxygen carriers by using coke oven gas as reducing agent. Appl Catal B. 2022;301: 120778.
273. Yuan K, Zheng Y, Li K. Enhanced resistance to carbon deposition over $La_xCe_{1-x}Fe_xNi_{1-x}O_3$ oxygen carrier for chemical looping reforming. Energy Fuels. 2021;35:15867–78.
274. Zhang L, Xu W, Wu J. Identifying the role of A-site cations in modulating oxygen capacity of iron-based perovskite for enhanced chemical looping methane-to-syngas conversion. ACS Catal. 2020;10:9420–30.
275. Zhang L, Hu Y, Xu W. Anti-coke $BaFe_{1-x}Sn_xO_{3-\delta}$ oxygen carriers for enhanced syngas production via chemical looping partial oxidation of methane. Energy Fuels. 2020;34:6991–8.
276. Huang C, Wu J, Chen Y-T. In situ encapsulation of iron(0) for solar thermochemical syngas production over iron-based perovskite material. Commun Chem. 2018;1:55.
277. Zhang J, Haribal V, Li F. Perovskite nanocomposites as effective CO_2-splitting agents in a cyclic redox scheme. Sci Adv. 2017;3: e1701184.
278. Wang X, Du X, Yu W. Coproduction of hydrogen and methanol from methane by chemical looping reforming. Ind Eng Chem Res. 2019;58:10296–306.
279. Chen C, Yu W, Duan Y. Chlorine-promoted perovskite nanocomposite as a high-performance oxygen transfer agent for chemical looping methane-assisted CO_2 splitting. Chem Eng J Adv. 2020;4: 100052.
280. Zhu Y, Liu R, Sun X. Metal modified hexaaluminates for syngas generation and CO_2 utilization via chemical looping. Int J Hydrog Energy. 2019;44:10218–31.
281. Zhu Y, Sun X, Liu W. Microstructure and reactivity evolution of LaFeAl oxygen carrier for syngas production via chemical looping CH_4-CO_2 reforming. Int J Hydrog Energy. 2017;42:30509–24.
282. Zhu Y, Jin N, Liu R. Bimetallic $BaFe_2MAl_9O_{19}$ (M = Mn, Ni, and Co) hexaaluminates as oxygen carriers for chemical looping dry reforming of methane. Appl Energy. 2020;258: 114070.
283. Sun Z, Lu DY, Symonds RT. Chemical looping reforming of CH_4 in the presence of CO_2 using ilmenite ore and NiO-modified ilmenite ore oxygen carriers. Chem Eng J. 2020;401: 123481.
284. Gu H, Cui X, Wang J. Natural iron ore as oxygen carrier modified with rare earth metal for chemical looping hydrogen production. Energy Fuels. 2021;35:15234–42.
285. Lu C, Li K, Wang H. Chemical looping reforming of methane using magnetite as oxygen carrier: structure evolution and reduction kinetics. Appl Energy. 2018;211:1–14.
286. Lu CQ, Xu RD, Muhammad IK. Thermodynamic evolution of magnetite oxygen carrier via chemical looping reforming of methane. J Nat Gas Sci Eng. 2021. https://doi.org/10.1016/j.apenergy.2017.11.049.
287. Lu C, Li K, Zhu X. Improved activity of magnetite oxygen carrier for chemical looping steam reforming by ultrasonic treatment. Appl Energy. 2020;261: 114437.
288. Tian H, Siriwardane R, Simonyi T. Natural ores as oxygen carriers in chemical looping combustion. Energy Fuels. 2013;27:4108–18.
289. Gu H, Lang S, Song G. Enhanced chemical looping hydrogen production based on biomass ash-promoted iron ore oxygen carrier. Chem Eng J. 2019;360:260–70.
290. Wei G-Q, Zhao W-N, Meng J-G. Hydrogen production from vegetable oil via a chemical looping process with hematite oxygen carriers. J Cleaner Prod. 2018;200:588–97.
291. Huang Z, He F, Feng Y. Synthesis gas production through biomass direct chemical looping conversion with natural hematite as an oxygen carrier. Bioresour Technol. 2013;140:138–45.
292. Lewis W, Gilliland E, Reed WA. Reaction of methane with copper oxide in a fluidized bed. Ind Eng Chem. 1949;41:1227–37.
293. Lewis W, Gilliland E, Sweeney M. Gasification of carbon-Metal oxides in a fluidized powder bed. Chem Eng Prog. 1951;47:251–6.
294. Abuelgasim S, Wang WJ, Li TL. The effect of alkali and alkaline earth metals oxides addition on oxygen uncoupling rate of copper-based oxygen carrier: a kinetic and experimental investigations. Sep Purif Technol. 2021. https://doi.org/10.1016/j.seppur.2021.119176.
295. Johansson M. Screening of oxygen-carrier particles based on iron-, manganese-, copper-and nickel oxides for use in chemical-looping technologies. Sweden: Chalmers University of Technology Göteborg; 2007.
296. Noorman S, Gallucci F, van Sint AM. Experimental investigation of a CuO/Al_2O_3 oxygen carrier for chemical-looping combustion. Ind Eng Chem Res. 2010;49:9720–8.
297. Zhao H-Y, Cao Y, Orndorff W. Study on modification of Cu-based oxygen carrier for chemical looping combustion. J Therm Anal Calorim. 2013;113:1123–8.
298. Son SR, Go KS, Kim SD. Thermogravimetric analysis of copper oxide for chemical-looping hydrogen generation. Ind Eng Chem Res. 2009;48:380–7.
299. De Diego LF, García-Labiano F, Adánez J. Development of Cu-based oxygen carriers for chemical-looping combustion. Fuel. 2004;83:1749–57.
300. Keller M, Leion H, Mattisson T. Use of $CuO/MgAl_2O_4$ and $La_{0.8}Sr_{0.2}FeO_3/\gamma$-$Al_2O_3$ in chemical looping reforming system for tar removal from gasification gas. AIChE J. 2016;62:38–45.
301. Keller M, Fung J, Leion H. Cu-impregnated alumina/silica bed materials for chemical looping reforming of biomass gasification gas. Fuel. 2016;180:448–56.
302. Rodriguez JA, Grinter DC, Liu Z. Ceria-based model catalysts: fundamental studies on the importance of the metal–ceria interface in CO oxidation, the water–gas shift, CO_2 hydrogenation, and methane and alcohol reforming. Chem Soc Rev. 2017;46:1824–41.
303. Montini T, Melchionna M, Monai M. Fundamentals and catalytic applications of CeO_2-based materials. Chem Rev. 2016;116:5987–6041.
304. Campbell CT, Peden CH. Oxygen vacancies and catalysis on ceria surfaces. Science. 2005;309:713–4.
305. Sugiura M. Oxygen storage materials for automotive catalysts: ceria-zirconia solid solutions. Catal Surv Asia. 2003;7:77–87.
306. Otsuka K, Ushiyama T, Yamanaka I. Partial oxidation of methane using the redox of cerium oxide. Chem Lett. 1993;22:1517–20.
307. Otsuka K, Wang Y, Nakamura M. Direct conversion of methane to synthesis gas through gas–solid reaction using CeO_2–ZrO_2 solid solution at moderate temperature. Appl Catal A. 1999;183:317–24.

308. Zhu X, Donat F, Imtiaz Q. Chemical looping beyond combustion–a perspective. Energy Environ Sci. 2020. https://doi.org/10.1039/C9EE03793D.
309. Hong W, Zhang L, Miao L. Co/CeO_2 for ethanol steam reforming: effect of ceria morphology. J Rare Earths. 2013;31:565–71.
310. Dong W-S, Jun K-W, Roh H-S. Comparative study on partial oxidation of methane over Ni/ZrO_2, Ni/CeO_2 and Ni/Ce–ZrO_2 catalysts. Catal Lett. 2002;78:215–22.
311. Wang Y, Zheng Y, Wang Y. Syngas production modified by oxygen vacancies over CeO_2-ZrO_2-CuO oxygen carrier via chemical looping reforming of methane. Appl Surf Sci. 2019;481:151–60.
312. Ruan C, Tan Y, Li L. A novel $CeO_{2-x}SnO_2/Ce_2Sn_2O_7$ pyrochlore cycle for enhanced solar thermochemical water splitting. AIChE J. 2017;63:3450–62.
313. Hossain MM, de Lasa HI. Chemical-looping combustion (CLC) for inherent CO_2 separations—a review. Chem Eng Sci. 2008;63:4433–51.
314. Cheng X, Li K, Wang H. Chemical looping combustion of methane in a large laboratory unit: model study on the reactivity and effective utilization of typical oxygen carriers. Chem Eng J. 2017;328:382–96.
315. Adánez J, de Diego LF, García-Labiano F. Selection of oxygen carriers for chemical-looping combustion. Energy Fuels. 2004;18:371–7.
316. Costa T, Gayán P, Abad A. Promising impregnated Mn-based oxygen carriers for chemical looping combustion of gaseous fuels. Energy Procedia. 2017;114:334–43.
317. Bazhenova E, Honkala K. Screening the bulk properties and reducibility of Fe-doped Mn_2O_3 from first principles calculations. Catal Today. 2017;285:104–13.
318. Yin X, Wang S, Wang B. Perovskite-type $LaMn_{1-x}B_xO_{3+\delta}$ (B = Fe, CO and Ni) as oxygen carriers for chemical looping steam methane reforming. Chem Eng J. 2021;422: 128751.
319. Yin X, Shen L, Wang S. Double adjustment of Co and Sr in $LaMnO_{3+\delta}$ perovskite oxygen carriers for chemical looping steam methane reforming. Appl Catal B. 2022;301: 120816.
320. Zheng Y, Zhao L, Wang Y. Enhanced activity of $La_{1-x}MnCu_xO_3$ perovskite oxides for chemical looping steam methane reforming. Fuel Process Technol. 2021;215: 106744.
321. Yang ZY, Zheng YE, Li KZ. Chemical-looping reforming of methane over La-Mn-Fe-O oxygen carriers: effect of calcination temperature. Chem Eng Sci. 2021. https://doi.org/10.1016/j.ces.2020.116085.
322. Qin L, Cheng Z, Guo M. Morphology evolution and nanostructure of chemical looping transition metal oxide materials upon redox processes. Acta Mater. 2017;124:568–78.
323. Alalwan HA, Cwiertny DM, Grassian VH. Co3O4 nanoparticles as oxygen carriers for chemical looping combustion: a materials characterization approach to understanding oxygen carrier performance. Chem Eng J. 2017;319:279–87.
324. De los Rios T, Gutierrez DL, Martínez VC. Redox stabilization effect of TiO_2 in Co_3O_4 as oxygen carrier for the production of hydrogen through POX and chemical looping processes. Int J Chem Reactor Eng. 2005. https://doi.org/10.2202/1542-6580.1260.
325. Hwang JH, Son EN, Lee R. A thermogravimetric study of $CoTiO_3$ as oxygen carrier for chemical looping combustion. Catal Today. 2018;303:13–8.
326. Shen Q, Zheng Y, Li S. Optimize process parameters of microwave-assisted EDTA method using orthogonal experiment for novel $BaCoO_{3-\delta}$ perovskite. J Alloys Compd. 2016;658:125–31.
327. Lee M, Lim HS, Kim Y. Enhancement of highly-concentrated hydrogen productivity in chemical looping steam methane reforming using Fe-substituted $LaCoO_3$. Energy Convers Manag. 2020;207: 112507.
328. Kodama T, Ohtake H, Matsumoto S. Thermochemical methane reforming using a reactive WO_3/W redox system. Energy. 2000;25:411–25.
329. Shimizu T, Shimizu K, Kitayama Y. Thermochemical methane reforming using WO_3 as an oxidant below 1173 K by a solar furnace simulator. Sol Energy. 2001;71:315–24.
330. Kwak JH, Han GY, Yoon KJ. Zirconia-supported tungsten oxides for cyclic production of syngas and hydrogen by methane reforming and water splitting. Int J Hydrogen Energy. 2013;38:8293–305.
331. Zhao K, He F, Huang Z. $La_{1-x}Sr_xFeO_3$ perovskites as oxygen carriers for the partial oxidation of methane to syngas. Chin J Catal. 2014;35:1196–205.
332. Chen Y, Galinsky N, Wang Z. Investigation of perovskite supported composite oxides for chemical looping conversion of syngas. Fuel. 2014;134:521–30.
333. Otto S-K, Kousi K, Neagu D. Exsolved nickel nanoparticles acting as oxygen storage reservoirs and active sites for redox CH_4 conversion. ACS Appl Energy Mater. 2019;2:7288–98.
334. Zeng D, Cui D, Qiu Y. Mn-Fe-Al-O mixed spinel oxides as oxygen carrier for chemical looping hydrogen production with CO_2 capture. Fuel. 2020;274: 117854.